Politechnika Wrocławska

FIELD OF SCIENCE: Engineering and Technology

DISCIPLINE OF SCIENCE: Mechanical Engineering

DOCTORAL DISSERTATION

Fatigue behavior and life assessment of CFRP structures under global non-proportional multiaxial loading conditions

M. Sc. Eng. Szymon Duda

Supervisor:

Ph.D., D.Sc., Eng. Grzegorz Lesiuk, Assoc. Prof.

Auxiliary supervisor:

Ph.D, M.Sc., B.Sc., Eng. José A.F.O. Correia, Assist. Prof, University of Porto

Keywords: *carbon fiber reinforced polymer, multiaxial fatigue, mechanics of composite materials, fatigue life prediction*

WROCŁAW 2024

Preface

This Ph.D. thesis was submitted to the Faculty of Mechanical Engineering at Wroclaw University of Science and Technology. The Ph.D. thesis presents the research carried out during the course of a Ph.D. project in the Department of Mechanics, Material Science and Biomedical Engineering at Wroclaw University of Science and Technology from September 2020 to May 2024. The dissertation has received sponsorship from the Polish National Research Center, grant no. 2021/41/N/ST8/03365. The support received is gratefully acknowledged.

The central part of the research is put on the redeveloped damage parameter based on the Fatemi – Socie parameter. This aspect plays a crucial role in assessing multiaxial fatigue regardless of mean stress and phase non-proportionality. Finally, the parameter is used to predict the fatigue life of different materials using data taken from the literature. On the basis of the delivered results, one paper has been published in international scientific journals with peer review, whilst the two others are both undergoing review for possible publication in international journals at the time of printing of this thesis. This thesis is structured by covering nine chapters that answer the assumed scientific theses. The main goal of this dissertation is to provide a general approach for fatigue life estimation for composite materials that undergo non-proportional multiaxial loading.

The dissertation has been supervised by Associate Professor Grzegorz Lesiuk, Department of Mechanics, Material Science and Biomedical Engineering, Wroclaw University of Science and Technology, and Professor Jose AFO Correia, affiliated with Department of Mechanical Engineering, FEUP, Faculty of Engineering of the University of Porto. I express my sincere gratitude to all of my supervisors for the excellent guidance and support I received throughout the dissertation period.

Parts of the research in this Ph.D. dissertation have been carried out during international placements. I have spent five months at the University of Memphis, United States, in the research group of Fracture and Fatigue of Materials under the supervision of Professor Ali Fatemi thanks to support provided by the Fulbright commission. Another month was spent at the Department of Management and Engineering at NTNU, Norway, under the supervision of Professor Filippo Berto and Professor Gao Chao. I am very grateful for the guidance, support, and fruitful discussions during these external collaborations, which significantly impact the quality of my research.

I would like to thank my friends, lab mates, colleagues and research team – mgr inż. Paweł Zielonka, dr. inż. Paweł Stabla, dr inż. Michał Smolnicki, mgr inż. Tomasz Osiecki, Tomasz Markiewicz, dr inż. Wojciech Pawlak for valuable suggestions and unparallel support which was really influential in shaping my research. My appreciation also goes out to my family especialy my parents, grandparents, sister and fiance for their encouragement and support all through my studies.

English summary

The dynamic development of composite materials in industry is driven by the development of modern manufacturing technology and the superior properties these materials exhibit, such as high specific strength, low density, high resistance to corrosion, fatigue, and chemical environment. Moreover, the freedom of shaping geometry allows the production of new, more geometrically complex parts and objects sufficient to overstand significant load conditions with satisfactory mass.

Important examples of elements made of composite materials are wind turbine blades, drive shafts, high-pressure tanks, and even aircraft bodies. Taking into account the above-mentioned applications, it can be noticed that they are subjected to various cyclic loads. For example, the drive shaft is subjected to time-varying torsional and bending loads. These conditions significantly affect the operation of the elements and require their consideration at the design stage. The process of designing elements made of composite materials is very complex and advanced due to the anisotropy of the material. In order to ensure safety and reliability in operation, a costly experimental procedure is often required to describe the mechanical behavior of the element. This process can be optimized by mathematical description of individual phenomena that affect the strength of the designed element.

The dissertation focuses on the description of the fatigue process of a thin-walled cylindrical element made of carbon fiber reinforced polymer material (CFRP), which is subjected to axial forces and torsion. Moreover, the acting load is out of phase. This process is still not clearly described in composite materials, unlike metallic materials. Knowledge of this process will allow the fatigue life of an element to be estimated. The scientific literature provides several fatigue criteria that are used in the design of components exposed to fatigue damage. However, the available criteria do not cover all factors influencing the fatigue degradation of composite structures, such as load phase shift or mean stress. In the doctoral thesis, a fatigue criterion based on the critical plane approach was proposed. The developed fatigue criterion, based on the stress damage parameter defined for the critical plane, allows the assessment of material damage taking into account the mean stress and the phase shift of the load.

The doctoral dissertation is divided into two main stages: experimental and analytical. The first phase includes experimental work, i.e. fundamental research used for the fatigue modeling process. In this section, cylindrical CFRP specimens produced by filament winding technology are subjected to tensile, compressive, and torsional loads. The load is generated by a biaxial hydraulic testing machine equipped with special grips to ensure suitable loading conditions.

The second phase is related to modeling the fatigue process and predicting durability. Based on the developed numerical model, a stress analysis is performed to define the value of the failure parameter. The correlation of data for durability and failure parameters allowed for the description of the S-N curves, which were used to predict fatigue life. Moreover, this part of the work shows the applicability of the developed approach to other materials of the same class.

The experimental part is enriched with nondestructive (ND) methods to investigate damage mechanisms. Several failure mechanisms can occur in composite materials, such as delamination, debonding, matrix cracking, or fiber pullout. ND methods allow the

determination of defects that appear in the technological process and their development during the experiment. Computed tomography is a reliable method to assess the quality of the microstructure, among others such as defects and inclusions resulting from the technological process. Furthermore, in situ analysis using acoustic emission showed the global evolution of emerging defects and failure mechanisms during the fatigue test. In addition, a digital image correlation (DIC) device was used to measure strain during the test, providing information about defects that occur on the outer surface of the sample and the strain distribution. The data were used to verify the numerical method.

The proposed approach allows for a comprehensive filling of the existing gap in the literature regarding models predicting fatigue life, taking into account the phase shift of the load, the stress state, and its mean value.

Polish Summary

Wzrost udziału materiałów kompozytowych w przemyśle dyktowany jest przez rozwój nowoczesnej technologi wytwórczej, satysfakcjonujących właściwości, jakie te materiały wykazują, takich jak wysoka wytrzymałość właściwa, niska gęstość, wysoka odporność na korozję, zmęczenie i środowisko chemiczne. Ponadto dowolność kształtowania geometrii pozwala na wytwarzanie nowych, bardziej skomplikowanych geometrycznie części i obiektów dostosowanych do przemoszenia znaczynych obciążeń przy zachowaniu niższej masy w stosunku do odpowieników wykonanych z materiałów metalicznych.

Istotnymi przykładami elementów wykonanych z materiałów komopozytowych są łopaty turbin wiatrowych, wały napędowe, zbiorniki wysokociśnieniowe czy nawet korpusy samolotów. Biorąc pod uwagę przytoczone zastosowania można zauważyć, że są one poddawane różnym obciążeniom cyklicznym. Na przykład wał napędowy jest poddawany obciążeniom skręcającym i zginającym zmiennym w czasie. Warunki te w istotny sposób wpływają na eksploatację elementów i wymagą uwzględnienie ich na etapie projektowym. Proces projektowanie elementów z materiałów kompozytowych jest bardzo kompleksowego i zaawansowany z uwagi na anizotropię materiału. W celu zapewnienia bezpieczeństwa i niezawodność w eksploatacji, bardzo często wyamgana jest kosztowna procedura eksperymentalna pozwalająca opisać zachowanie mechaniczne elementu. Proces ten można zoptymalizować przez opis matematyczny poszczególnych zjawisk wpływających na wytrzymałość projektowanego elementu.

Dysertacja skupia się na opisie proces zmęczeniowego cieńkościennego elementu cylindrycznego wykonanego z materiał polimerowego wzmocnionego włóknem węglowym (CFRP), który poddany jest działaniu sił osiowych i skręcania. Ponadto działające obciążenie jest przesunięte w fazie. Proces ten wciąż nie jest jednoznacznie opisany w materiałach kompozytowych w przeciwieństwie do materiałów metalicznych. Literatura naukowa podaje kilka kryteriów zmęczeniowych, które wykorzystuje się w projektowaniu elekemtów narażonych na uszkodzenie zmęczeniowe. Jednakże, dostepne kryteria nie obejmują wszystkich czynników wpływających na degradację zmęczeniową konstrukcji warstwowych jak np. przesunięcie fazowe obciążenia lub naprężenie średnie. W roprawie doktorskiej zaproponowano kryterium zmęczeniowe bazujące na podejściu płaszczyzny krytycznej. Opracowane kryterium zmęczeniowe, oparte na naprężeniowym parametrze uszkodzenia definiowanego dla płaszczyzny krytycznej, pozwala ocenić uszkodzenie materiału biorąc pod uwagę naprężenie średnie oraz przesunięcie fazowe obciążenia.

Rozprawę doktorska podzielona jest na dwa główne etapy: eksperymentalny i analityczny. Pierwsza faza obejmuje prace eksperymentalne, czyli badanie statyczne oraz cykliczne wykorzystane do opisu procesu modelowania zmęczenia wieloosiowego. W tej części cylindryczne próbki CFRP wytwarzane metodą nawijania poddawane są obciążeniom rozciągającym/ściskającym oraz skręcającym. Obciązenie generowane jest przez dwuosiową hydrauliczną maszyna wytrzymałościowa wyposażona w specjalne uchwyty zapewniającą odpowiednie warunki obciążenia.

Druga faza związana jest z modelowaniem procesu zmęczeniowego oraz przewidywanie trwałości. W oparciu o opracowany model numeryczny, analiza naprężeń jest przeprowadzona w celu zdefiniowana wartości parametru zniszczenia. Korelacja danych dla trwałości oraz parametru zniszczenia pozwoliła uzyskać krzywe S-N, które wykorzystane zostały do przewidywania trwałości zmęczeniowej. Ponadto ta część pracu pokazuje aplikacyjność opracowanego podejścia w przypadku innego materiału tej samej klasy.

Część eksperymentalna zostanie wzbogacona o metody nieniszczące (ND) w celu zbadania mechanizmów uszkodzeń. W materiałach kompozytowych może wystąpić kilka mechanizmów niszczenia, na przykład rozwarstwienie, odspojenie, pękanie osnowy lub wyrywanie włókien. Metody ND pozwalają na określenie defektów pojawiających się w procesie technologicznym oraz ich rozwój w trakcie eksperymentu. Tomografia komputerowa jest niezawodną metodą oceny jakości struktury m.in. defektów i wtrąceń będących następstwem procesu technologicznego. Ponadto analiza in-situ z wykorzystaniem emisji akustycznej wykazała globalną ewolucję pojawiających się defektów i mechanizmów uszkodzeń podczas testu zmęczeniowego. Dodatkowo do pomiaru odkształceń podczas testu użyte zostało urządzenie do cyfrowej korelacji obrazu (DIC), które dostarczyło informacji o defektach występujących na zewnętrznej powierzchni próbki oraz dystrybucję odkształceń. Dane zostały wkorzystane do weryfikacji metody numerczynej.

Zaproponowany podejście pozwala na kompleksowe wypełnienie istniejącej luki w literaturze w zakresie modeli przewidujących trwałość zmęczeniową uwzględniając przesunięcie fazowe obciążenia, stan naprężenia oraz jego wartość średnią.

Contents

Nomenclature

α	- material non-linearity factor
γ_{ij}	- shear strain in "ij" direction
δ	- phase shifting between applied loads
θ	- composite layup fiber orientation
$\lambda_{t/12}$	- biaxiality ratio of stress components
ν_{ij}	- Poisson ratio in "ij" direction
$\sigma_{x,amp}$	- geometrical normal stress amplitude
$\tau_{xy,amp}$	- geometrical shear stress amplitude
σ_i	- normal stress component, i – direction
τ_{ij}	- shear stress, ij - direction
CDS	- characteristic damage state
$CFRP$	- carbon fiber reinforced polymer
COV	- coefficient of variation
DIC	- digital image correlation
e_m	- matrix tensile/compressive failure criterion
e_{fs}	- fiber – matrix shearing criterion
e_b	- fiber buckling criterion
E_1	- Young's modulus along fibers (1st-direction)
E_2	- Young's modulus perpendicular to fibers
FEM/A	- Finite Element Method/Analysis
FV	- Field Variable
FW	- filament winding
k	- calibration parameter for damage equation
G_{ij}	- shear modulus in "ij" plane
$GFRP$	- glass fiber reinforced polymer
HCF	- high cycle fatigue
N_f	- number of cycles to failure
ND	- nondestructive
PS	- principal strain
R	- load ratio
S_c	- ply shear strength

SD - standard deviation

$USDFLD$ - user-defined field

UTS - Ultimate Tensile Strength

WP - winding pattern

Y_c - matrix compressive strength

Y_t - transverse tensile strength

X_c - longitudinal compressive strength

1 Introduction

The chapter presented includes the theoretical background required to correctly understand the investigated phenomena within the dissertation. Due to the complex structure of composite materials, in many cases, even under uniaxial load, the multiaxial stress state is induced and is assumed to be a local multiaxiality; on the other hand, if more than one load case acts on the object, the global multiaxiality can be defined. In the case of this dissertation, global loading conditions are considered to refer to the multiaxial stress state generated by axial and torsional loading conditions. Apart from that, the problem and motivation have been described to show the need to consider and investigate this scientific subject.

Motivation

The regulations of the European Union regarding net zero emission balance by 2050, force many industrial fields to put the CO_2 emission aspect as a priority. It can be achieved by applying various solutions, i.e. mass reduction. Industries such as civil engineering, the automotive industry, and aerospace increase the number of lightweight composite members to reduce costs, consume energy, and reduce greenhouse gas emissions [1]. In terms of engineering industry, mass optimization holding a suitable stiffness of the system is one of major interest. This optimum (mass – stiffness) can be reached using composite materials, whose demand on the market increases every year [2]. Their extraordinary mechanical properties, such as high fatigue resistance and specific strength with a combination of low global density, enable one to design structural elements that meet demanding requirements. The Boeing 787 is a shining example of a structure made of 50% composite materials by weight (80% by volume). In addition, it is the first airplane to be equipped with an airframe made of a composite material [3].

The design process of structural elements requires a comprehensive and detailed design process that provides safety and reliability in service. This design process is even more sophisticated if composite materials have been considered. Their anisotropic material symmetry causes the multiaxial stress state even under static uniaxial loading. In practice, this stress state is compounded by alternating loading conditions that act on physical objects. Therefore, understanding the fatigue behavior of these materials is crucial in many applications (i.e., wind turbine blades, high-pressure vessels) in predicting maintenance or repair service, as well as in guaranteeing long-term service.

Problem overview

The superior engineering properties of composite materials attract engineers in many industrial fields. However, a complex design process remains a significant barrier to the wider application of these materials. The complexity of the design process is laid in many aspects, i.e. material inhomogeneity and anisotropic material symmetry, technology, loading conditions, and required experiments.

The inhomogeneity of the material causes the evolution of the damage to proceed differently from accumulation in metallic materials according to Fig. 1. Considering composite materials, the curve passes through three stages associated mainly with a particular failure mechanism. The first stage is dominated by microcracking of the matrix, and its density increases until the

point of characteristic damage state (CDS) is reached, which indicates the highest level of crack saturation that can be obtained. This point initiates the interfacial debonding caused by a high content of cracks and their coupling. During the same time, local delamination and fiber breakage may occur. The progression of interfacial debonding leads to delamination, which in the final stage, in combination with fiber breakage, completely eliminates the structural integrity of the laminate [4], [5]. On the accumulation of other hand, the damage in metallic materials progresses differently; the failure initiates a certain number of cycles and begins to grow up to the critical size that causes the fracture.

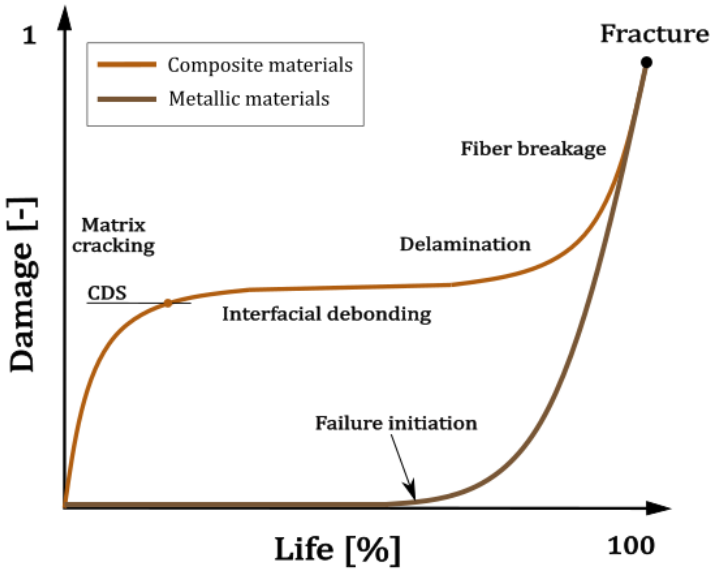

Fig. 1. General nature of damage accumulation in composite materials and metallic materials

Fiber reinforced polymers are multifaced materials that contain initial flaws such as broken fibers, voids, and damage from machining operations such as local delamination that challenge predictive methods used in the design process [6], [7], [8]. The consecutive issue is placed in the detection method to determine the discontinuity and failure mechanisms of the structure that occur within the operation in service. There are several methods applied to composite materials that support defect analysis and in situ damage accumulation monitoring, i.e. Visual testing (VT or VI), Ultrasonic testing (UT), Thermography, Radiographic testing (RT), Electromagnetic testing (ET), Acoustic emission (AE) and shearography testing [9].

Characterization of composite materials under the fatigue regime is crucial in terms of design in many applications to ensure safe long-term service. Many solutions in the field of computational mechanics have been proposed to overcome these problems; however, they require deep scientific knowledge and understanding of material physics. The mentioned issues require a holistic design procedure that combines all factors that influence the mechanical performance of composite materials.

The scope of the presented dissertation covers the problem of assessing the multiaxial behavior of thin-walled CFRP cylindrical members under multiaxial loading conditions. Axial load conditions (tension / compression) and torsion load were established on the basis of the analysis of industrial applications such as airplane wings, shafts, high-pressure vessels, or wind turbine blades. These objects are very often subjected to loads acting in various directions and are

usually coupled together. The wind turbine blade is a shining example of complex loading conditions generated by aerodynamic load, that is, bending (tension/compression) coupled with torsion (shear); the investigation of this state is well justified and has not yet been fully described [10].

Along with load complexity, the technology used in manufacturing plays a crucial role. To manufacture the aforementioned thin-walled CFRP structure, a filament winding method was applied. It is commonly used in the production of high-pressure vessels or shafts. However, it generates a complex structure that causes local stress concentrations at the fiber tow interweaving.

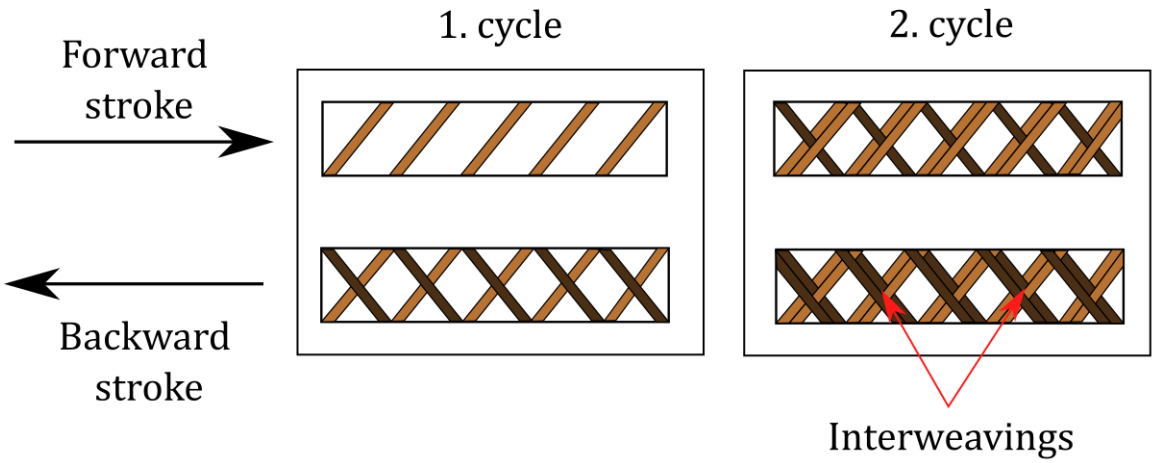

Fig. 2. Schematic presentation of filament winding processes in the example of two cycles. Graphic by authors, first published in [11] under https://creativecommons.org/licenses/by/4.0/

The continuous process of filament winding technology gives a specific structure of the composite with interweaving as it is presented in Fig. 2. They are an inseparable part of the filament wound structure (excluding pure hoop winding). In this area, the fibers are distorted from the linear path and cause stress concentration.

Applied technology requires several parameters to define. The most important point of view of mechanical performance is the orientation of the fiber of the wounded cylindrical structure. It is commonly reported in literature that fiber orientation has a significant influence on mechanical strength and performance. In this investigation, a 30° fiber orientation was assumed based on the following factors:

- Since torsion, tension and compression is considered. The variation in fiber orientation was constrained by the fact that the 45° angle of the fiber resists the most effective shear stress caused by the torsion load and the bending is carried the most by the fiber oriented in the 15° direction.
- To precisely choose the dissipative factor provided by Morozov [12] was considered as a final indicator. The dependence of the dissipative factor on the fiber orientation is presented in Fig. 3.

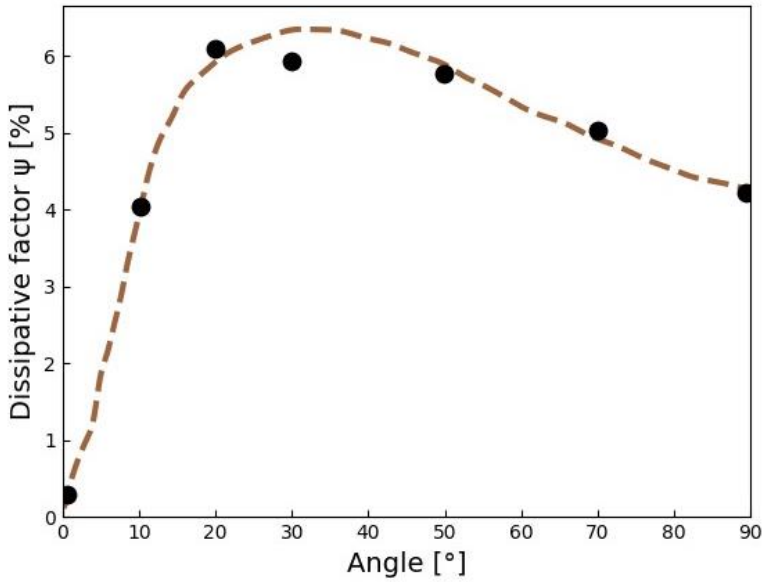

Fig. 3. Calculated (dot line) and experimental (black points) dependencies of the dissipation factor on the ply orientation for unidirectional carbon epoxy. Graphic by the authors, first published in [11] under https://creativecommons.org/licenses/by/4.0/

1.1 State of the art

The survey of the literature shows a shortage of research on the multiaxial fatigue behavior of composite materials. In the world, only several research groups deal with multiaxial phenomena, mainly at Padova University, the University of Bristol, and the Technical University Dresden. The demanding specification of the experiment under multiaxial loading conditions excludes many research groups from this field. Furthermore, the experiment is time-consuming and cost-consuming, which cannot be afforded by every research team in the scientific field.

Identification of a literature gap

M. Quaresimin [10], [13], [14], [15], [16], [17], [18] is the leading scientist in the field of damage-oriented fatigue modeling of composite materials. The researcher published valuable articles on the multiaxial fatigue behavior of composite materials. The research team of Quaresimin examined a cylindrical glass fiber reinforced polymer tube (GFRP) subjected to various load combinations, for example, tension/stress loading conditions, investigating factors that influence fatigue strength such as the stress ratio (R), the biaxiality ratio (λ), the degree of non-proportionality and the layout configuration. Their work focuses on experiment simplification by investigating a flat specimen reflecting the same stress state as in the cylindrical sample under multiaxial loading conditions [19]. Recently, spectrum loading has been an area of interest for the Quaresimin research team [20]. Considering their research, it needs to be noted that published papers give results for specific material and its particular configuration with some layup variations. Based on the articles cited, it is still necessary to investigate other material configurations and various load proportionality, including the influence of load nonproportionality [21].

Jifa Mei [22] provided an example of systems in which the non-proportionality of loading conditions appears, for instance, the loading histories plot recorded for the lower wing skin of

an aircraft, which exhibits non-proportionality between stress components. Considering the previous example of Boeing 787, the airplane wings are made in large part from CFRP, it leads to a genuine need to examine phase shifting in CFRP material.

To provide established multiaxial loading conditions, the appropriate specimen should be manufactured. Olsson [23] submitted a paper giving an overview of multiaxial test procedures, suggesting that a tubular specimen is an obvious choice for these assumptions (material and loading conditions). Moreover, this type of specimen presents an absence of a free edge effect (lack of stress concentration at the edges due to cutting process). There are two possibilities to manufacture this type of specimen using the filament winding or mandrel wrapping and curing process in an autoclave [14].

Mechanics of FW members

FW cylindrical members are an interest for many scientists and significant effort is put into the effect of winding pattern on mechanical performance. Lately, de Menezes et al. [24] analyzed the influence of the WP on filament-wound cylinders under axial compression, torsion, and internal pressure loads. An original approach to generate the geometric pattern was developed by the aforementioned author. It allowed to numerically analyze parameters such as the number of layers, the winding angles, and winding pattern using the finite element method. The results obtained demonstrate that the interweaving area is the location of the significant stress concentration. This effect can be reduced by the higher number of layers, according to the research mentioned.

Lisboa et al. [25] presented another scientific paper on experimental and numerical investigation of the winding pattern. The authors' conclusions demonstrate that the winding pattern determines the mechanical behavior (from yielded progressive to brittle manner) and the manner of failure (delamination, transverse cracks). Furthermore, the stiffness of the tube did not change significantly in relation to the absorbed energy. Winding pattern is also the objective of the research by Azevedo et al. [26]. Hydrothermally aged filament wound composite cylinders show that water uptake depends on the mosaic pattern. A lower degree of interweaving allows for greater water uptake. Subsequently, the investigated compressive strength and stiffness were sensitive to WP. The compressive strength generally increases with the winding pattern (number of interweaving); however, the stiffness does not follow this scheme.

It is crucial to refer to Morozov [27], [28], which shows that stress analysis based on conventional mechanics could underestimate this value. The results show the sensitivity of the composite shells to winding patterns, resulting in divergent stress and strain distributions. This survey provides direction in terms of stress/strain analysis in terms of FW members investigated within the research framework. In summary, it is important to consider the mosaic pattern, which has a significant impact on the stress distribution.

Shear nonlinear material models

To perform stress analysis, a proper material model needs to be chosen and calibrated. In terms of composite materials, it is also desirable to apply progressive failure due to the complexity of the failure (many failure mechanisms act simultaneously). Due to the large group of available

material models, only those for composite materials with shear nonlinearity were taken into account.

An analytical solution for damage analysis proposed by Chang [29] in 1987 includes an approach for stress analysis of composite laminate with a notch subjected to compressive loading. This stress analysis is incorporated with the damage-based model, which takes into account the damage state in the material. The theory of finite deformation with nonlinearity (material and geometrical) gives the formula for stress and strain calculations. Simultaneously, the set of failure criteria and degradation models predicts the failure mechanism and gives a real damage state in the material. The prediction agrees well with the experimental results [11].

Two decades later, Van Paepegem et al. [30] proposed a semi-empirical model derived from experimental data based on two state variables, that is, shear damage and permanent shear strain. The researcher highlighted that shear damage can be adequately described by the developed model; however, the effect of normal stresses cannot be neglected. An additional damage law should be included to consider the transverse stiffness of the material [11].

Subsequent evaluation of the non-linear shear stress-strain relationship was developed by He et al. [31] in 2012. The research combined finite method analysis along with digital image correlation to analyze material deformation. The Ramberg-Osgood equation and classical beam theory were incorporated to conduct a stress analysis of a glass-epoxy composite in a short beam shear test. The conclusions drawn by the author confirm a good agreement between the experimentally generated strain field and the FE-computed strain field [11].

The impact of the non-linear shear effect on damage was also studied by Fedulov et al. [32] in 2016. In this investigation, the stress-strain relationship proposed by Chang [29] for the open-hole compression test was adopted and the results showed good agreement with the experiment.

In 2021, O'Brien [33] conducted research on hybrid composites (composed of glass and steel fibers) as a potential alternative to conventional glass fiber reinforced polymers, with the aim of improving energy dissipation and strength. The proposed approach is based on two user-defined materials models. The nonlinear behavior of the glass fiber reinforced polymer is reflected by the material model based on continuum damage mechanics. On the other hand, stainless-steel fibers exhibit ductile behavior, which is based on the plasticity model. The developed approach shows good agreement in the strain field validated by the correlation of the digital image during the experiment.

The literature survey gives an overview of 5 material models with progressive failure. On the basis of this and the static experimental campaign conducted, the model developed by Chang [29] was chosen and applied in this dissertation research.

Multiaxial fatigue models

The previous literature review gives an overview of damage-based material models in static conditions. It is crucial from the perspective of stress analysis. However, if the alternating stresses are considered, the modeling process is understood as a way of predicting the durability of the material. The fatigue prediction methodologies are more often based on the development of the empirical relationship between the applied load and the fatigue lifetime of the investigated material at different scale lengths depending on the group of approaches. The

theories are divided into four classes, i.e. macroscopic, damage-based models, probabilistic and multiscale theories as presented in Fig. 4. Except for probabilistic approaches, remaining give the deterministic solution. Each of them provides various advantages that result in various engineering applications.

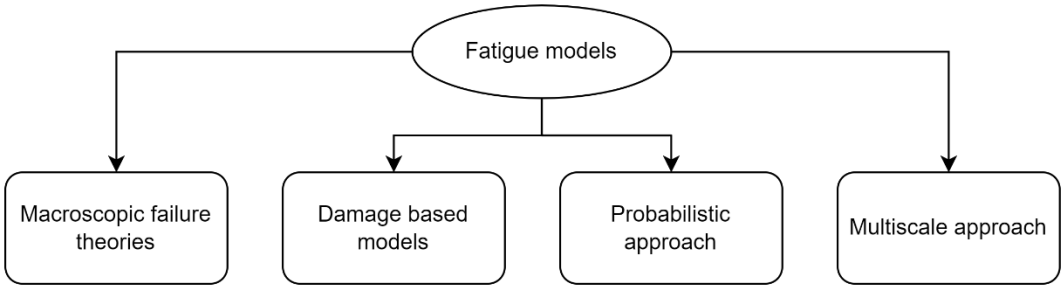

Fig. 4. The groups of fatigue models

Based on the classification presented, a more precise description of the models is provided.

- Macroscopic failure theories – group of phenomenological models. These models are based on the delivery of an S-N or ε-N. This group follows the trend of experimental fatigue data (best fit) and does not take into account the damage state of the material. The literature provides several models for the approximation curve, such as Sendeckyj [34], Kohout – Vechet [35], or Weibull [36]. In this method, a large number of experimental data is needed, and real damage mechanisms such as fiber and resin failure are not considered [37]. Additionally, within this group, strength and stiffness degradation theories are placed. These theories consider the actual state of damage in the material expressed by a representative damage indicator. Taking into account this damage indicator, theories are based on residual strength or residual stiffness. The latter theory is not related to macroscopic failure; it predicts material behavior in terms of stiffness degradation. The main advantages of these theories are greater changes in stiffness during their lifetime. Residual strength theories assume that failure occurs when the maximum applied cyclic stress level. There is a weakness of these methods that the change of the strength along the fatigue lifetime is minimal, it changes rapidly before the final failure happens. This group cannot be applied to complex loading patterns when multiaxial stress states appear.
- Probabilistic approach - The stochastic nature of fatigue behavior leads to this group of approaches. The probabilistic approach describes fatigue behavior according to the distribution (Weibull or Normal) of the applied parameters (load, strength). Otherwise, to the deterministic approaches, the material properties have a value of a certain level of reliability. The intense development of those techniques has begun in the last several years. It is caused by novel computational techniques available presently, including genetic algorithms, artificial intelligence, or neural networks [38], [39].
- Multiscale approach - Composite materials exhibit various mechanical performances depending on the length scale. The idea of those theories is placed into investigating damage state at various scales, i.e. initiation phase at nano- or microscale, propagation at micro- or macroscale. Currently, many research groups work on those methods, as they provide

reliable results; however, they require large experimental campaigns and deep knowledge of material physics. Basically, this group is a combination of models from different groups.

- Damage-based methods - This group is based on the actual damage state in the material. As a shining example concept based on the observation of the initiation and propagation of fatigue cracks along the planes, the known as the critical plane should be highlighted [40]. The Critical-plane approach is based on two aspects, the definition of the critical plane and the definition of representative damage parameter, which can be in the form of energy-based parameter, but it is not limited to energy.

Despite the fair number of models available in the literature, there are limitations to using such models for the characterization of life prediction. There are no comprehensive models considering all the factors that influence the multiaxial fatigue behavior of the composite material. Some of them are detailed described in the following review.

The author Quarisimin [17] examined some semi-empirical fatigue criteria, including those proposed by Ellyin. The main advantage is the reduced number of parameters that need to be determined experimentally, but this criterion is highly sensitive to the adopted calibration curve. The Tsai–Hill quadratic polynomial criteria according to date seem to be a reasonable alternative in estimating fatigue life strength considering global (external – load) and local (internal – material anisotropy) multiaxiality, but its use requires three (3) calibration curves. The author also examined the Smith-Pascoe criterion, which has some limitations regarding fiber symmetry (cannot be applied for unidirectional laminates).

A decade ago, Quaresimin et al. [14], [18] developed a multiscale damage-based approach for the estimation of fatigue lifetime. Predicts the onset of matrix cracks by considering the local maximum principal stress or the local hydrostatic stress. Since the first crack initiates, and propagate other cracks can initiate, at this stage the crack density function needs to be described. This step ends with the initiation of delamination and, finally, propagation and fiber breakage. All of these stages need to be considered on different length scales. The papers show good agreement between the experiment and the predictions.

Recently, Fatemi et al. [41], [42] expanded a critical plane approach to life prediction in short fiber polymer composites under multiaxial loading conditions. The concept is based on the modified Fatemi – Socie damage parameter that takes into account the notch effect, means stress and multiaxiality effect, debonding damage, and fiber orientation effect. The results show a good agreement with the experimental data. The Fatemi approach appears to be a good alternative to further extend it to long fiber materials subjected to multiaxial loading conditions.

Weng et al. [4] proposed a multiscale model used to predict the multiaxial fatigue life of composite laminates. They investigated the fatigue behavior of composite laminates under tension–torsion biaxial loading conditions, including various loading paths. Their numerical results showed good agreement with the experimental data. However, a couple of points are highlighted that differentiate the research in dissertation. First, they used a different modeling method to predict fatigue life. Instead of an energy-based approach, the multiscale finite element analysis method was applied. Furthermore, research excludes the influence of the mean stress effect for the investigated composite material. Finally, insufficient data were provided,

and only a few specimens for the S-N curves are presented. It shows that a more detailed analysis is needed.

The summary of the models available in the literature is provided in Table 1.

Table 1. Summary of the fatigue lifetime prediction models reviewed

Authors	Year	Approach	Concept	Loading conditions	Material system
Labossiere et al. [43]	1988	Macroscopic failure criterion	Modified Tsai–Hill criterion	Multiaxial	FRP
Smith et al. [44]	1989	Macroscopic failure criterion	Modified Tsai–Hill criterion	Multiaxial	FRP
Ellyin et al. [45]	1990	Macroscopic failure criterion	Strain energy density parameter	Multiaxial	glass fiber/epoxy resin, boron fiber/aluminum matrix, and graphite fiber/epoxy resin
Ellyin et al. [46]	1994	Macroscopic failure criterion	Empirical	Multiaxial	FRP
Plumtree et al. [47]	1999/ initial SWT parameter 1970	Damage based - critical plane	Fatigue damage parameter based on the Smith-Watson-Topper parameter (SWT)	Uniaxial	UD GFRP
Petermann et al. [48]	2001	Damage based - critical plane	Fatigue parameter	Uniaxial	UD CFRP and GFRP
Shokrieh et al. [49]	2006	Macroscopic failure criterion	Elastic strain energy density	Uniaxial	UD CFRP
Qi et al.[50]	2008	Damage based - critical plane	Effective stress	Multiaxial	GFRP
Tan et al.[51]	2010	Damage based	Hysteresis-based damage parameter	Uniaxial	GFRP
Movaghghar et al. [52]	2012	Macroscopic failure criterion	Dissipative energy of the cyclic and creep energy described as functions	Uniaxial	GFRP
Naderi et al. [53]	2013	Damage based	Heat dissipation, hysteresis energy	Uniaxial	GFRP
Quaresimin et al.[14], [18]	2014	Damage based	Local stresses/crack density function/energy release rate	Multiaxial	GFRP Tube

Weng et al. [4]	2020	Damage based	Energy-based fatigue damage parameter	Multiaxial	UD GFRP
Plumtree et al. [54]	2023	Damage based	Weibull model/continuum damage mechanics	Uniaxial	UD FRP
Fatemi et al. [41], [42], [55]	2020 – 2024/ initial FS form 1988	Damage based - critical plane	Based on the Fatemi – Socie (FS) parameter	Multiaxial	Short fiber reinforced polymers

CFRP – carbon fiber reinforced polymer
FRP – fiber reinforced polymer
GFRP – glass fiber reinforced polymer
NA – non applicable
UD – unidirectional

Experimental data published in scientific journals

From the modeling point of view, it is important to review the available experimental data, already done in the field of multiaxial fatigue. The experimental data available in the literature are presented in Table 2. The survey was carried out based on the scientific databases of Google Scholar and Scopus. As shown, 13 scientific papers were found that touch on this subject and data on multiaxial fatigue.

Table 2. Summary of the experimental results generated under external biaxial loading available in the literature

Authors	**Year**	**Matrix**	**Fibers**	**R**	**Lay-up**	**Specimen Type**
Smith et al. [56]	1989	Polyester	Glass Woven	-1	$[0/90]_{13}$ $[22.5/112.5]_{13}$ $[\pm45]_{13}$	Cruciform
Amijima et al. [57]	1991	Polyester	Glass Woven	0	$[0/90]_n$	Tubular
Atcholi et al. [58]	1992	Epoxy	Glass UD	-1	$[0]_n$	Bar
Fuji et al. [59], [60]	1995; 2016	Polyester	Glass Woven	0	$[0/90]_n$	Tubular
Wafa et al. [61]	1997	Polyester	Glass Woven	-1	$[0/90]_n$ $[\pm45]_n$	Tubular
Qi et al. [62]	2007	Epoxy	Glass Woven	0/-1	[±35] [±55] [±70]	Tubular

Quaresimin et al. [21], [63]	2013; 2015	Epoxy	Glass Woven	0.05/0.1/0.5/-1	$[90]_n [0/50_2/0/-50_2]_S$ $[0/60_2/0/-60_2]_S$	Tubular
Qiao et al. [64]	2019	Epoxy	Glass UD	0.1	$[+45/90/-45/0]_s$ $[0/90]_{2s}$	Notched specimen
Skinner et al. [65]	2019	Epoxy	Carbon Woven	0.1/0.3	$[0/90]_S$	Cruciform
Weng et al. [4]	2020	Epoxy	Carbon Woven	NR	[45/70/0/-70/-45]	Tubular
Zumaquero et al. [5]	2022	Epoxy	Carbon UD	NR	$[0]_n$	Cruciform

NR – non – reported.

Conclusions drawn on the basis of the conducted survey

The following conclusions can be drawn from the literature survey performed:

- There is still a lack of sufficient fatigue database in the field of composite materials, especially considering the global multiaxiality case. The lack of data drastically limits the possibility of developing a general formula for the estimation of fatigue life of this class of materials.
- Some research is done in the field of nonproportional multiaxial fatigue mainly for GFRP material manufactured differently from FW. There is still a need for a deeper understanding of the multiaxial fatigue behavior of composite anisotropic materials considering global multiaxial loading conditions, especially in terms of FW members and CFRP.
- Due to the complex material architecture provided by FW, a proper material model needs to be used to analyze the mechanical performance of the material that includes the stress non-linearity experience of members due to the shear softening effect caused by fiber undulation.
- There are many divisions of fatigue models that can be applied for fatigue prediction. However, the fatigue criteria available in the literature are usually limited to specific factors, which allows them to be used only for certain loading cases, very often excluding many important parameters affecting fatigue life, and these available in the literature do not comprehensively exemplify the scale of the problem in the cognitive sense.
- Identification of the failure mechanism that acts while in service is still an issue to overcome.

The developed approach and the knowledge of multiaxial phenomena will contribute to the proper design of composite members, especially in the aerospace, energy and automotive industries. Existing models very often lead to an overestimation of durability, which has a direct impact on the economy and ecology of designed parts.

1.2 Mechanics of composite materials

The mechanics of composite materials introduce the constitutive relation between stress and strain. To describe this relation, the stiffness matrix needs to be determined on the basis of the elastic properties of the material. Determining the elastic constants of the composite material requires a comprehensive experimental campaign. There are two ways to determine the elastic properties of the investigated composite materials, i.e., macroscopic and micromechanical approaches.

The composite material is a combination of at least two different materials in terms of physical and chemical properties, the assembly of which provides improved qualities. Due to this inhomogeneous nature, the elastic properties are not always easy to determine experimentally, or to determine stiffness matrix many tests are required. The micromechanical approach allows to calculate the elastic properties of the homogeneous composite layer or laminate based on the elastic properties of the constituents and fiber volume. Several approaches may be introduced, including the Rule of Mixtures, Halpin-Tsai (interpolation procedure) or Abolin'sh [66]. These approaches describe composite behavior by considering interaction of constituent materials on the basis of the following assumptions: homogeneity of matrix and fibers, isotropy, and elastic behavior of constituents. Moreover, uniform fiber distribution with the absolute adhesion matrix – fibers is considered. Highlighted criteria are feasible to calculate elastic properties of the material such as Young's modulus in the first and second directions and Poisson ratio. Those methods do not allow to calculate strength properties such as UTS. There is one exception, compression strength, which can be approximate using, for instance, the Rule of Mixtures. These methods require defining the elastic parameters for constituents, i.e. resin and fibers, and fiber content volume. For that reason, special devices, for instance, micro-tensile machines for single fiber, are required.

Increasing the level of the scale length, the more common is to investigate material properties in a macroscopic way. The complete experimental campaign is included in Table 3, which shows the number of experiments necessary to fully determine the elastic properties of the composite material system. Each load case (tension, compression) should be conducted for at least 0° and 90° unidirectional fiber orientation. Additionally, some industries (i.e. Aerospace) require conducting a tensile test for quasi-isotropic laminates. This test prevents edge effect softening in angle ply laminates, which may result in an underestimation of the strength and modulus of angle ply laminates. Otherwise, in steel, the compression strength of composite materials is significantly lower. Due to the high sensitivity for this loading case, an experimental procedure needs to be carried out.

Table 3. Static experimental procedures for determining in a complex way the mechanical properties of orthotropic composite material

Experiment	Standard	Layup configuration
Tensile 0°		$[0]_8$
Tensile 90°	ASTM D3039 [67]	$[90]_{16}$
Laminate tensile QI		$[45/0/-45/90]_{2S}$
Compression 0°		$[0]_8$
Compression 90°	ASTM D6641 [68]	$[90]_{16}$
Laminate compression QI		$[45/0/-45/90]_{2S}$
In-plane shear	ASTM D7078 [69]	$[45/-45]_{4S}$

QI – quasi - isotropic

Composite laminates are frequently described as transversely isotropic or orthotropic materials. This assumption significantly reduces the components of the linear theory of elasticity for anisotropic materials. The fully anisotropic (triclinic) description requires 21 elastic parameters; however, the orthotropic description requires only 9 independent components [70].

The essential point of view of composite mechanics is the latter case of symmetry. Most laminates belong to this group. The material possesses orthotropic symmetry if there are three mutually orthogonal symmetry planes. The axes created by inter-sectioned planes cover the principal axes of the material. In the case of composite materials, a two-coordinate system should be considered. If the lamina is taken into account, the material coordinated system is denoted 1st (along fiber direction), 2nd (perpendicular to the fiber direction), and 3rd according to Fig. 5. Simultaneously, these directions refer to stress principal directions. Considering laminate (as an integral structure), the load direction coordinate system has a very often priority and is usually denoted as x, y, z [70]. In terms of thin-walled structure, the 3rd or z direction is excluded due to the plane stress conditions that fulfill the geometry. There is a direct relationship between those coordinate systems, which allows the transformation of stresses from one coordinate (for instance, according to the load coordinate system) to a material coordinate system. Using the transformation matrix (considering fiber orientation) it can be calculated as presented in Eq. (1).

$$\begin{bmatrix} \sigma_1 \\ \sigma_2 \\ \tau_{12} \end{bmatrix} = \begin{bmatrix} cos^2\,\theta & sin^2\,\theta & 2\sin\theta\cos\theta \\ sin^2\,\theta & cos^2\,\theta & -2\sin\theta\cos\theta \\ -\sin\theta\cos\theta & \sin\theta\cos\theta & cos^2\,\theta - sin^2\,\theta \end{bmatrix} \begin{bmatrix} \sigma_x \\ \sigma_y \\ \tau_{xy} \end{bmatrix} \quad (1)$$

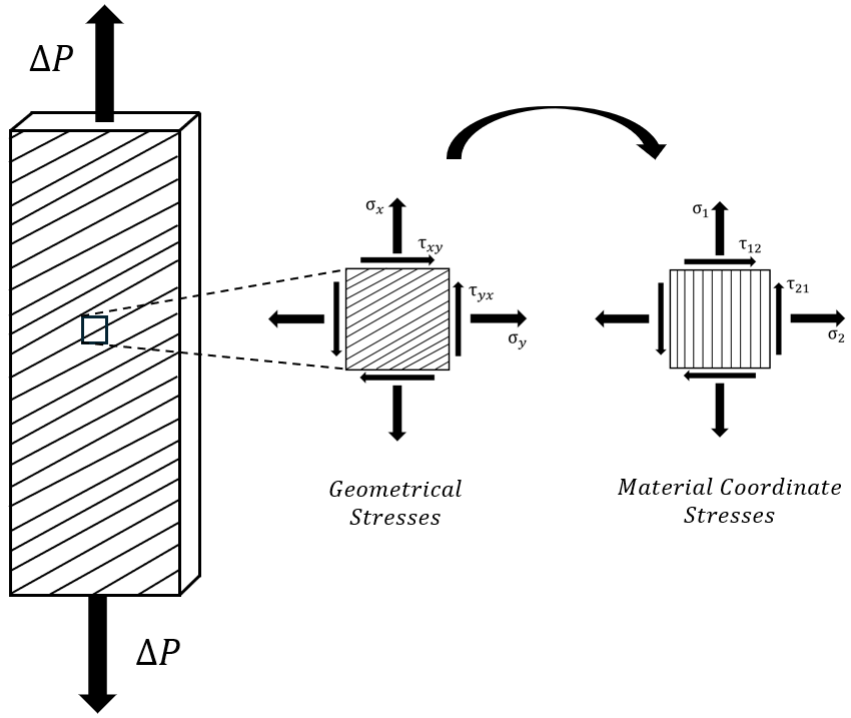

Fig. 5. Relationship between stress states for the material and load coordinate system in orthotropic composite materials under plane stress conditions

Proceeding to the constitutive relationship of composite materials, the tensor or Voigt notation might be introduced. Mainly in the mechanics of composite materials, Voigt notation is used for simplicity as well as convenience reasons. This allows avoiding complicated tensor operations. The physical equations in the Voigt contraction are presented below:

$$\sigma_i = Q_{ij}\varepsilon_j \tag{2}$$

$$\varepsilon_i = S_{ij}\sigma_j \tag{3}$$

where
i, j = 1, 2, …, 3
Q_{ij} – stiffness matrix,
S_{ij} – compliance matrix,
$Q_{ij} = 1/S_{ij}$ – relationship between the matrices.

It may be shown that the physical equations for materials that possess orthotropic symmetry have the form as follows:

$$\begin{Bmatrix} \sigma_1 \\ \sigma_2 \\ \sigma_3 \\ \tau_{23} \\ \tau_{31} \\ \tau_{12} \end{Bmatrix} = \begin{bmatrix} Q_{11} & Q_{12} & Q_{13} & 0 & 0 & 0 \\ Q_{21} & Q_{22} & Q_{23} & 0 & 0 & 0 \\ Q_{31} & Q_{23} & Q_{33} & 0 & 0 & 0 \\ 0 & 0 & 0 & Q_{44} & 0 & 0 \\ 0 & 0 & 0 & 0 & Q_{55} & 0 \\ 0 & 0 & 0 & 0 & 0 & Q_{66} \end{bmatrix} \begin{Bmatrix} \varepsilon_1 \\ \varepsilon_2 \\ \varepsilon_3 \\ \gamma_{23} \\ \gamma_{31} \\ \gamma_{12} \end{Bmatrix} \frac{E(1-\nu)}{(1-2\nu)(1+\nu)} \tag{4}$$

The decreased number of components is the result of the symmetry properties with respect to the designated planes. It is noticeable that there is no feedback between normal stresses and tangential strains, tangential stresses and normal strains, and tangential stresses and strains in the Eq. (4).

Further simplification may occur for transverse isotropy symmetry; in this case, components such as Q_{55} and Q_{66} need to be replaced as follows, $Q_{55} = Q_{44}, Q_{66} = (Q_{11} - Q_{12})/2$. For materials with transverse isotropic symmetry, only five elastic constants have been required.

There is another important aspect which needs to be considered. To reduce computational and modeling resources, it is common to use a 2D approximation in engineering analysis. This approximation is divided into plane stress and plane strain material conditions. Plane stress conditions appear when the stress vector is zero in a particular plane. For plane strain conditions, no strain occurs in a particular direction. This fact may also be applied to composite materials; usually, members made from composite materials can be treated as plates or shells (thickness of laminates is significantly lower with respect to other dimensions). In that case, the plane stress conditions are very often inquired and benefit the following assumptions:

$$\sigma_3 = 0;\ \tau_{23} = 0;\ \tau_{13} = 0 \tag{5}$$

This assumption leads to the major simplification of constitutive equations. It is presented in the form of the relationship for strains using a compliance matrix (Eq. 6). This form of linear theory of elasticity is more common and useful because it is a simpler form of compliance than the stiffness matrix.

$$\begin{Bmatrix} \varepsilon_1 \\ \varepsilon_2 \\ \gamma_{12} \end{Bmatrix} = \begin{bmatrix} \frac{1}{E_1} & -\frac{\nu_{21}}{E_2} & 0 \\ -\frac{\nu_{12}}{E_1} & \frac{1}{E_2} & 0 \\ 0 & 0 & G_{12} \end{bmatrix} \begin{Bmatrix} \sigma_1 \\ \sigma_2 \\ \tau_{12} \end{Bmatrix} \tag{6}$$

The number of independent components in compliance, as well as in stiffness matrix and engineering constants, decreased to 4 compared to 9 required for a general orthotropic case. The independent engineering constants determined for the composite material are:

E_1 – Young's modulus along the 1st direction (longitudinal Young modulus),
E_2 – Young's modulus along the 2nd – direction (transverse Young modulus),
G_{12} – in plane shear modulus,
ν_{12} – Poisson's ratio,
and dependent constant ν_{21} – minor Poisson ratio defined as $\nu_{21} = \frac{E_2}{E_1}\nu_{12}$.

In most cases, the aforementioned elastic properties are applied to describe the material behavior of composite laminates in the elastic regime under mechanical load.

Static failure criteria

The analysis of failures is an important part of the mechanics of composite materials. It consists of two main elements that must be considered, lamina failure analysis and laminate stress analysis, including reduction of stiffness due to lamina failure. The complex microstructure of these materials causes a loss of integrity resulting from several failure mechanisms that act simultaneously. It significantly increases the difficulty level of predicting mechanical performance. In this section, the static failure criteria for the unidirectional lamina are discussed.

Failure criteria for the lamina determine the strength and mode of failure of a unidirectional composite layer. The available criteria, mainly phenomenological based on linear elastic analysis, do not cover detailed processes of fracture. Moreover, they predict only the initiation, which means that there is failure or not, there is no damage growth phase included. The lamina failure criteria can be divided into three groups:

- Limit criteria (e.g. maximum stress or maximum strain), this group predicts failure by comparing the stress or strain component with the corresponding strength.
- Interactive criteria (e.g. Hill – Tsai, Tsai – Wu), they combine all stresses or strain by using a single quadratic or higher-order polynomial equation to predict the failure. The stress strength ratios are compared to define the failure mode as long as the equation is satisfied.
- Separate mode criteria (e.g. Hashin – Rotem, Hashin), widely used group, those criteria differentiate the failures, there are separate failure criterion for matrix and fiber. The equation can depend on one or more stress components with an interaction of stress. As this group covers various failures and separates them, predictability is relatively high [71].

One of the most commonly used failure criteria for damage initiation is Hashin, widely implemented in many software suit for finite element analysis. The highlighted criterion takes into account four failure modes, such as fiber tension/compression and matrix tension/compression. The equations that describe particular failure modes are presented below.

$$\text{Fiber failure (tension)} = \left(\frac{\sigma_{11}}{X}\right)^2 + \left(\frac{\tau_{12}}{S}\right)^2 = 1 \tag{7}$$

$$\text{Fiber failure (compression)} = \left(\frac{\sigma_{11}}{X'}\right)^2 = 1 \tag{8}$$

$$\text{Matrix failure} = \left(\frac{\sigma_{22}}{Y}\right)^2 + \left(\frac{\tau_{12}}{S}\right)^2 = 1 \tag{9}$$

where
X – tensile strength, fiber direction [MPa],
X ' – compression strength, fiber direction [MPa],
Y – tensile strength, transverse direction [MPa],
S – shear strength [MPa].

The next stage, important from an engineering point of view, covers the stress analysis of the laminate, which is layered structures of differently oriented laminae. In this case, the situation is more sophisticated due to the variety of failure mechanisms and their coupling. There is no universal failure criterion describing the mechanical performance in general for composite materials, each case should be treated separately, and on the basis of the gathered experimental data, a particular approach can be chosen.

1.3 Fatigue phenomenon

The design of a fatigue testing campaign contains many variables that directly affect the results. The clue of fatigue experiment is to provide the loading conditions that reflect the stress state in the sample approximately to the in-service conditions. These parameters and their importance are presented in this subchapter.

The design of the specimen for the fatigue experiment plays a crucial role in the observation and description of damage. There are several various geometries, which allow to obtain various kinds of experimental data. If a smooth specimen (unnotched) is considered, the total fatigue life is obtained that includes the damage initiation and the damage growth life. On the other hand, the damage growth data can be observed and measured by notched specimen. The fatigue experiment is conducted for a thin-walled cylindrical smooth specimen that allows the application of gloabal multiaxial loading conditions and excludes the free edge effect (source of delamination).

In the beginning, the understanding of multiaxiality needs to be highlighted. There are two adjectives that describe this term as presented in Fig. 5. Considering the anisotropic inhomogeneous composite material, the multiaxial stress state is generated even by a simple uniaxial loading case, and this state refers to local multiaxiality. Global multiaxiality is concerned when the two separate loading cases are applied and act on the material system, which also generate the multiaxial stress state. However, the magnitude of the stress components might be significantly multiplied.

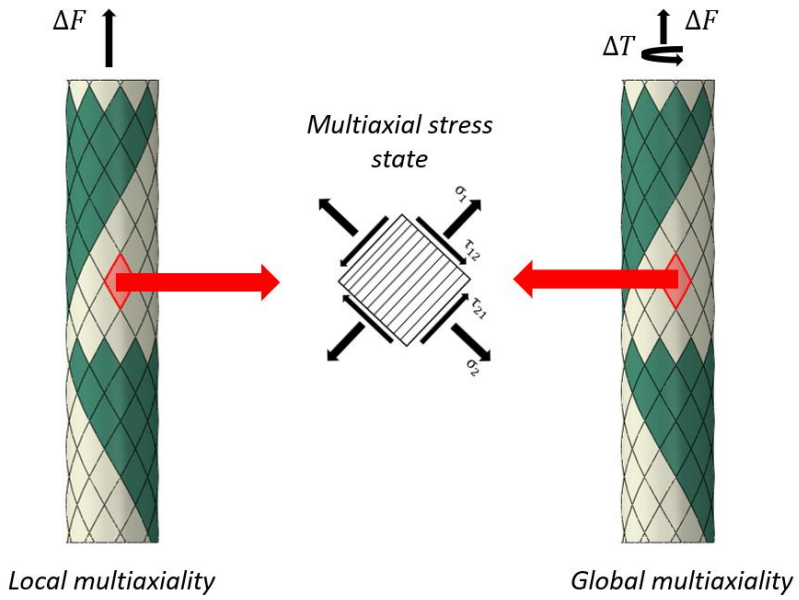

Fig. 6. Schematic explanation of local and global multiaxiality

There are at least two loads that act simultaneously on the material considering the global multiaxial load. It gives another parameter that needs to be taken into account, i.e., load proportionality. Considering the sinusoidal signals for axial and torsional load, there is a proportional load also called in phase in Fig. 7a, the peak values for both signals act at the same time. On the other hand, in Fig. 7b, the peak values are shiften with respect to time, this fact refers to load nonproportionality or out of phase loading case. In general, by changing the loading phase, the signals are shifted with respect to time. By shifting the loading phase, the stress path changes shape according to Fig. 7c. This fact affects the development of fatigue fractures, as well as fatigue life.

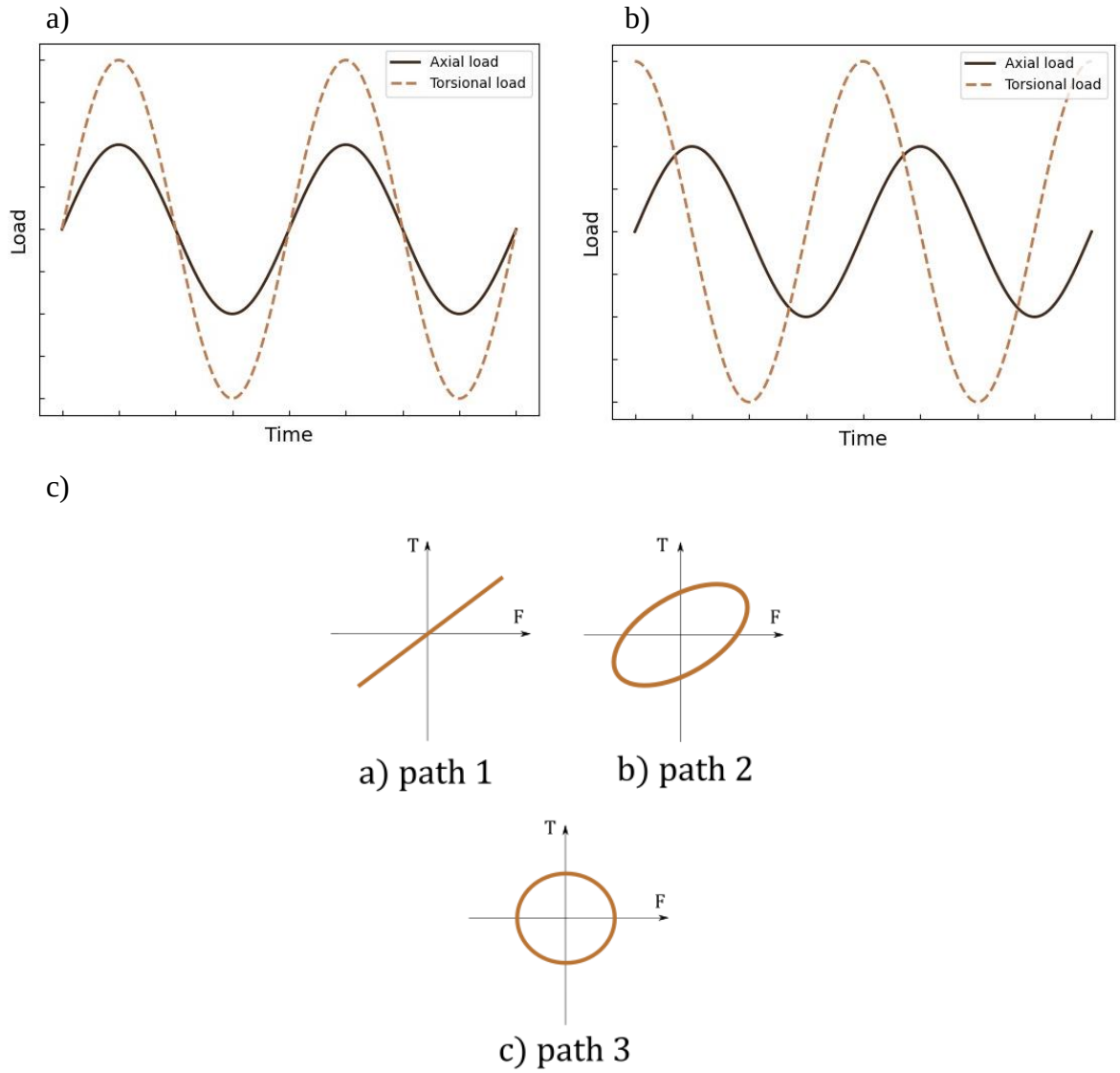

Fig. 7. Examples of a) in phase, b) 45 out of phase sinusoidal signals, c) stress paths for multiaxial load for path 1 (λ = 1, 0, δ = 0°), path 2 (λ = 1, δ = 45°) and path 3 (λ = 1, δ = 90°), where T – torque and F – force;

The aforementioned parameters refer directly to multiaxial fatigue; however, there are several other more general parameters that must be defined in every experimental fatigue test. The following can be identified:

- Load or stress ratio (R) - It is a ratio of minimum over maximum cyclic stress or load ($R = \sigma_{min}/\sigma_{max}$). Specifying, it says whether tensile, compression, or a combination of both loading cases act on the sample. The mean stress effect should be pointed out here, which is expressed by formulae $\sigma_M = (\sigma_{max}+\sigma_{min})/2$. Investigating various stress ratios exhibits the influence of mean stress [72]. Mean stress effects are important in metals for the analysis of high cycle fatigue (HCF) and are well defined [73]. In contrast to metals, in composites, the mean stress effects are likely to be more significant but still require a detailed analysis [74]. Some exemplary stress ratios are plotted in Fig. 8.
- Loading pattern – considering this parameter, two aspects are brought to the point. At first, the testing amplitude may be constant or variable. Most existing fatigue data are provided for constant amplitude; however, more complicated loading patterns can be

applied, such as block loading [72], and variable amplitude loading [75], [76], [77]. The need for these experiments is various. For example, block loading conditions can investigate the effect of sequence, especially the effect of creep [78], [79], [80]. More representative and realistic loading conditions can be reflected by applying variable amplitude load, this can also provide more reliable fatigue life prediction results [81]. As a second aspect, the complexity of the load needs to be discussed. As a result of the anisotropy of the material, even with uniaxial loading conditions, a multiaxial stress state can be obtained. However, multiaxial loading conditions (e.g., tension/torsion) can be applied to the material. To distinguish both cases, local and global multiaxiality needs to be defined. Local multiaxiality is caused by material anisotropy, since global multiaxiality is imposed by loading conditions [82]. Global multiaxiality is used to investigate material behavior under complex stress states, as well as to establish models to predict fatigue life under such conditions [10], [83], [84]. Fig. 8 presents some examples of constant and various amplitude loading conditions.

- Waveform – the applied waveform can differ in shape and affects the fatigue results. The most used is sinusoidal because of the effortlessness to generate this signal. Concerning signals such as triangular, square, or sawtooth, a conclusion can be drawn that sinusoidal does not generate sudden changes, which may better reflect realistic conditions. Investigating creep or recovery effects, more sophisticated signals can be selected. Sims [81] investigated the influence of waveform for fatigue data obtained for glass-fiber/epoxy. The results show that with longer lives there is no difference. The difference in shorter lives may be related to the mean load applied in each type of cycle, with the highest mean load for the square wave and the lowest for the triangular one. Different waveforms are presented in Fig. 8.

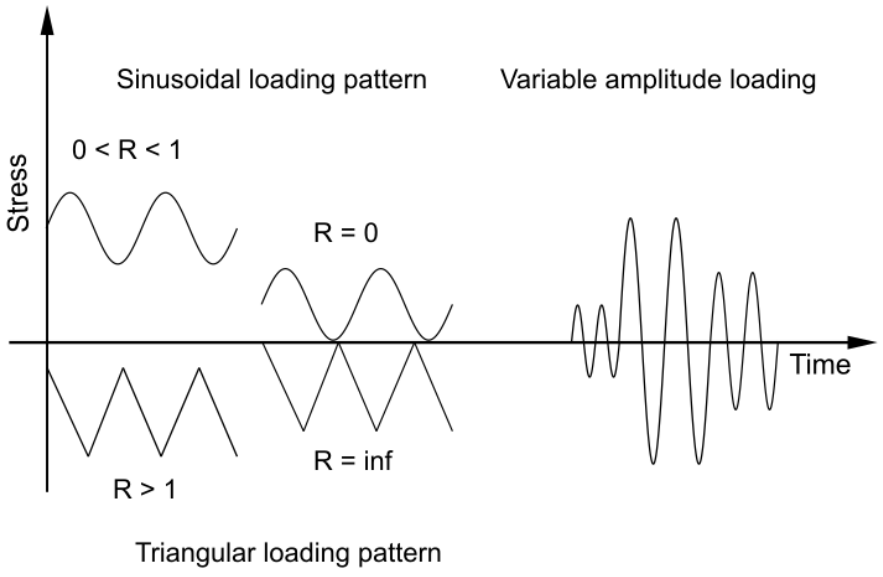

Fig. 8 Comparison of stress ratio, waveforms, and loading patterns

- Frequency/strain rate - Unlike metallic materials, composite materials are affected by frequency. The reason for this is due to the heating of the material at higher frequencies or creep fatigue at lower frequencies, also a combination of both [85], [86]. The

mechanical energy dissipated during the hysteresis loop is restated in heat; when the energy increases and it cannot be rejected in the environment, it simultaneously increases local temperature, which affects fatigue lifetime, especially if the glass transition temperature of the matrix is exceeded. Citing ASTM D3479 [87], no significant changes in temperature must be observed during constant-amplitude load until failure.

- Control mode - The fatigue experiment can be conducted under load/displacement/strain control. For delivering standard S-N curves, force control is preferred. Since the load is constant, the deformation increases with load cycles caused by the accumulation of damage. In the case of displacement control, a smoother evolution of the damage is observed. That way, the material does not fail suddenly. This control mode might be used especially in materials with large deformation, such as hyperplastic materials. Investigating fatigue in low cycle fatigue (in the plastic region, usually up to 100 000 cycles) the strain rate control should be applied. This control mode is the most challenging because it requires an additional sensor (strain gage or extensometer) and special limit levels must be activated in the testing machine to prevent undesirable movements of the machine.
- Testing temperature – this factor is also very important from the fatigue strength perspective and in-service loading conditions. Real objects are very often subjected to combined thermomechanical loading conditions i.e. airplanes or wind turbine blades [88]. However, for nonstructural structures, fatigue tests are normally carried out under ambient environmental conditions. This is due to simplicity and cost (less expensive).

The parameters need to be defined to examine the fatigue behavior of the material experimentally. The knowledge included in this chapter allows understating factors that influence fatigue life and provides an overview of components that should be taken into account in analytical divagation.

However, the fatigue behavior of composite materials is governed by other aspects related in general to the material itself and manufacturing. The following factors should be noted:

- Fiber orientation – the static and fatigue strength depend highly on the fiber orientation. Taking into account the uniaxial tensile load capacity, the direction of the fiber parallel to the applied force provides the highest performance in both static and fatigue. However, if the pure torsional load is considered the 45° fiber orientation provides the leading performance. There are several studies, i.e. [89], [49], [14], [62] giving an overview of the influence of fiber on fatigue strength. In general, the fiber orientation that defines the principal directions of the material needs to correspond to the principal directions introduced by the load to achieve the maximum mechanical performance of the material.
- Constituents – this aspect covers the basic materials for fibers and matrices and the form of reinforcement. Considering the composite material as the assembly of two or more materials with different chemical and physical properties on a macroscopic scale to form a third with improved qualities, a variety of forms of reinforcement can be highlighted: fiber (i.e. continuous, short) and particle-based (i.e. large particles, dispersion

strengthened) and structural reinforcement (fabrics, sandwich panels). Additionally, various materials for fibers (i.e. carbon, glass, aramid, basalt, etc.) and for matrices (i.e. epoxy, vinyl ester, etc.) can be used to provide different mechanical performance of the final material composition defined by dissimilar elastic properties of each submaterial.

- Layup configurations - Composite materials are usually in the form of laminates which consist of several layers stacked together. In this configuration, a variety of layer orientations can be used, which are normally governed by the loading conditions that the material needs to withstand. Those laminates are subdivided into classes: unidirectional (each layer is aligned in the same direction), cross-ply (alternating layers in perpendicular direction i.e. 0° – 90°), angle – ply (alternating layer oriented in $\pm\theta°$ direction) and multidirectional (various fiber orientation for each layer). This aspect is important and has an impact on fatigue strength, as reported in [14], [90].
- Manufacturing method - There are many methods for manufacturing parts from composite materials i.e. hand layup, spray layup, pultrusion, filament winding machine, autoclave-based processing, resin transfer molding, etc. Each technology provides some advantages and limitations in use. Therefore, the geometry and the required quality of the material frequently define the manufacturing process. There are manufacturing processes that possess the same possibilities, but the final product may provide a different quality in terms of microstructural discontinuity. The aspect of material imperfection is challenging but important; recently, it is a very vital subject to incorporate technological imperfections into failure analysis of composites. It is investigated in a comprehensive way by R. Tarleja and presented in [91].

The highlighted factors show the very complex nature of composite materials. However, it is challenging to consider all of these factors for economic reasons. In this study, only some of them are taken into account and analyzed.

Analysis of fatigue data

The fatigue experimental data for smooth samples are presented in the form of S – N curves as presented in Fig. 9. The graph presents stress (usually the stress amplitude) as a function of life to failure, which is understood as total material decohesion. Constant ampitude S – N curves can be plotted on log-log or semilog coordinates. The S – N behavior covers the total fatigue life; it means the damage iniation (crack nucleation and small crack growth) as well as propoagation of macrodamage. However, the designed specimen can exhibit very rapid and unstable damage; in that case the S – N curves refer to damage initiation. The most common way to deliver the S – N curve is the regression analysis described in [92]. However, there are more models that provide the S – N curves in addition to regression analysis; currently, stochastic methods are widely used.

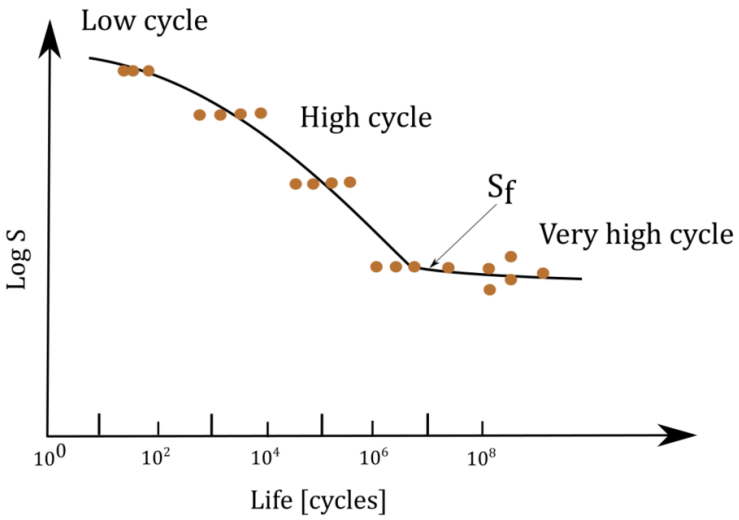

Fig. 9. Typical S - N diagram; S – stress [MPa], S_f – fatigue limit [MPa]

The S – N behavior can be divided into a low-cycle, high-cycle, and very high-cycle fatigue regime, which is defined for a particular number of cycles according to the investigated material. If low cycle fatigue is considered, the material usually experiences plastic defermation and fatigue life is short; in terms of high cycle fatigue, elastic behavior is considered. Taking into account the behavior of S - N, fatigue strength should be noted; this value refers to the highest stress that a material can withstand for a given number of cycles without fracture. The second term refers to the fatigue limit, S_f, the stress condition below which a material may endure an infinite number of cycles before failure. However, recent investigations in the very high cycle fatigue (possible due to modern resonance high frequency testing machines) showed that the fatigue limit is not a constant value, the S – N curve in this regime exhibits some slope. The S – N curves allow to design elements with respect to defined life time or predict the life time of the object under certain loading conditions.

1.4 Damage mechanisms

Due to the inhomogeneity of the material, several failure mechanisms affect the fatigue life of the composite material. Otherwise, to well-known metallic materials where normally a single crack starts to grow, in these materials, several failure mechanisms are coupled with each other and occur consecutively within the entire volume of the material. When considering plastic material reinforced with fibers (mainly continuous), different failure mechanisms can be considered for each length scale. The microscopic scale includes debonding (interface single fiber – matrix), single fiber breakage, and matrix microcracking. Taking into account separately each lamina, the mesoscale has been introduced. This scale length allows for investigating failures such as translaminar failure of the lamina, splitting, kinking (local buckling), and local delamination. When the entire thickness of the laminate is taken into account, the macroscale is introduced. On this scale, delamination plays an important issue [93], [94].

One of the first damage mechanisms in composite materials that develops during cycling loading is cracking of the matrix. They usually have an elliptical shape or narrow openings. This damage is not catastrophic but as the number of cracks increases, the material properties decrease, and at the final stage, they generate consequential failure mode, which is detrimental

for the drop in stiffness. In addition to the external load that causes cracks, the manufacturing process is also the source of microstructure discontinuity, including microcracks. Furthermore, the sources of cracks and their growth are the result of loss of adhesion along fibers and loss of matrix and resin bridges between fiber regions in the early stage of material degradation. Joining those microcracks with interlaminar cracks results in translaminar failure on the mesoscopic scale. The rich resin regions generate a second mechanism that causes matrix micro-and meso- cracking. This fact is a result of exceeding the local boundary strain value [95], [96].

The most detrimental failure mechanism that refers to the debonding of alternate laminae is delamination. This process occurs mainly in fiber-reinforced laminates [97]. As a source of stress singularity that induces delamination, the following examples are quoted, free edges, notches, ply drop, and joints [98]. Delamination can be divided into 3 stages as follows: initiation phase, stable propagation, and unstable propagation phase [99]. Several approaches allow investigating this phenomenon, mainly implemented at FEM. The most common are Cohesive Zone Modeling (CZM), Extended Finite Element (xFEM), and Virtual Crack Closure Technique (VCCT). These techniques require determining the critical strain energy density and initiation parameters to define the traction–separation law to reflect the behavior of the interface between the composite layers. Linear elastic fracture mechanics (LEFM) is widely used to investigate the propagation phase of delamination. In general, the border between the applicability of the LEFM and the S-N approach is placed in the length of the defect. For the S - N approach, the small cracks and its initiation phase are considered; on the other hand, for analyzing the propagation phase, LFEM should be used.

The nature of composite failures is comprehensive, especially for advanced laminates (various fiber orientations), which results in various failure modes, often the last one covered by fiber breakage. It should be stated that the degree of failure that classifies material for further exploitation may be considerably higher before the final breakage [96].

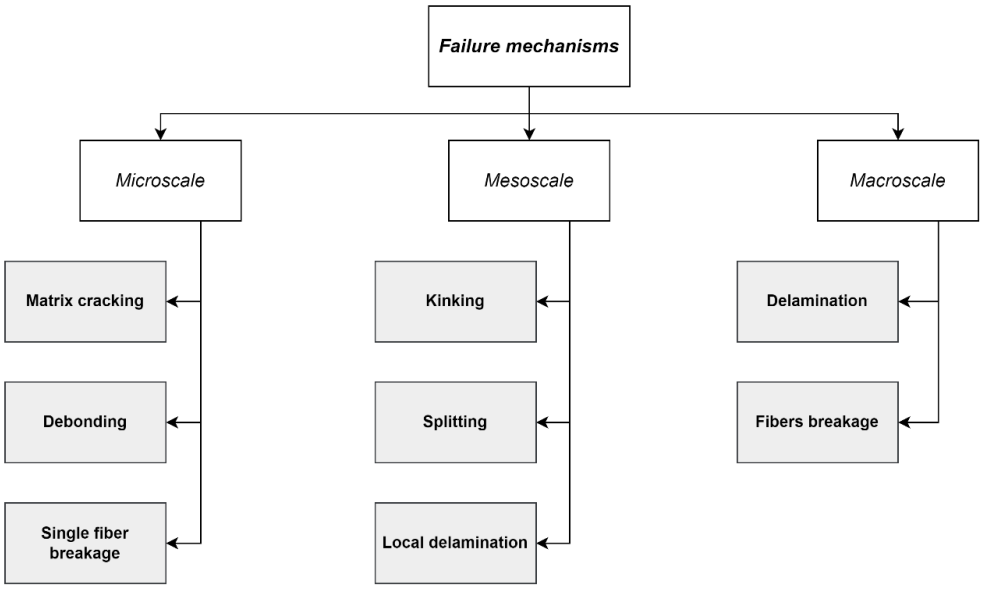

Fig. 10. Failure mechanism divisions in terms of length scale

When fatigue phenomena are considered, three major failure mechanisms, i.e., matrix cracking, debonding, and delamination, are frequently considered during the analysis of the fatigue behavior of the composite material. Recognition of fracture behavior is crucial from a modeling point of view, which results in good agreement on fatigue life prediction. The division of the failure mechanisms in terms of scale is presented in Fig. 10.

Non-destructive methods used in fracture analysis of composite materials

Modern ND methods allow for in situ or ex situ material examination in terms of defect distribution, their initation, and nuckleation. It is important to monitor the health condition of many objects, especially structural parts. Increase its safe operation and prevent disasters. One of the most presice; however very expensive method is micro-computerized tomography, which gives the exact 3D microstructure image. There are some limitations in the use, the scale of the investigated objects. It cannot be used for large structural elements. However, the analysis can be performed on a laboratory scale and implemented on real objects. References [100], [101], [102] shows the use of computed tomography even with a connection to the DIC method to comprehensively investigate the evolution of damage. This connection of modern techniques allows to determine the failure mechanism that leads to failure. There are other methods, such as electrical methods, ultrasonic methods, optical methods, or acoustic methods. Due to the relatively large number of methods, some criteria of choice need to be defined. In the case of this research, the acoustic method was applied because of its accessibility and dynamic development in the field in the past few decades.

The Acoustic Emission Method is based on the acquisition of the elastic weaves appearing in the material by the piezoelectric sensor and their analysis. Each failure within the material caused the acustic signal which can be collected and described by the parameters presented in Table 4. Considering the number of parameters it is not easy to define primary the failure modes unless it is a homogeneous and anisotropic material. In other cases, due to the complex failure nature, this task is extremely challenging because failure acts simultaneously.

Table 4. Basic parameters used in description of acoustic signal collected by the AE method

Parameter	**Description**
Count	Every peak signal, which exceeds the threshold value
Amplitude	The highest value of the signal recorded within one signal. Measured in mV but presented in relativ way in dB
Duration	It is a time between the duration of the initial and end signal over the threshold limit [μs]
Rise Time	The time of the first signal rises to reach the maximum amplitude in the cycle [μs]
Energy	Usually integration of the signal over time
Frequency	Delivered on the basis of the applied analysis of waveforms
Root mean squared of noise	The root of the arithmetic mean of the squares of the noise values. It is observed that its higher values are often registered during rupture events.

The development of new algorithms allowed the analysis of signals in a more efficient and effective way; however, it required a deep understanding of programming and signal analysis. Some of the possibilities of using machine learning are shown in [103], [104], and [105]. For analysis of damage in material, for the purpose of this research, an acoustic emision is used. Signal analysis covers only basic possibilities provided by the Vallen system. Any further analysis is not considered within the investigation.

1.5 Summary

The introduction chapter covers the following aspects, identification of the scientific problem along with the motivation for conducting the research. Furthermore, a comprehensive literature survey is included in the field of multiaxial fatigue. Finally, the theoretical background is given, which is important for understanding the research pursued. In summary, the following major aspects are investigated in the presented dissertation.

- Material model definition based on the static experimental campain.
- Effective stress analysis of the FW composite structure under multidirectional loads acting on the material system using the numerical method.
- Experimental evaluation of the multiaxial fatigue behavior of the thin-walled CFRP tube.
- S-N behavior modeling of the multiaxial proportional and non-proportional loading phase.
- Analysis of the impact of the mean stress and load proportionality on the behavior of S - N.
- Assessment of damage accumulation assesment monitored by the acoustic emission system during cycling loading.
- Life prediction approach for CFRP material investigated subjected to multiaxial fatigue load.

2 Objective and research methods

2.1 Objective and content

The presented dissertation investigates the multiaxial fatigue behavior of thin-walled carbon fiber reinforced polymer (CFRP) under nonproportional loading conditions. The main objective of the research is the mechanical characterization of multiaxial behavior considering parameters such as nonproportionality (phase shifting), and variable load ratios. Characterization includes S-N curves established for the examined parameters that show their influence on the general behavior of the investigated material. The filament winding method is applied to manufacture thin-walled members with fiber orientation [+/- 30°]. Damage analysis performed within the research is based on digital image correlation (for quasi-static loading conditions) and acoustic signals acquired during the fatigue experiment. The modeling part based on the experimental data is carried out based on the critical plane approach and the redeveloped Fatemi – Socie parameter based on stress components. The defined damage parameter is applied to predict the fatigue life in terms of the S-N curve. Moreover, the approach was confronted with data from the literature for glass fiber reinforced polymer (GFRP).

The research framework is presented in Fig. 11. The core of the dissertation is covered by 4 main tasks, i.e., preliminary material examinations, multiaxial fatigue experiment, fatigue behavior modeling, and fatigue life prediction.

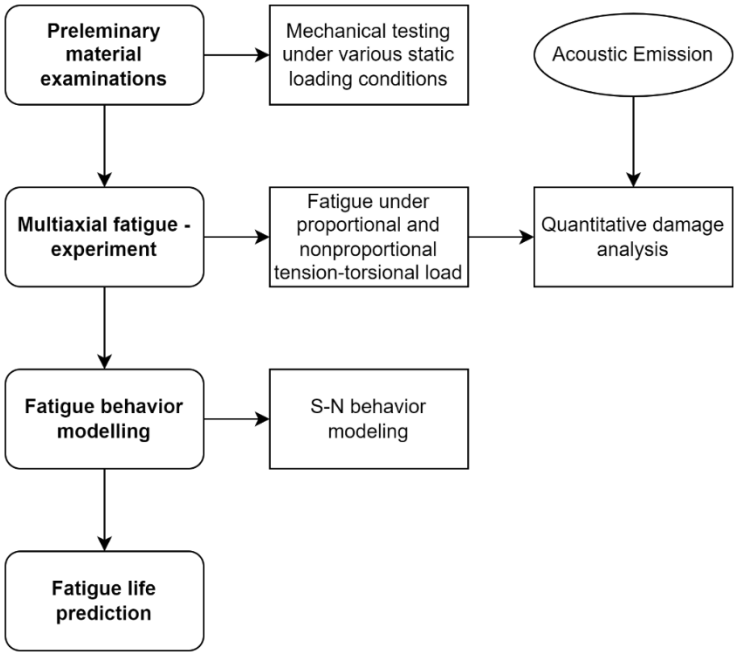

Fig. 11. Research task flow of the dissertation

2.2 Research Hypotheses

Based on the literature review, the following research hypotheses are introduced.

(1) Phase shift has a negative impact on the slope of the fatigue S-N characteristics compared to proportional loading considering the multiaxial fatigue loading conditions.

(2) The impact of the mean stress on the fatigue behavior of the S - N of CFRP is negative and can be modeled using the critical plane approach.

(3) It is possible to describe the mean stress and phase-shifting effects in polymers reinforced with continuous fibers using the damage parameter based on the principal stresses.

To answer these questions, the following research tasks were established.

1. Static tests of constituents – elastic properties
2. Calculation of the effective elastic properties for the investigated FW composite member.
3. Static tests of CFRP tubes under various loading conditions.
4. Numerical modeling of a FW thin-walled tube.
5. Fatigue testing of CFRP material under tension/compression and torsion loading conditions.
6. Fatigue data analysis (description of the S-N behavior) for multiaxial loading.
7. Modeling of multiaxial fatigue behavior based on numerical stress analysis and damage parameter.
8. Fatigue life prediction based on the approach developed for the experimental data delivered.
9. Applicability of the approach for different materials.

The methods used within the research framework are consecutive; the first phase of the dissertation includes static and fatigue experiments. It allows for the calibration of the material model, stress analysis, and the delivery of S-N curves. This is a fundamental study to proceed with fatigue modeling and life assessment considered in the second phase. The analytical part of the dissertation relates to the assessment of fatigue behavior. This part is proposed to estimate the fatigue lifetime, especially under multiaxial loading conditions. With respect to the anisotropy nature of CFRP materials, a proper description of the fatigue process in terms of mathematical methods is crucial to provide long-term safety. To date, no unambiguous mathematical description of the behavior of this type of material (CFRP manufactured by FW) under multiaxial loading conditions has been identified in the literature.

The modeling process is based on a high cycle fatigue experiment of CFRP tubular specimens under proportional (reference) and nonproportional tension, compression, and torsion loading conditions. Additional non-destructive (ND) methods, such as digital image correlation (DIC) and in situ acoustic emission, are applied to analyze the material deformation and damage accumulation during the fatigue experiment.

2.3 Research methods

Investigated parameters

The multiaxial stress state that appears in composite materials due to anisotropy and very often due to material inhomogeneity under basic and multiaxial load conditions needs to be properly characterized. In reference [14] a parameter, that is, the biaxiality ratio, has been proposed,

which describes the degree of multiaxiality of the stress state. In this investigation, the biaxiality ratios of the geometrical stresses (λ_T) along with the biaxiality of the material stressess (λ_{12}) are considered. They are assumed to be as follows.

- The biaxiality ratio (λ), is a ratio of the particular stress components as follows:

$$\lambda_T = \frac{\tau_{xy}}{\sigma_x}, \tag{10}$$

$$\lambda_{12} = \frac{\tau_{12}}{\sigma_2}, \tag{11}$$

  where τ_{12} is a shear stress, and σ_2 is a normal stress with respect to the material coordinate system (1-2), τ_{xy} is a geometric shear stress, and σ_x is a geometric normal stress. To control mechanical tests (static and fatigue), the λ_T is taken into account, for maximum stresses. However, a description of the S-N behavior requires a more precise description of the actual stress state in the material. As the material behavior in the high-cycle regime is matrix-dominated, the biaxiality λ_{12} is introduced [84]. For λ_{12} When the biaxiality ratio is applied, the stress amplitude is applied with respect to fatigue loading.

- Phase shifting (δ), between sinusoidal axial and torsional load signals causing various relationships of stress components.

Static and fatigue experimental campaign

The static campaign covers 2 phases; first, the elastic properties of constituents are determined. It is devoted to estimating the effective elastic properties of the CFRP tube using the micromechanical approach. The second phase includes the experiments carried out on the tubular specimen subjected to various static loading conditions.

Multiaxial fatigue investigations are performed for two phase shift values (δ) with constant biaxiality ratios (λ_T) for each phase shift. As a reference, a proportional loading condition is examined. Furthermore, a minimum of 9 samples per variation of each *R*-ratio (*R*= -1/0.05/0.5) are taken into account. Fig. 12 presents a flow chart of the parameters investigated within the research framework.

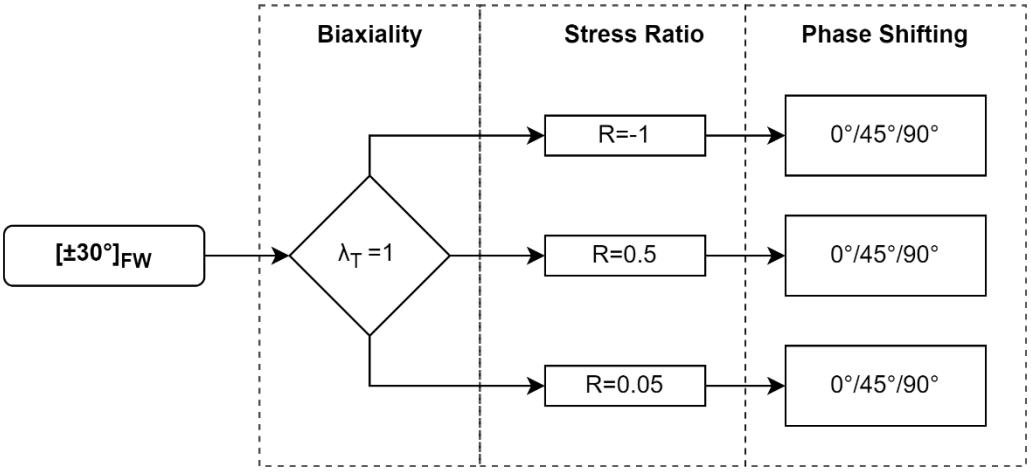

Fig. 12. Flow chart of the fatigue experiment parameters.

The experimental procedure presented is used to assess the impact of phase shifting and mean stress effect on fatigue performance of the thin-walled CFRP tubular member. In addition, multiaxial fatigue data are used to model the process and predict fatigue life.

Work plan concerning the research plan

Dissertation is divided into 4 major tasks as follows:

(1) Preliminary material examination under static load

(2) Fatigue testing

(3) Defect and damage analysis

(4) Fatigue life prediction

A detailed task description is presented below.

Preliminary material examination and mechanical properties under static loads	
Objectives	This task focuses on the characterization of the material in terms of its static mechanical properties. The determination of the maximum static force is important in estimating the stress amplitudes in the fatigue test. These tests are carried out on the thin-walled tubular specimen. Additionally, the strength of the components (resin, fibers) is examined. It is significant in the determination of effective elastic properties based on the micromechanical approach.
Multiaxial fatigue testing	
Objectives	This task aims at characterizing the fatigue behavior of selected materials under proportional and nonproportional multiaxial (tension/compression/torsion) loading conditions. The multiaxial behavior is analyzed in terms of parameters such as non-proportionality, and load ratios for geometrical stresses.
Defect and damage analysis	
Objectives	The defect and damage analysis allows for observation of the evolution of the defects during the (in situ) fatigue test and after the test. Damage accumulation is investigated with acoustic emission during fatigue testing. Additionally, in terms of static tests, digital image correlation is applied to analyze the deformation of the outer surface. Post-failure analysis is performed by optical observation and by using μCT.
Fatigue life prediction based on energy approach	
Objectives	The final task combines the results from the previous work packages. To estimate fatigue lifetime, especially under multiaxial loading conditions including load non-proportionality and mean stress effect, a comprehensive approach is needed. Within this task, the approach for fatigue life prediction is proposed.

Novelty of the research

A comprehensive review of the literature shows that there are few research groups dealing with multiaxial fatigue phenomena in composite materials. However, research within these groups is based mainly on GFRP tubes manufactured by autoclave-based processing.

The novelty of this research is placed in two aspects: nonproportional multiaxial fatigue and life assessment using the critical plane approach. The multiaxial fatigue behavior of composite materials, specifically under non-proportional loading, is not yet precisely described in the literature considering CFRP manufactured using filament winding technology. This multiaxial fatigue experiment is time-consuming and cost-consuming and requires a special apparatus (multipurpose servo hydraulic testing system). In the wake of that, not every research team can afford this, causing a limitation in data in this field.

The life assessment proposed within the investigation is based on the critical plane approach and the stress-based damage parameter. It is a useful tool to predict fatigue life in a continuous fiber-reinforced polymer under multiaxial loading conditions, including mean stress and phase shift effect. The proposed approach is based on the Fatemi – Socie parameter, which was redeveloped for this class of material, and it was never used before for continuous fiber polymers.

3 Material testing under static conditions

This chapter includes the description and results of an experimental campaign for various static load conditions. A significant aspect of this chapter is placed in delivering the material properties for stress analysis of thin – walled CFRP cylindrical members with shear nonlinear material model and progressive damage failure covered in next chapter.

3.1 Constitutes materials – micromechanical approach

For the determination of elastic constants, the micromechanical approach developed by Abolin'sh [106] has been applied. Following the requirements, a mechanical investigation of the constituents has been conducted. The following materials as constituents were used for the manufacturing of the thin – walled CFRP tube investigated in the dissertation. The continuous carbon fibers were purchased from Zoltek^{TM} company. Based on manufacturer data, the fiber has a diameter of 7.2 microns and a carbon content of 95%. The epoxy resin supplied by Huntsman is Araldite LY1564 with Aradur 3474 hardener.

Experimental investigation was carried out for fibers involving the Textechno FAVIMAT+ machine (equipped with a 1N high-resolution load cell 1μN at 200 cN range and presented in Fig. 13) for the single fiber tensile test. It allowed the tensile strength (UTS) of a single fiber as well as the Young's modulus. The Poisson ratio was not measured, which was taken from the literature. Taking into account the epoxy resin, the dog bone test specimens were molded in silicon cast. From the tensile test of epoxy resin except for the UTS and Young's modulus, the value of the Poisson ratio was determined using 2 extensometers for longitudinal and transverse strain. The results obtained for the reinforcement and matrix are provided in Table 5.

a)

b)

c)

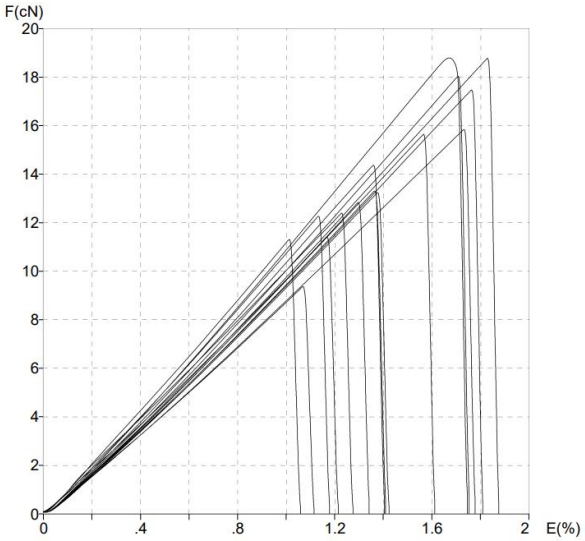

Fig. 13. a) Experimental Textechno setup for testing single fiber; b) single carbon fiber during the test; c) obtained results from the test as a function of force vs. elongation

Table 5. Mechanical properties of constituents used in manufacturing process for thin – walled CFRP tube

	ZOLTEK™ PX35 – continuous carbon fiber	**Araldite LY1564 - epoxy resin**
Material overview	**experimental data**	**experimental data**
Tensile strength	2422 MPa	49.5 MPa
Young Modulus	230 GPa	2.7 GPa
Elongation	1.42%	1.8%
Poisson	0.3 from [107]	0.4

Digital image analysis of SEM pictures allowed for determining volume fiber content. The experimental data provided was applied to the Abolin approach to predict the effective elastic properties of the thin-walled CFRP tube with a fiber content of 55%. In this method, it is assumed that the ply is transversely isotropic in the normal plane of the fibers and ignores the normal Poisson effect of the fibers under longitudinal load.

3.2 Specimen manufacturing method

The filament winding method was applied to manufacture the thin-walled tubular specimen subjected to various loads under static and fatigue loading conditions. The technology used provided a CFRP tube with a winding pattern of 1/1 (see Appendix 1). The specimen along with the fiber orientation is shown in Fig. 14. The presented cordinate systems refer to the material cordinate system (123).

To manufacture tubes using this technology, a chrome-coated steel mandrel with a diameter of 20 mm was used. The surface preparation of the mandrels was crucial for facilitating the demolding process. For this purpose, the wax was placed and then polished; this procedure was repeated before each winding process. When the appropriate fiber placement process on the mandrel was completed, a special shrink tape was applied to cover the still wet surface of the tube to remove the resin overflow and receive sufficient seamlessness of the outer surface. The obtained structure is cured at ambient temperature and rotated continuously for several hours. The post-curing process is suggested by the resin producer following the temperature steps of 1 h at 80° C and 4 h at 120° C. It is carried out after being dumped from the steel mandrel and cut into the specimen.

a)

b)

Fig. 14. a) Thin-walled specimen manufactured using FW – general view, b) specimen fiber orientation where 1 – fiber direction, 2 – direction perpendicular to fiber

According to Fig. 15, some discrepancy is noticeable. The measured angle is in a small error margin with respect to the reference angle of 30°, which may be caused by technology or measurement inaccuracy.

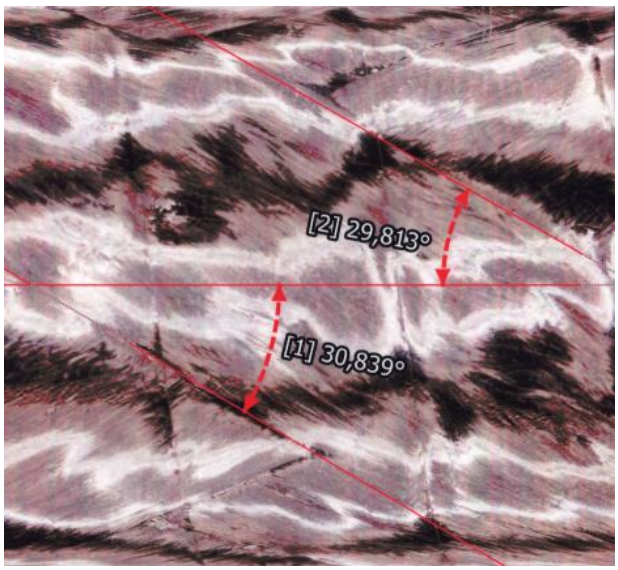

Fig. 15. Fiber orientation verification using the optical method. The fiber orientation is in the range of 30°, some variance may occur due to the inaccurate measurement or technology discrepancy

Using the 3D scanning optical method, measurement of the geometry and fiber orientation was carried out. A discrepancy with a standard deviation of 0.45° was defined for fiber orientation with respect to the reference angle of 30°. The measurement of the outer diameter was conducted by measuring the length of the sample, the mass and the density of the material (0.00152 g/mm^3). This method provides a mean diameter value of 21.894 mm with a standard deviation of 0.091 mm.

The manufactured samples were indicated using the following code: the load ratio/biaxiality/phase shift/number of samples, for example, sample no -1/1/0/13, refers to the load ratio (R= -1), biaxiality (λ_T =1), phase shift (0°) and the number of samples in this set is equal to 13.

3.3 Static testing of thin-walled tubular members

Taking into account the research framework, the first step is to characterize the material under static loading conditions. The experimental campaign requires proper preparation of the specimen in terms of the gripping system in the hydraulic testing machine. Composite materials are sensitive to compressive load, which causes the matrix to crack, accelerating the initiation of delamination. This aspect should be taken into account during the design of the gripping system to minimize impact. In terms of the tubular specimen, the two additional parts needed to be designed, i.e. solid part, which fits the inside diameter of the tube, another part covers the external surface in the form of bearing shell as it is presented in Fig. 16.

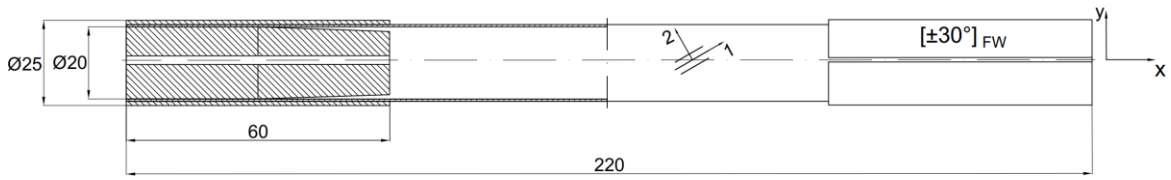

Fig. 16. Dimensions of the test specimen used for experimental multiaxial fatigue characterization

Various load cases are applied within this framework to assess the static mechanical behavior of a thin-walled CFRP tubular specimen. Additionally, strain measurement during mechanical experiment is carried out using two independent techniques, i.e. strain gauges and digital image correlation (DIC). To analyze sample deformation by image correlation, the stochastic pattern needs to be provided; in general, the black background was covered with white particles to analyze external surface deformation and describe strains acting on this surface. The MTS 809 axial/torsional hydraulic testing system with 50 kN load cell was used to apply tensile, compressive and torsional loads. The following experiments were carried out with a constant load ratio of 2 Nm/sec for torsion, 200 N/sec for tension and 100 N/sec for compression test. The loading conditions are presented in Fig. 17. Rosette strain gages adhered to the external surface following the principal directions of the lamina (1st, fiber direction, 2nd – perpendicular to the fibers). Additionally, a strain gauge was used in the angle of 45°, respectively, to direction 1 - clockwise direction.

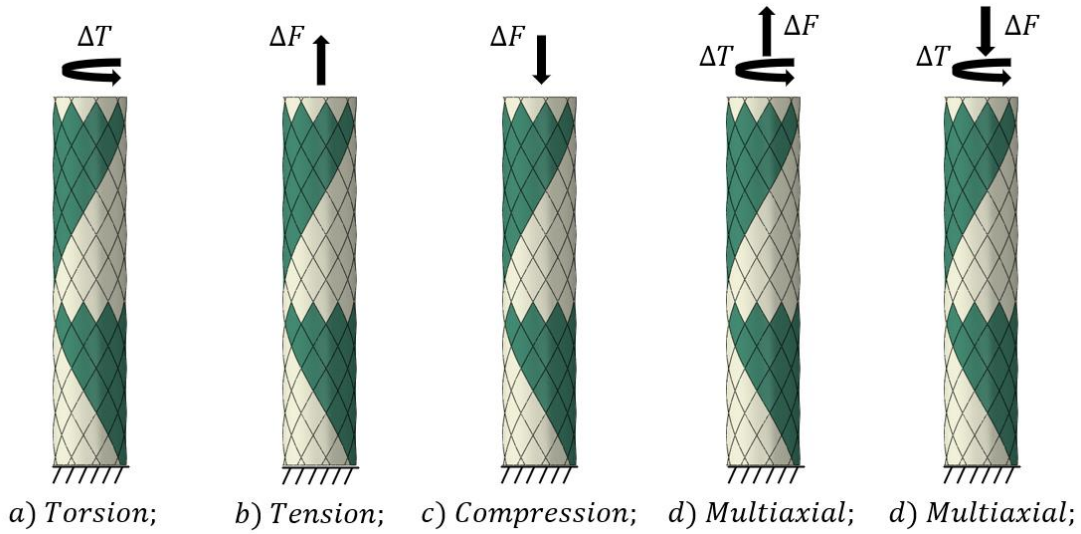

Fig. 17. The static loading conditions; a) torsion, b) tension, c) compression, d) multiaxial (tension/compression and torsion)

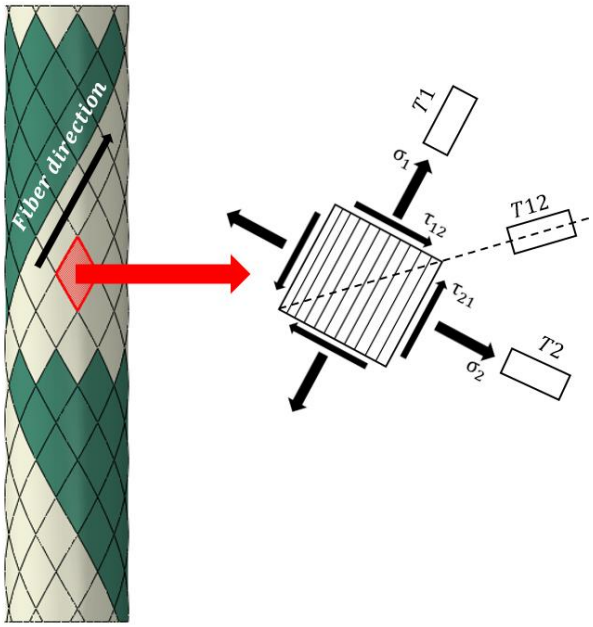

Fig. 18. Position and orientation of the strain rosette during mechanical tests under static loading condition

Considering the axial load (tension or compression) – torsional load (Fig. 17d), the force control mode was involved to provide a constant biaxiality ratio (λ_T) and load proportionality $\delta = 0°$. The experiment covers the biaxiality ratio (λ_T) equal 1. In the case of these experiments, the value of the biaxiality ratio for geometrical stresses is applied.

The entire experimental setup used in this investigation is presented in Fig. 19. Two cameras were used as part of the digital image correlation (Dantec dynamic Q300).

Fig. 19. Experimental setup used in the presented research equipped with a camera I used for sample monitoring, camera II as part of the DIC system used, and strain gauges. Graphic by the author, first published in [11] under https://creativecommons.org/licenses/by/4.0/

The average experimental curves are shown in Fig. 20. The results are divided into two sections, first, the axial loads, i.e., tensile/compression in Fig. 20a and torsional load in Fig. 20b. For each static test, 3 specimens were used, and only average curves were plotted.

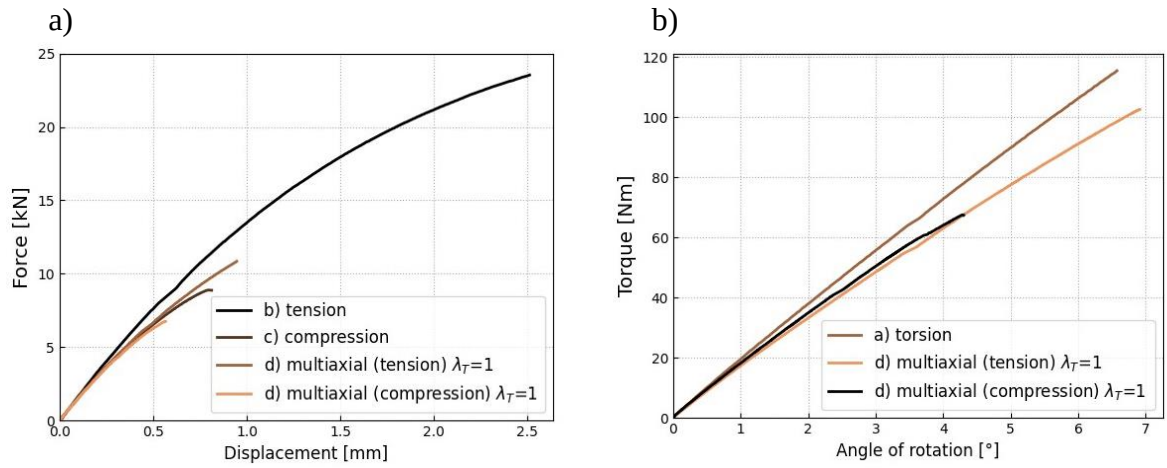

Fig. 20. a) Average curves of mechanical tests for tensile and compression; and b) for torsional; both graphs include results for multiaxial load.

Statistical analysis performed on mechanical results is presented in Table 6. There are three statistical parameters calculated as following mean value, standard deviation (SD), and coefficient of variation (COV). The COV gives information on data dispersion around the mean value; in case of presented data, the largest variability is observed for the torsion test, whereas other values are below 10%. In general, in small period around the mean value can be assumed, suggesting high repeatability of results.

Table 6. Statistical analysis of the maximum values of force and torque obtained from the static mechanical experiment

	Mean value	**Standard deviation**	**Coefficient of variation**
Torsion	114.3 Nm	21.4 Nm	18.7%
Tension	23.5 kN	1.9 kN	8.1%
Compression	- 8.3 kN	0.5 kN	6.0%
Multiaxial (tension-torsion)	108.0 Nm	9.8 Nm	9.1%
	10.8 kN	1.0 kN	9.2%
Multiaxial (compression – torsion)	-67.4 Nm	5.6 Nm	8.3%
	-6.7 kN	0.6 kN	8.9%

The following results were obtained; the uniaxial tensile test gives a maximum force value of 23.5 kN with a standard deviation of 1.9 kN. The tensile curve exhibits nonlinear behavior up to the final failure, which suggests the nonlinearity of one of the stress tensor components. This aspect might be explained by the large influence of friction-induced shear in the interweaving areas (caused by FW technology). Furthermore, the tensile capacity of the FW member is significant until the continuity of the fibers is damaged, even if there is no adhesion between the matrix and the fiber.

When considering the compression capacity of the thin-walled tubular member, there is a large reduction with respect to the tensile capacity. The mean value of the maximum compressive force is 8.3 kN with a standard deviation of 0.5 kN. This fact shows the sensitivity of the material to compressive load. Moreover, this loading case strongly depends on microstructure quality.

The applied torsional load resulted in a torque capacity of 114.3 Nm with a relatively large standard deviation of 21.4 Nm. During the experiment, the differences in maximum torque were noticeable. It can be a result of the gripping system, which cannot carry the higher value of torque acting on the sample in a sufficient way. Moreover, sample imperfection can also affect the maximum torque value.

When multiaxial loading conditions are considered, the sample subjected to compression and torsion experienced the lowest load capacity with a maximum compressive force of 6.7 kN (SD 0.6 kN) and a maximum torque of 67.4 Nm (SD 5.6 Nm). On the other hand, the sample subjected to the tension-torsion load exhibits a maximum tensile load of 10.8 kN (SD 1.0 kN) and a maximum torque of 108 Nm (SD 9.8 Nm).

The experimental tests confirmed the material sensitivity to the compression load by showing the lowest load capacity for both loading cases, i.e. uniaxial and multiaxial. Moreover, the mechanical tests exhibit the nonlinear material behavior for axial loads and linear for torsional loads.

Strain measurement was performed using the strain rosette and digital image correlation. The principal strains obtained from the strain gauges and the DIC are presented in Fig. 21. Due to the strain inhomogeneity (due to the specimen architecture provided by the FW technology) a more reliable method is the digital image correlation as it takes into account a larger specimen area. However, to confirm its correctness, the strains measured in particular places by the strain gauges are correlated. These data are also used for the verification of numerical models. On the basis of the presented results, the non-elastic behavior of the investigated thin-walled tubular member is confirmed. This behavior is described in the literature and is known as the shear softening effect caused by the high influence of the shear stress component [30], [31], [32], [33], [108]. An important conclusion can be drawn that commonly used failure criteria (i.e. Hashin, Tsai-Hill, or Chamis) cannot be applied to this research case as they are based on the linear elastic material behavior.

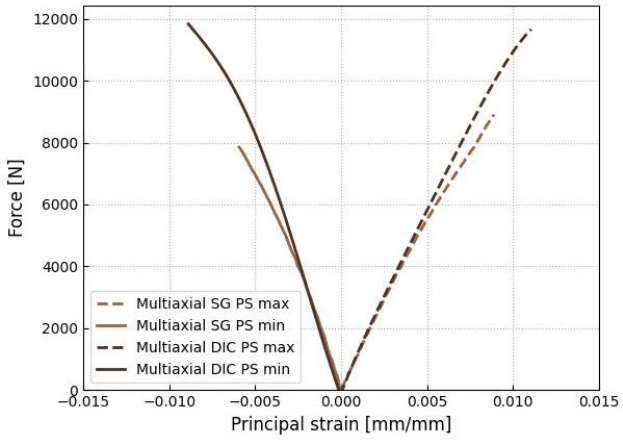

Fig. 21. Maximum principal stresses for multiaxial loading (λ_T=1) obtained from strain gauges compared to those obtained from digital image correlation. Data and graphs by author, first published in [11] under https://creativecommons.org/licenses/by/4.0/

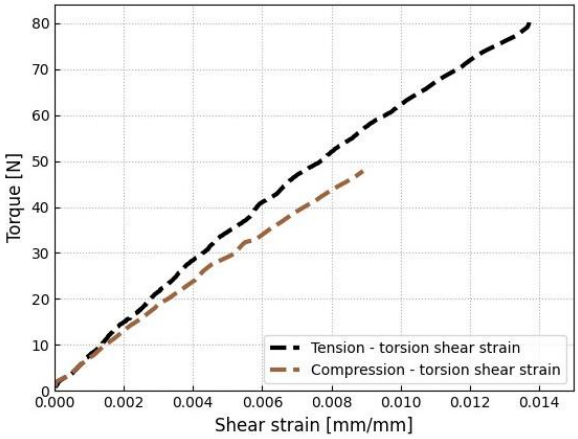

Fig. 22. Shear strains measured by strain rosette for multiaxial loads

The shear strains relationship with respect to torque for measurement point is presented in Fig. 22. Some nonlinearity is observed; however, locally this effect might be hidden for some areas due to strain inhomogeneity and the measurement point with respect to thickness of the specimen. It should be noted that each region might experience different varieties from the linearity between applied load and deformation.

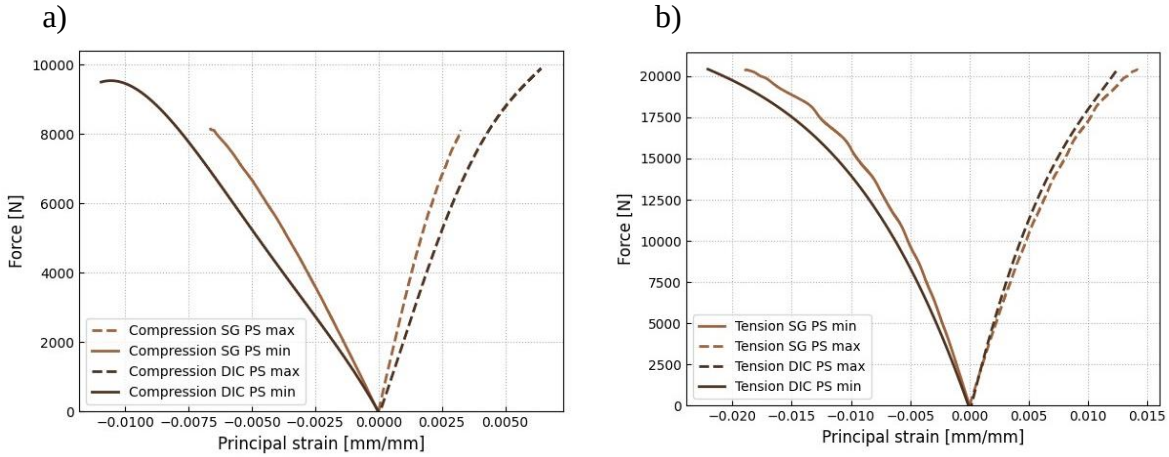

Fig. 23. a) Principal stresses for compression obtained from strain gauges (SG) compared with those obtained from digital image correlation (DIC), b) maximum principal stresses for the tension obtained from the strain gauges compared with those obtained from digital image correlation. Data and graphs by author, first published in [11] under https://creativecommons.org/licenses/by/4.0/sscc

It should be noted that due to the relatively large deformation of the specimen, it was not possible to measure strain at failure. The strain gauges deboned after a certain load value. Hence, the comparison of the results and the calculation of the error for the force level of 5 kN are provided in Table 7.

Table 7. Comparison of results along with the relative error calculated at force 5 kN used from [11]

Loading case	DIC	Strain gauge	Relative error at force 5 kN [%]
Max PS – tension [mm/mm]	0.012	0.013	2
Min PS – tension [mm/mm]	-0.22	-0.18	13
Max PS – multiaxial (λ_T=1) [mm/mm]	0.010	0.008	2
Min PS – multiaxial (λ_T=1) [mm/mm]	-0.008	-0.005	8
Max PS – compression [mm/mm]	0.005	0.003	26
Min PS – compression [mm/mm]	-0.010	-0.006	28

PS – principal strain

As presented in Table 6, the relative error shows the discrepancy in the strain results. The highest error appears for the compression test, if the digital image correlation is considered, and there are some factors that influence the accuracy. It is likely that the stochastic pattern was not accurately introduced into the sample. Furthermore, the area taken into account for strain calculation by the DIC is slightly shifted with respect to the strain gauges.

3.4 Summary

The results of the comprehensive static experimental campaign are presented in Chapter 3. An experimental investigation brought the following conclusion:

- The designed gripping system was able to transfer the applied loading conditions within the entire load range. The observed failure in the gauge length of the specimen does not show a negative impact of clamping.
- The applied DIC and strain gauge measurement allowed the strains to be defined at the measurement point for the SG and strain distribution using the DIC method. It confirms the non-linearity of the strains. The shear strains do not exhibit significant discrepancies from linearity; however, it could be expected that a more precise measurement point for shear stress would be in the middle section of the thickness, i.e. between two layers. It would provide a more valuable correlation, but it can be assumed that the nonlinearity is likely to increase at the middle section due to load transmission of two composite layers with opposite fiber orientation. The experimental campaign carried out proved the reasonability of applying the nonlinear material behavior.
- The experiments gave fundamental data for numerical modeling of static performance under mechanical load. A properly defined material model is crucial for effective stress analysis.

4 Numerical modeling

The numerical modeling of the thin-walled tubular specimen is presented in Chapter 4. The finite element method is used to analyze the mechanical performance of CFRP material under various loading conditions. In this chapter, the steps that cover the formulation of discrete models with the implementation of the material model are given. The objective of this chapter is to provide a reliable tool for stress analysis that is used to model fatigue performance. Moreover, the buckling analysis presented in the chapter allowed to assess safety margin for fatigue load under compressive load.

4.1 Modeling of nonlinear shear behavior

Description of the behavior of the mechanical material requires the determination of the elastic properties. Based on the elastic properties of the constituents and the fiber volume content (55%), the micromechanical approach proposed by Abolin'sh [106] was used to provide the elastic properties of CFRP material. The calculated elastic properties used for the numerical analysis are presented in Table 8. To reflect the mechanical stress-strain relation, the non-linear shear model proposed by Chang [29] was used and calibrated according to the mechanical experiments carried out.

Table 8. Elastic properties of the CFRP compound with 55% fiber volume calculated on the basis of Abolin'sh micromechanical approach [11]

	E_1 [MPa]	**E_2 [MPa]**	**ν_{12} [-]**	**G_{12} [MPa]**
CFRP	128 100	5 378	0.345	3 132

The applied material model with progressive damage requires data of the strength parameters and determination of the parameter that describes the non-linearity of the material (α). These values were approximated using FEM on the basis of the experimental tests conducted. The available literature [29], [32] allowed to set the range of α parameter; however, the final value was delivered by FEA.

Table 9. Strength parameters used in the non-linear shear model [11]

Transverse tensile strength (Y_t)	**Longitudinal compressive strength (X_c)**	**Transverse compressive strength (Y_c)**	**Ply shear strength (S_c)**
160 MPa	1 500 MPa	160 MPa	50 MPa

The applied approach combines the material model, which includes the shear softening effect and progressive damage. The constitutive relation takes into account the shear impact by introducing the second term in Eq. (12), which combines the nonlinearity parameter (α) and shear stress (τ_{xy}). Furthermore, progressive damage is considered by the implementation of failure criteria for particular failure modes. The approach is implemented into Abaqus FE software in the form of the user-defined Fortran code.

The applied stress-strain relation is described in Eq. (12).

$$\gamma_{12} = G_{12}^{-1}\tau_{12} + \alpha\tau_{12}^{3} \tag{12}$$

Where:

G_{12} is the (initial) ply shear modulus and non-linearity is characterized by the factor α (2.44×10^{-6} MPa $^{-3}$) [11]

The executed model sets the elastic constants depending on the three field variables implemented in the Abaqus by using user defined field subroutine (USDFLD). The following variables are executed:

Field variable 1 (FV1) – binary variable indicates matrix tensile/compression failure according to Eqs. (13 – 14).

Field variable 2 (FV2) – binary variable indicating fiber matrix shear failure according to Eq. (15).

Field variable 3 (FV3) – Material shear damage indicated by the value range between [0, 1] described in Eq. (17)

The filed variables are defined on the basis of failure mechanisms that occur in the investigated CFRP thin-walled member. The equations used to describe the particular failure mechanisms are presented below.

Matrix tensile cracking

$$e_m^2 = \left(\frac{\sigma_2}{Y_t}\right)^2 + \frac{\frac{2\tau_{12}^2}{G_{12}} + 3\alpha\tau_{12}^4}{\frac{2s_c^2}{\tau_{12}} + 3\alpha S_c^4} \tag{13}$$

where
S_c – shear strength [MPa]

Matrix compressive failure

$$e_m^2 = \left(\frac{\sigma_2}{Y_c}\right)^2 + \frac{\frac{2\tau_{12}^2}{G_{12}} + 3\alpha\tau_{12}^4}{\frac{2s_c^2}{\tau_{12}} + 3\alpha S_c^4} \tag{14}$$

$$\begin{cases} e_m^2 \geq 1 \rightarrow FV1 = 1 \\ e_m^2 < 1 \rightarrow FV1 = 0 \end{cases}$$

Fiber-matrix shearing

$$e_{fs}^2 = \left(\frac{\sigma_1}{X_c}\right)^2 + \frac{\frac{2\tau_{12}^2}{G_{12}} + 3\alpha\tau_{12}^4}{\frac{2s_c^2}{\tau_{12}} + 3\alpha S_c^4} \tag{15}$$

$$\begin{cases} e_{fs}^2 \geq 1 \rightarrow FV2 = 1 \\ e_{fs}^2 < 1 \rightarrow FV2 = 0 \end{cases}$$

Fiber buckling – independent of the other stress components

$$e_b = -\frac{\sigma_1}{X_c} \tag{16}$$

An important aspect of failure in terms of the investigated thin-walled member is buckling phenomena. This phenomenon might be considered on a global or local material scale. It is a catastrophic failure (global scale) that excluded material to withstand any load. On the other hand, on a local scale, it significantly decreased material load capacity. In an applied model, shear stiffness degradation due to fiber matrix failure can subsequently cause fiber buckling, and in this case it is assumed that the material cannot withstand any load.

Damage parameter

$$d = \frac{3\alpha G_{12}\left(\tau_{12}^{(i)}\right)^2 - 2\alpha\left(\tau_{12}^{(i)}\right)^3/\gamma_{12}^{(i)}}{1 + 3\alpha G_{12}\left(\tau_{12}^{(i)}\right)^2} \tag{17}$$

The progressive damage in its final form is described by the relation presented in Eq. (14).

$$\tau_{12}^{(i+1)} = (1-d)G_{12}\gamma_{12}^{(i+1)} \tag{18}$$

Table 10 presents the dependence of the elastic properties on the field variables (FV1 – FV3). The FV index (0 or 1) is governed by the formulas presented above (Eqs. 13 – 16). Elastic properties are equal to 0 when the appropriate FV exceeds 1 exhibiting a particular material state.

Table 10. Matrix of the material model presenting the damage states and elastic properties taken into account for various failure mechanisms

Material State	**Elastic properties**				**FV1**	**FV2**	**FV3**
No failure	E_x	E_y	υ_{xy}	G_{xy}	0	0	0
Matrix failure	E_x	0	0	G_{xy}	1	0	0
Fiber/matrix shear	E_x	E_y	0	0	0	1	0
Shear damage	E_x	E_y	υ_{xy}	0	0	0	1
Matrix failure and fiber/matrix shear	E_x	0	0	0	1	1	0
Matrix failure and shear damage	E_x	0	0	0	1	0	1
Fiber/matrix shear and shear damage	E_x	E_y	0	0	0	1	1
All failure modes	E_x	0	0	0	1	1	1

Boundary conditions

The interweaving areas are indispensable sections of the cylindrical members manufactured by FW technology. Taking into account this manufacturing method, the external layer can have fibers that run in $\alpha/-\alpha$ directions. This aspect significantly influences mechanical behavior, especially in terms of damage initiation and propagation, and should be considered. Research by the author [11] shows that simplification in excluding the winding pattern can lead to a result discrepancy.

The formulated geometric model is based on the sample geometry (Fig. 16) and the layer architecture. Introducing the precise geometry model, which includes the interweaving areas, is not an easy task and cannot be easily done manually. By incorporating computer programming, the task can be solved. The Simulia Abaqus environment used in the research framework allowed for the implementation of scripts based on the Python programming language. A special script presented in [109] allowed to precisely reflect the architecture of the sample layer that includes interweaving areas. The effect of this approach can be found in Fig. 24, the color regions shown by the assigned material sections, which reflect the different fiber orientations. The fiber orientation is measured with respect to the symmetry axis of the specimen and is positive when it is counterclockwise.

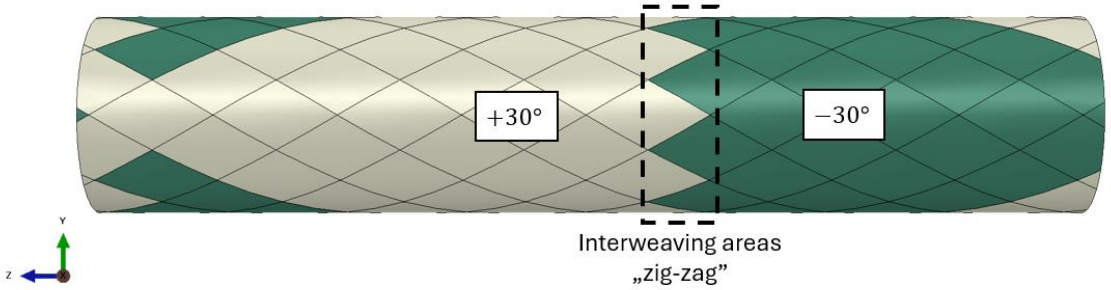

Fig. 24. FE modeling approaches – concept of including zigzag areas based on the numerical script from [109]

For the created geometry, the following boundary conditions according to Fig. 28b were applied to reflect particular loading conditions. Furthermore, the discrete model consisting of the mesh with 18 855 S4R elements is presented in Fig. 25a.

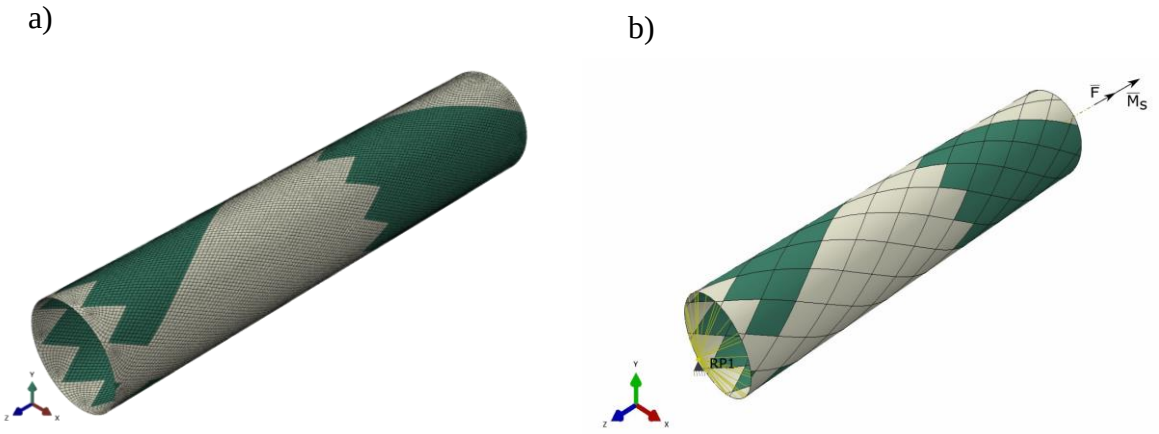

Fig. 25. a) Discrete model – material sections (various fiber orientations – different colors). b) boundary conditions applied to the FE model. Graphic by the author, first published in [11] under https://creativecommons.org/licenses/by/4.0/

To conclude the applied approach, the workflow chart is introduced and presented in Fig. 29. The methods described within this section, including geometry, material assignment, and boundary conditions, are implemented using a Python script, which generates geometry with diamond partitions and assigns materials based on the interweaving created during the FW process. Furthermore, the material model redefines the damage state and elastic properties after each iteration. This redefinition involves introducing user-defined fields through the USDFLD Fortran subroutine and assigning material properties based on the calculated values of field variables [11].

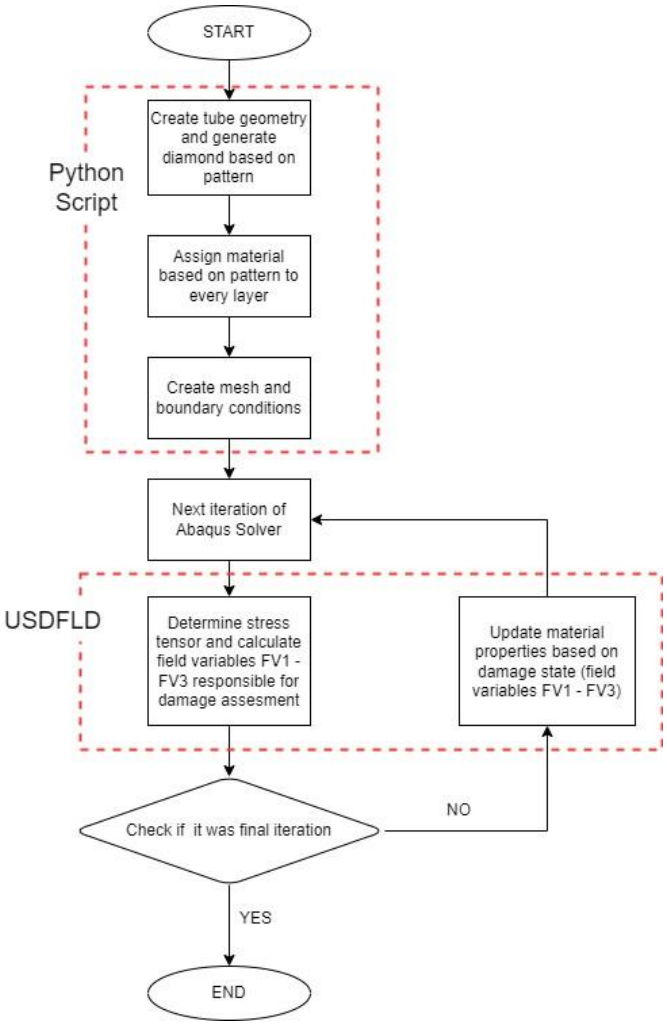

Fig. 26. Workflow of numerical simulations - Model is generated with Python script due to the complexity of geometry and material distribution. During the solution of the model, the USDFLD subroutine written in Fortran is used to update the material properties due to the accumulation of progressive damage. Graphic by the author, first published in [11] under https://creativecommons.org/licenses/by/4.0/

4.2 Numerical model calibration and validation

The applied model has been calibrated on the basis of the experimental data for the multiaxial loading case. Experimental results provide a reliable source of mechanical performance under static conditions; allowed nonlinear material parameter α and estimating strength parameters describing the progressive failure of the investigation thin-walled tubular member. The presented results are divided into two parts, i.e. axial loads are plotted separately, rather than rotational. The results of the fitting are presented in Fig. 27, in the form of the geometric normal and shear stresses. The maximum tensile strength (for multiaxial load) is underestimated. It might suggest that the strength parameters are not precisely fitted. However, since the strength parameters in this complex case are coupled together, a compromise solution needs to be applied. On the other hand, a good agreement was obtained in torsional conditions. Since fatigue analysis is performed in the static regime below the static maximum load values, the stiffness in this region is crucial, and it is achieved as presented in Fig. 27.

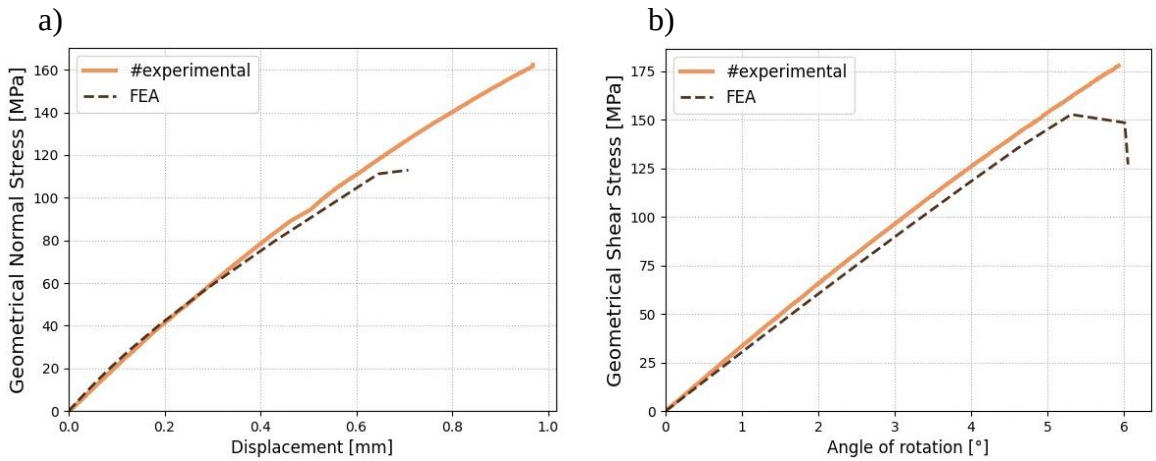

Fig. 27. Fitting of the model to the experimental data from multiaxial static loading, a) results for axial load, and b) results for torsional load

The calibrated model was examined by predicting the mechanical performance of the thin-walled CFRP cylindrical member under pure torsional and uniaxial tension loading. The results obtained are presented in Fig. 28 and compared with the experimental data. The numerical prediction shows some discrepancy in stiffness and maximum force. Considering the maximum load values, a more sophisticated optimization process would be required to precisely fit the strength parameters, as within the scope of the dissertation the fatigue phenomenon in high cycle fatigue (HCF) is evaluated, and this course was not researched deeper. In terms of stiffness, there are two aspects that should be considered. First, the elastic properties, which were estimated on the basis of micromechanical approach, this method gives the effective elastic properties that cannot be precise. However, the microstructure quality is more important, which also significantly influences the stiffness of the investigated CFRP thin-walled tubes. The microstructural imperfections due to technology are not considered, which does not allow to consider its impact on stiffness reduction. On the basis of the results, the prediction shows good agreement considering the load level applied in fatigue experiments.

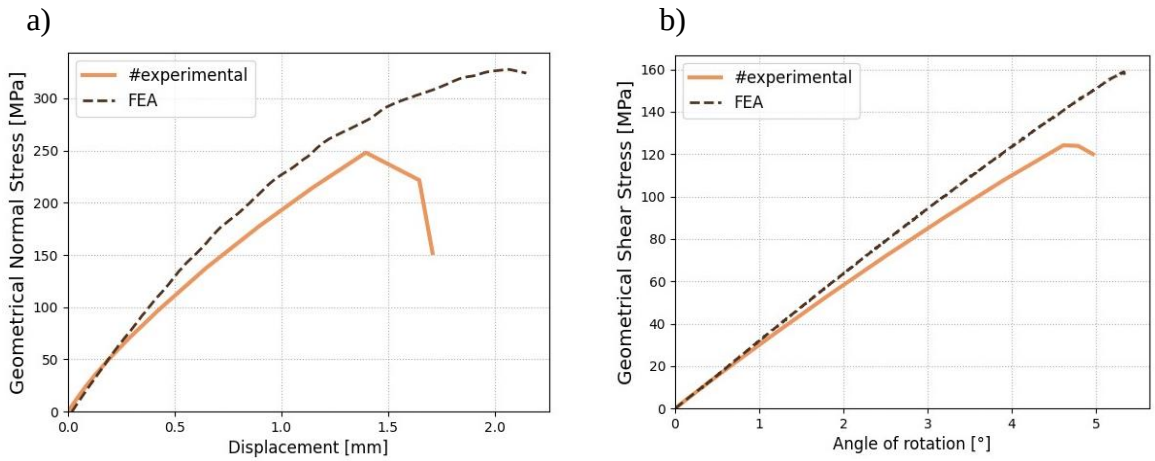

Fig. 28. Model evaluation a) comparison of the results of tensile load for FEA (based on the calibrated nonlinear shear model) and experiment. b) Torsional load results in comparison for FEA (based on the calibrated nonlinear shear model) and experiment. Results of the authors, first published in [11]

Taking into account the force level of 8 kN and the torsional load at 60 Nm, the relative errors were calculated. They were calculated with respect to the experimental values and are presented in Table 11.

Table 11. Comparison of experimental results with FEA. Data obtained by the author published in [11]

	Displacement at 8 kN – experimental value	**Displacement at 8 kN- FEA value**	**Relative error with respect to the experimental value at 8 kN**
Multiaxial (λ_T=1)	0.54 mm	0.54 mm	0%
Tension	0.49 mm	0.52 mm	5.7%
	Angle of rotation at 60 Nm – experimental value	**Angle of rotation at 60 Nm- FEA value**	**Relative error with respect to the experimental value at 60 Nm**
Multiaxial (λ_T=1)	3.03°	2.99°	1.3%
Torsional	2.97°	2.93°	1.4%

Combining the results for DIC, SG and FEA, the benchmark in form of the graph (load vs. strain) is presented in Fig. 29. The minimum principal strain value is better predicted by the FEA model; in terms of DIC there are discrepancies; however, the general nature of the relation is similar. On the other hand, the maximum value is more accurate for DIC in comparison to the SG reference curve. These differences in strain values from DIC result in the measurement of the strain at a different point from where the strain rosette was attached. In FEA the error can occur due to underestimation of elastic properties or considering incorrect integration point. Due to the inhomogeneous strain distribution, considering the same areas for each method is significant to get results agreement assuming that the material model is precisely calibrated. Due to the large deformation of the sample surface, the strain gauges deboned, and the value obtained from the strain gauges was inadequately lower and did not show the local extremal strain at failure.

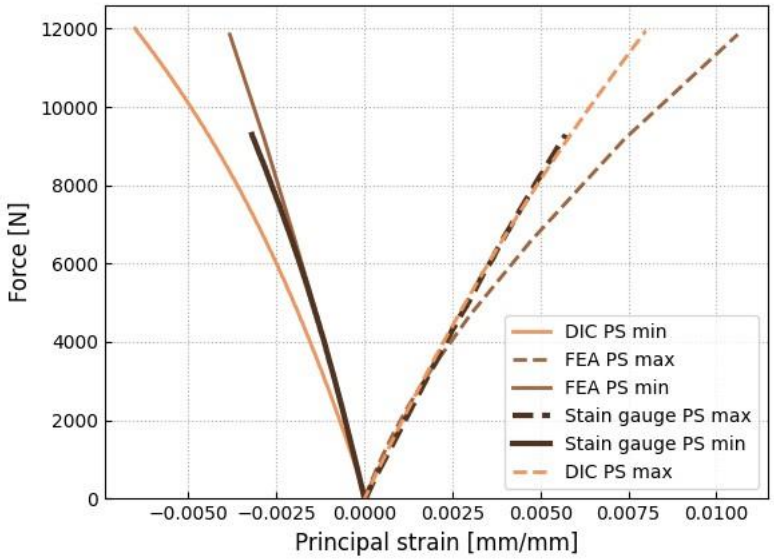

Fig. 29. Comparison of principal strains (PS) for multiaxial. The graph compares the values received from strain gauges, FEA and DIC

The deformation nature of the tubular specimen was captured by the DIC method and compared to the deformation obtained from FEA. The strain and displacement fields are placed along each other to compare them. As Fig. 30 - 31, there is good agreement between general material deformation behavior along the reference optical (DIC) and the numerical method (FEA). The strain and displacement fields presented by DIC show the deformation nature of the external surface of the CFRP tube. The FEA with WP accurately predicts this deformation pattern.

For the results obtained from multiaxial loading conditions, the relative error with respect to the strain value from the strain rosette was calculated and presented in Table 12. The calculations were made for strains obtained from FEA, DIC in comparison to the principal strains of maximum (0.0057 mm/mm) and minimum (-0.0032 mm/mm) principal strains obtained from the strain gauge rosette. As it is shown, the greater relative error provides FEA for maximum PS, on the other hand, DIC gives larger error for minimum PS.

Table 12. Comparison of the relative error values for FEA and DIC with respect to the maximum and minimum strain obtained from the strain gauges. Data obtained by the author published in [11]

	FEA	**DIC**
Relative error for maximum principal strain (0.0057)	29.8%	5.3%
Relative error for minimum principal strain (-0.0032)	12.5%	34.4%

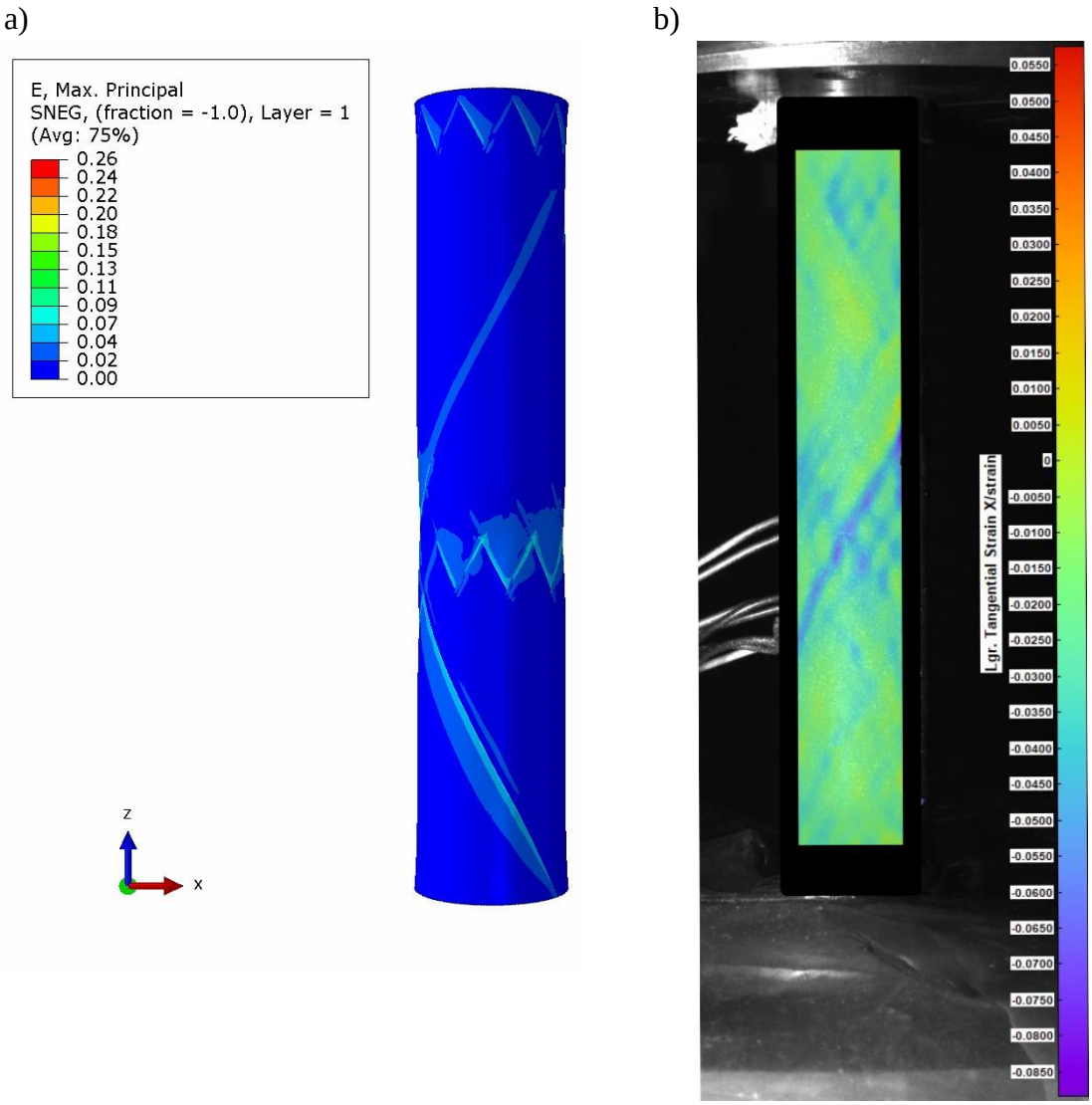

Fig. 30. Strain field comparison between a) FEA and b) DIC for multiaxial loading conditions. Graphic by the author, first published in [11] under https://creativecommons.org/licenses/by/4.0/

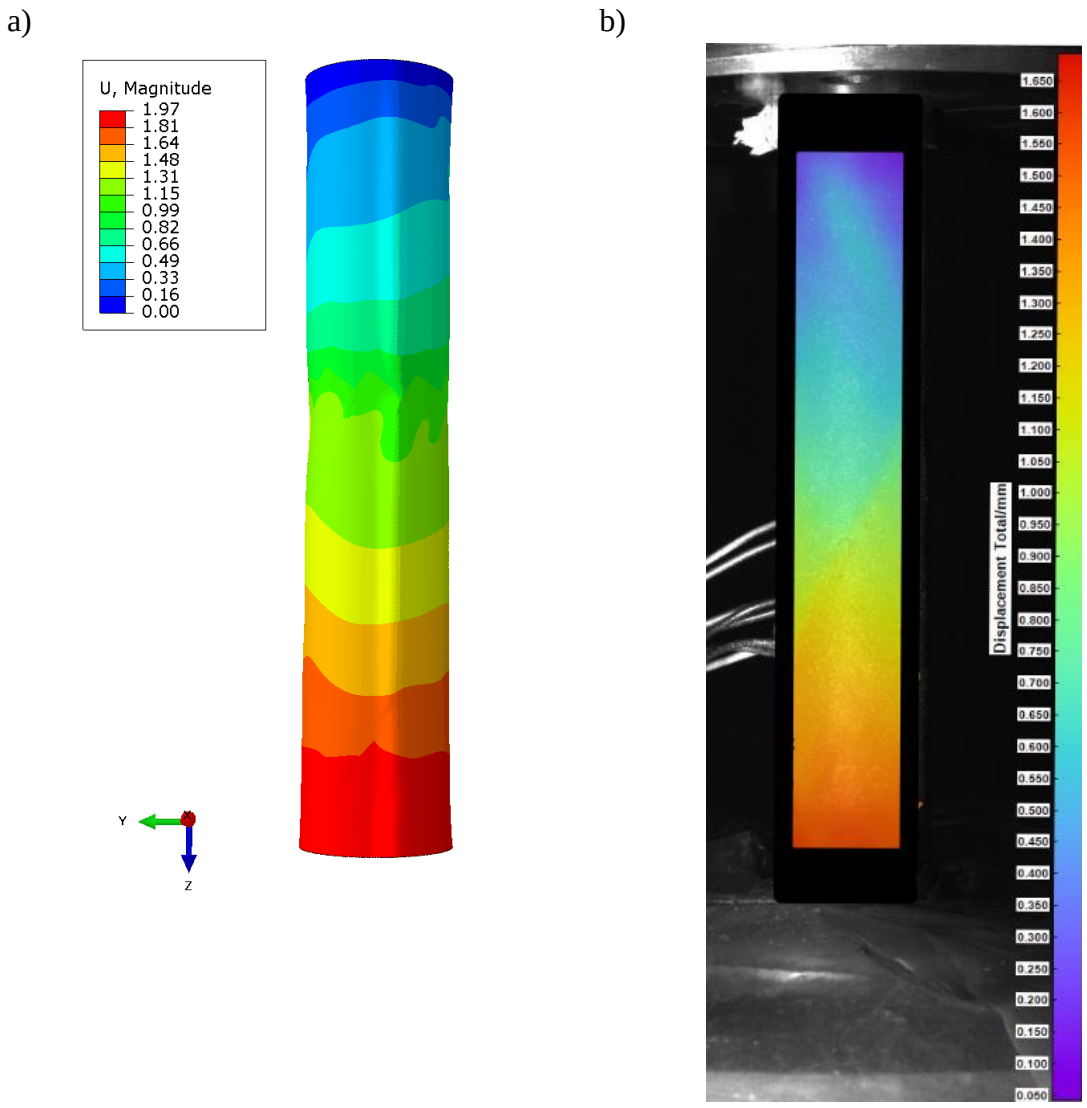

Fig. 31. Comparison of the total displacement field between a) FEA and b) DIC for multiaxial loading conditions. Graphic by the author, first published in [11] under https://creativecommons.org/licenses/by/4.0/

The results presented show the importance of modeling the zig-zag area and their effect on the local strain concentration and distribution. The thin-walled CFRP specimen investigated with a mosaic pattern of 1/1 consists of only one FW layer, which explains the significant impact of the zigzag area on the mechanical performance.

Taking into account the remaining load conditions, various sensitivitys to the local strain concentration in the zigzag area were noticed. The DIC method in terms of tension and compression was not able to capture local stress concentration in the zigzag area. However, the concentration along the fiber border was observed. In the case of torsional load, the zigzag area was detrimental and defined the failure area, in contrast to the delamination observed in other load cases.

The static experimental campaign conducted supported by optical and electrical strain gauge methods allowed the analysis of the strain field, calibration, and verification of the applied material model with shear nonlinearity. The DIC method allowed one to compare the deformation nature of the specimen with this obtained from the numerical method. The main

concentration of strain was placed in the zigzag area and, in case of tension and compression, along the fiber tow at the borders, which was confirmed by FEA and DIC. This static campaign draws an important conclusion to consider in further analysis. The interweaving area is crucial and has a significant impact on mechanical performance.

Damage results from numerical analysis

The numerical analysis was carried out with progressive damage; the general damage nature based on the 3 field variables implemented is presented in Fig. 32 and Fig. 33. Taking into account the tension – torsion load in Fig. 32, each damage variable exceeded 1, which indicates that the failure initiated and that a reduction in the elastic properties is needed. As it can be confirmed, the damage initiate at zig – zag area as well as along the fibers at the border that is defined by alternating fiber change.

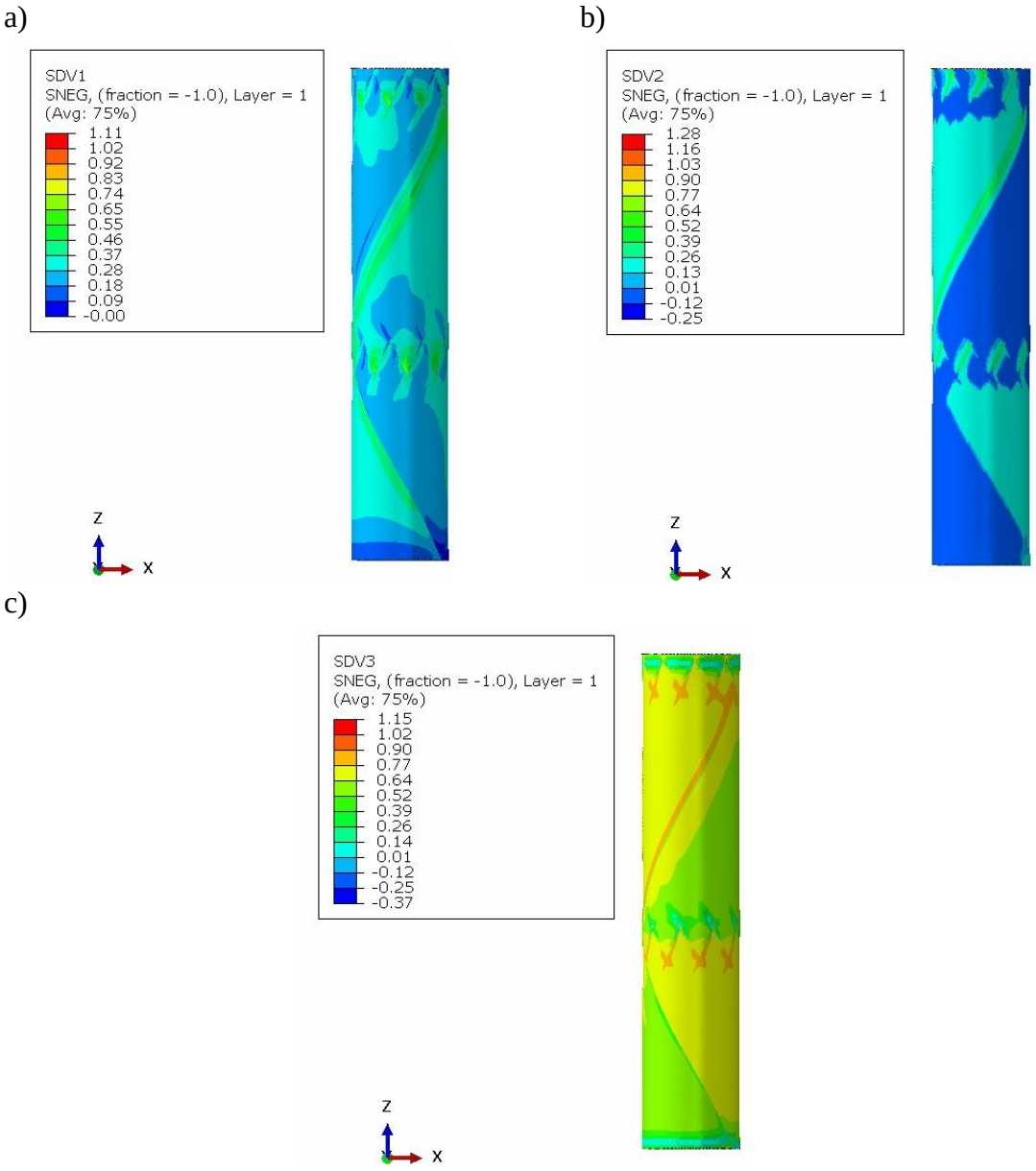

Fig. 32. Damage pattern for a) matrix tensile/compression failure, b) fiber matrix shear failure, and c) material shear damage for multiaxial load of 8.3 kN

The compression - torsion analysis was carried out up to maximum compression force of 2.6 kN, and the results are presented in Fig. 33. For this force value, the indicators did not exceed 1; however, for material shear damage the index reached 0.7, which suggests that damage initiation may occur soon.

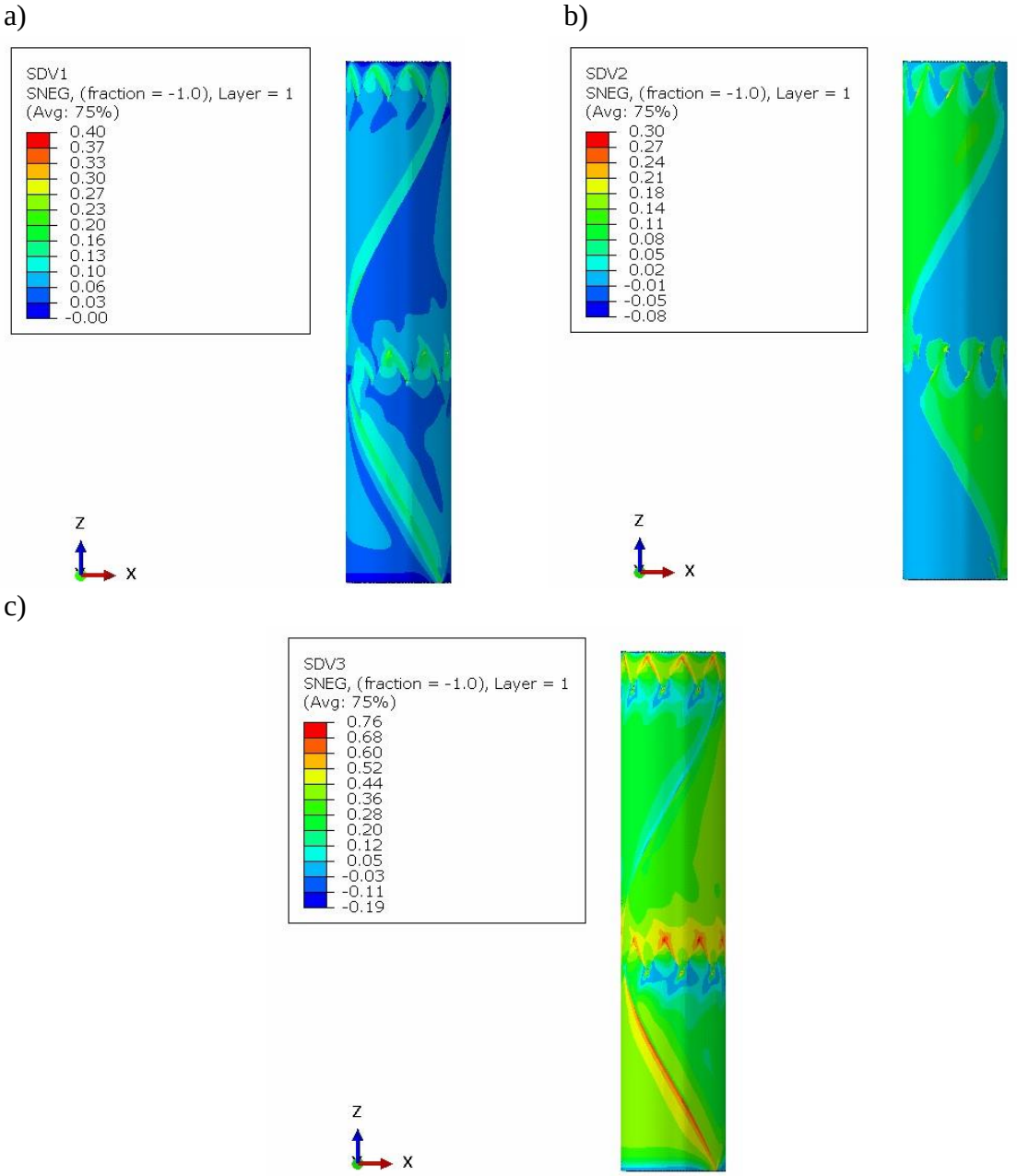

Fig. 33. Damage pattern for a) matrix tensile/compression failure, b) fiber matrix shear failure, and c) material shear damage for multiaxial load of -2.3 kN

The presented data confirm the proper application of progressive damage into thin-walled CFRP members.

4.3 Buckling analysis

The fatigue test under compressive load raises many doubts, especially for composite materials. As a result of the material sensitivity to compressive load, the buckling phenomenon needs to be considered and analyzed. This phenomenon affects fatigue behavior due to premature failure,

which affects the lifetime of the material. It affects the compressive capacity of the material and, therefore, a buckling analysis was performed to determine the safety margin of the buckling. A numerical analysis of nonlinear buckling was conducted to assess the material behavior under compression – torsion load in the static riks term. The results obtained were compared with the experimental data and presented in Fig. 34.

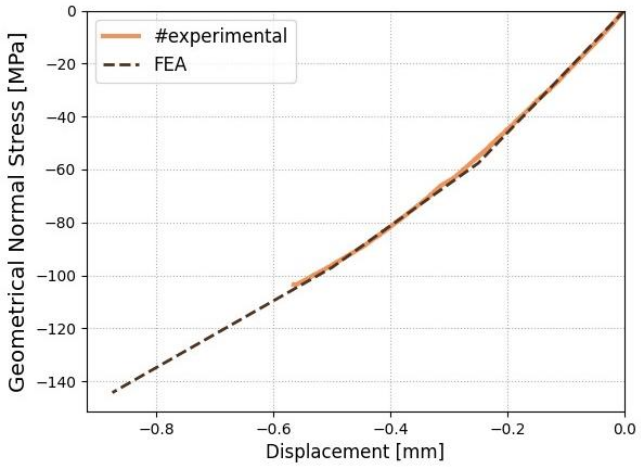

Fig. 34. Stress-displacement curve for quasi-static biaxial (compression-rotational) loading case presented along with the numerical results

Based on the results, the numerical model overestimated the maximum compressive strength (for multiaxial load) by more than 45 MPa. This discrepancy can be explained by considering the material sensitivity to imperfections, especially under compressive load; Since the numerical model does not include microstructural imperfections, it will not accurately predict the maximum compressive strength. When considering those materials, this aspect is always vital, as there are always some microstructure discontinuities. However, a good agreement is observed for the numerical analysis before the compressive strength is reached.

The numerical analysis conducted devoted to predicting the geometrically nonlinear collapse of a member delivered the critical force value of 12.7 kN. The simulation overestimated the maximum force; however, the importance of the analysis needs to be highlighted, it shows the member stability before reaching the maximum compressive force. Since it does not exhibit any loss of stability, the Euler force can be defined as an experimental value of 6.7 kN. The maximum compressive load applied during fatigue is 2.6 kN, which gives a safety margin of approximately 2.6. It gives a large safety margin before buckling occurs.

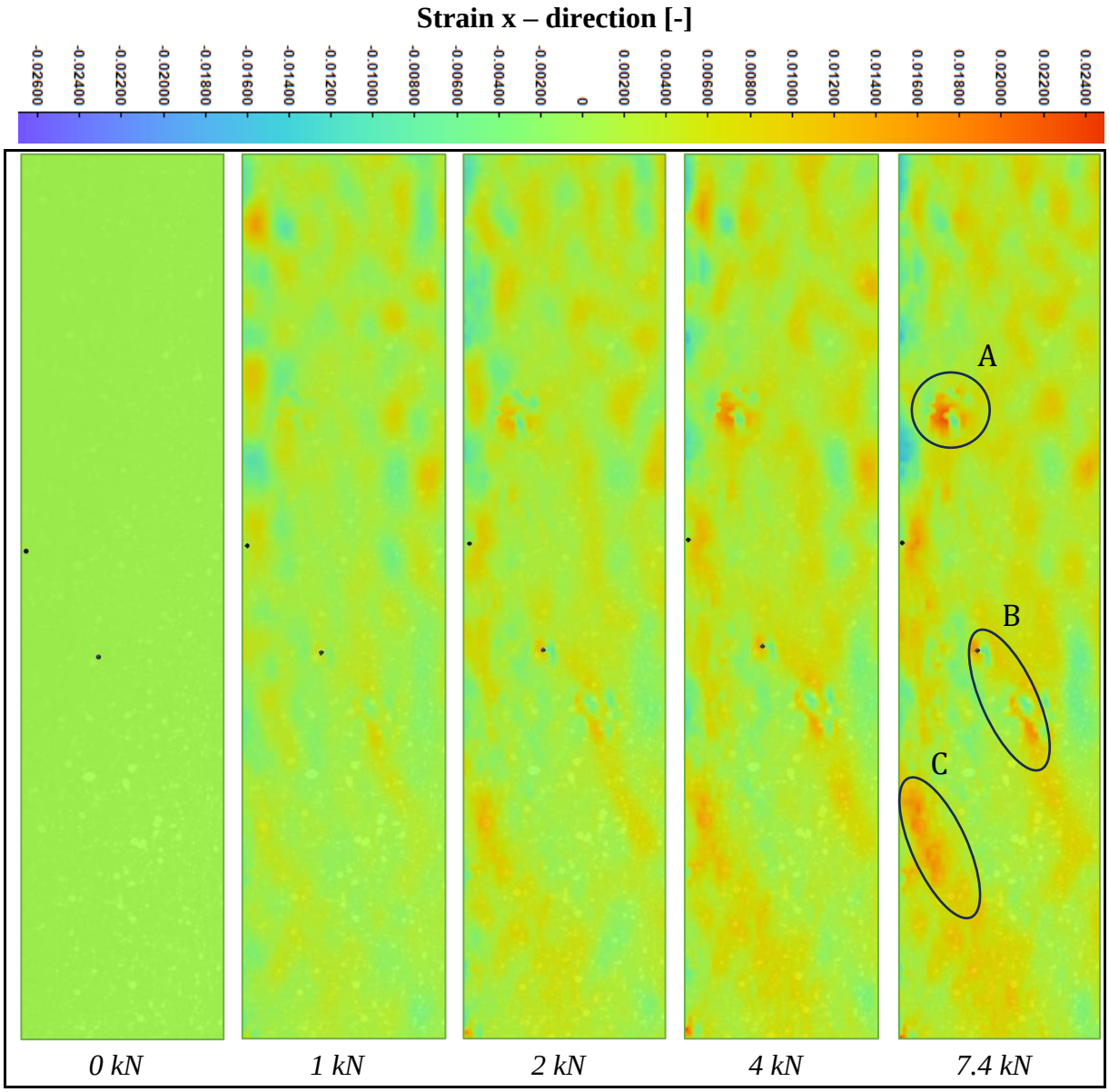

Fig. 35. Strain fields captured by DIC during the quasi-static compression-torsional test

The multiaxial compression test was performed to define the maximum compressive force and, simultaneously, the DIC method was applied to measure surface deformation. The strain fields obtained are presented in Fig. 35, as it can be seen that local strain concentrations are visible mainly along the fibers, at points B and C, and in the fiber interweaving area, at point C. Exceeding the compressive force of 2 kN, the areas covered by points began to be visible and after 4 kN reached a hot spot of strain concentration. These data confirm the safety of the load level applied to perform the fatigue experiment in terms of the global buckling phenomenon; however, buckling at lower length (e.g. kinking) cannot be excluded based on the performed numerical analysis.

4.4 Summary

To conclude the following chapter, several remarks need to be highlighted.

- The created numerical model contains a precise material architecture (mosaic pattern) considering fiber interweaving areas. It has been proven by the optical method that it is

an important aspect from the point of view of local strain concentration. Excluding this aspect may result in an over or underestimation of stress.

- The applied material model with shear non-linearity and progressive damage shows a similar strain nature in comparison to the DIC method. It is in good agreement with the experimental method; however, there are some small discrepancies in the stiffness of the material. On the other hand, larger discrepancies are seen in terms of maximum load obtained from FEA. It might suggest that the strength parameters were not fitted precisely. Due to many variables, the optimum set of strength parameters was defined to satisfy all static tests.
- The FE analysis performed allowed to define the buckling safety margin for compression – torsional load. The analysis showed a higher compressive strength compared to the experiment, which can be explained by the fact that the FE model is a perfectly built discrete body, which does not include any imperfections. In the case of composite materials, there are always material discontinuities because of technology and not only.
- The presented procedure and model validation show that the chosen material model in a good way reflects the performance of the thin-walled FW member under various loading conditions.

5 Multiaxial fatigue testing

Chapter 5 introduces the multiaxial fatigue testing campaign and presents the S-N data in terms of geometrical stresses and life. Regression analysis of fatigue data was performed and plotted along with the results. During the multiaxial experiment, in situ measurement of acoustic signals is conducted using a piezoelectric sensor. The main objective of this chapter is to provide fatigue data for analysis and to show the impact of the mean stress and load phase change on the cylindrical thin-walled CFRP tube.

5.1 Test procedure

Multiaxial fatigue tests on CFRP thin-walled cylindrical members were performed on the MTS series 809 axial / torsion test system. The test was controlled by an applied sinusoidal signal of the tension/compression/torsion load and its phase shift. The biaxiality (λ_T) was adopted to correlate geometrical shear and normal stresses and its equal 1, which gives the equality of shear and normal stresses. Three different load ratios *R* were considered, respectively -1, 0.05 and 0.5 for the in-phase and out of phase (45° and 90°) load according to the flow chart in Fig. 12. A frequency of 6 Hz was applied, and no significant temperature amplitude was observed by pyrometer and thermographic camera during the life of the specimen. The run-out life was set to $2x10^6$. During the experiment, the acquisition of acoustic signals within the material was carried out. The AMSYS-6 acoustic emission system provided by Vallen was used with a VS150-M piezoelectric sensor placed as shown in Fig. 36. A sensor was used with a frequency range of 50 to 600 kHz and mounted on the specimen using hot glue. Allows for a proper transfer of the elastic waves from the material to the sensor, which was verified by a pencil lead break test. The Acoustic Emission System allowed measuring the elastic waves in the specimen caused by any failure mechanisms. These collected signals are used for the quantitative analysis of the life stages of the CFRP specimens investigated. The experimental setup is presented in Fig. 36.

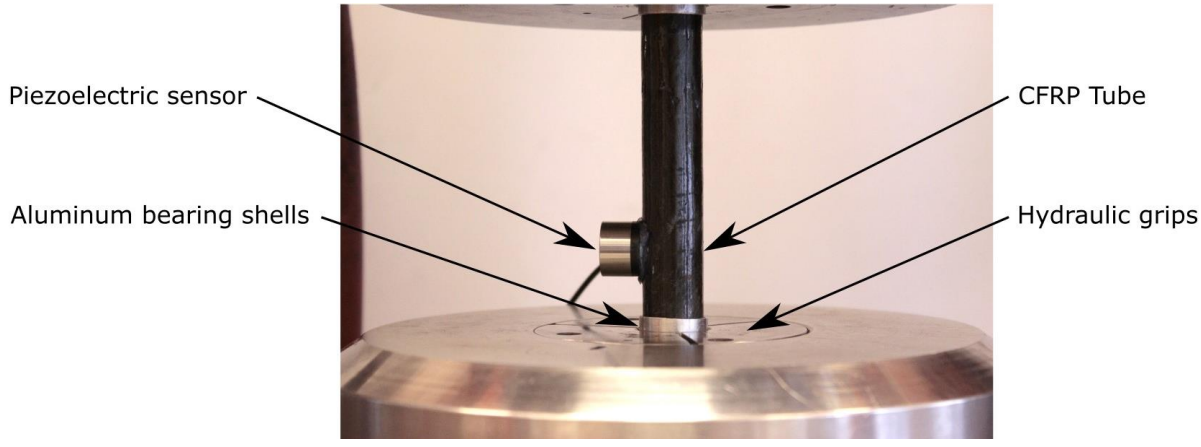

Fig. 36. Experimental setup used for providing multiaxial loading conditions and acquisition of acoustic signals

The applied sinusoidal axial force and torsional load provide various stress paths according to the phase shift. Considering the in-phase load, the straight line can be observed, on the other hand the out of phase load gives the ellipsoid as it is presented in Fig. 37.

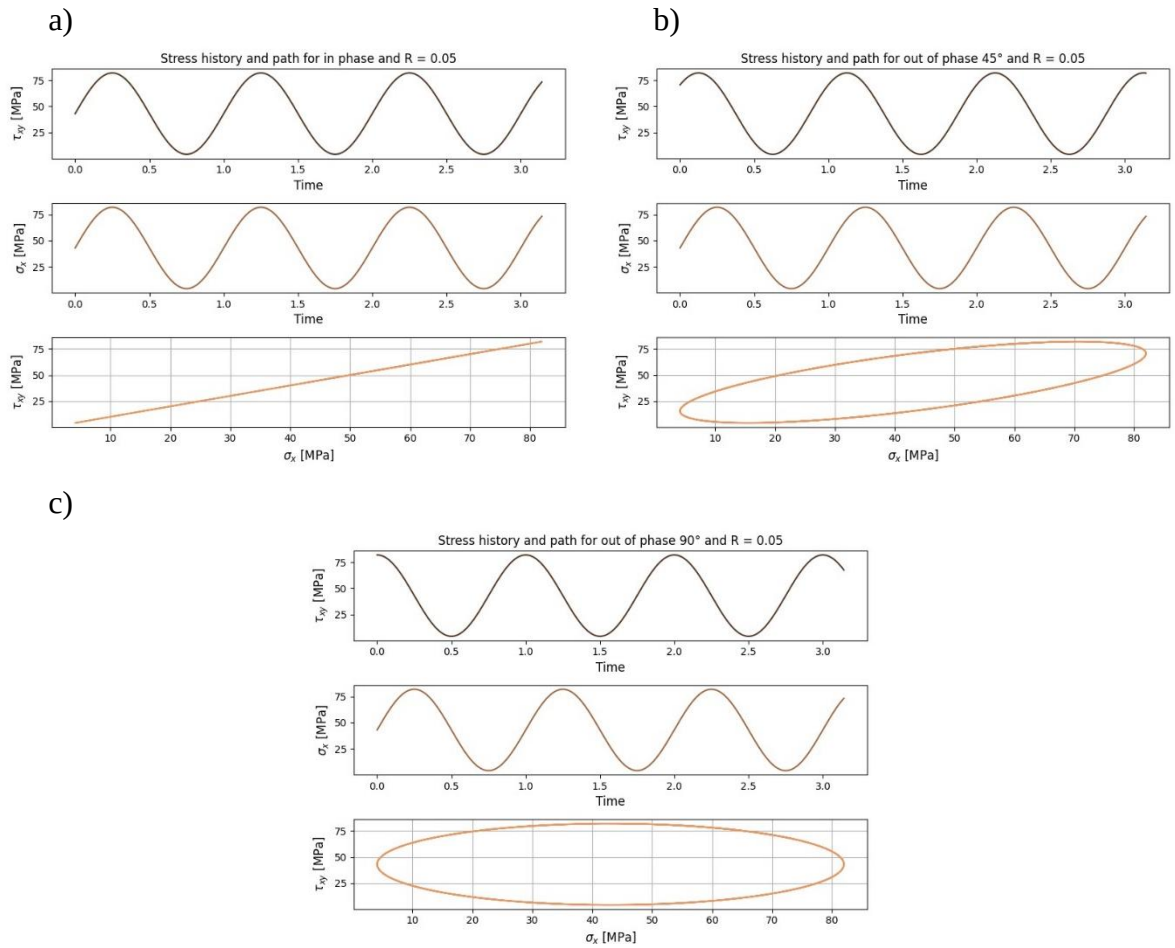

Fig. 37. Stress history and path for load ratio 0.05 where maximum force totals 5750 N and maximum torque 60 Nm for a) in phase load, b) 45° out of phase and c) 90° out of phase load

The gripping system developed for the static experimental campaign (Chapter 3 - Fig. 16) was also used in fatigue experiments. Each sample subjected to cycling loading was measured in the same way as described in Subchapter 3.2. The average external diameter of the sample is 21.993 mm with standard deviation 0.123 mm considering all samples used in the experiment.

5.2 Experimental fatigue data

The multiaxial fatigue data are presented in Fig. 38 – 44 in terms of the amplitude of geometrical normal stress $(\sigma_{x,amp})$ versus the life to the complete decohesion of the specimen. The results obtained are fitted using power law regression in the double logarithmic scales (Eq. 19).

$$Life = a * \sigma_{x,amp}^{k} \tag{19}$$

where, *a* is a constant, *k* is the exponent of the power law. Regression analysis has been performed for fatigue data considering stress as an independent variable.

In phase loading

The data for in-phase loading are shown with the scatter bands of 5. Taking into account the S – N plots for *R* = -1 and 0.5, the band lines cover all points. On the other hand, larger scatter bands can be observed for *R* = 0.05. In this case, 1 of 11 points are out of the scatter bands of

5. The slope for the regression lines is approximately similar for R = -1 and 0.5, where for R = 0.05 is much larger.

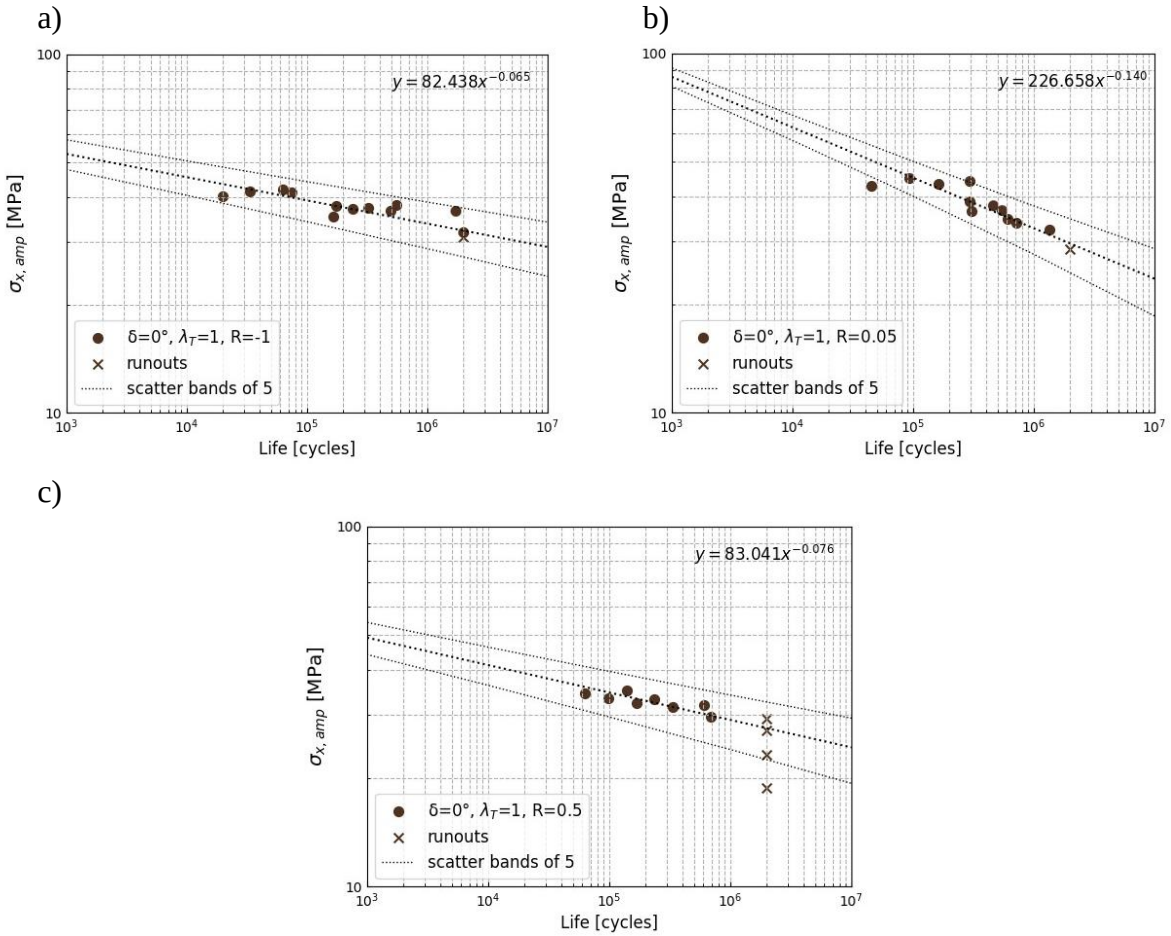

Fig. 38. Multiaxial fatigue S-N data for proportional loading for a) R = -1, b) R = 0.05, and c) R = 0.5

45° out of phase load

The phase lag of 45° gave the scatter bands of 5. In terms of R = 0.05 all points are within the scatter band. For R = -1, only one is outside the scatter band, and the largest discrepancy in the results exhibits R = 0.5, where 7 points out of 12 are not covered by the scatter band of 5. In the case of this data, the slopes are divergent.

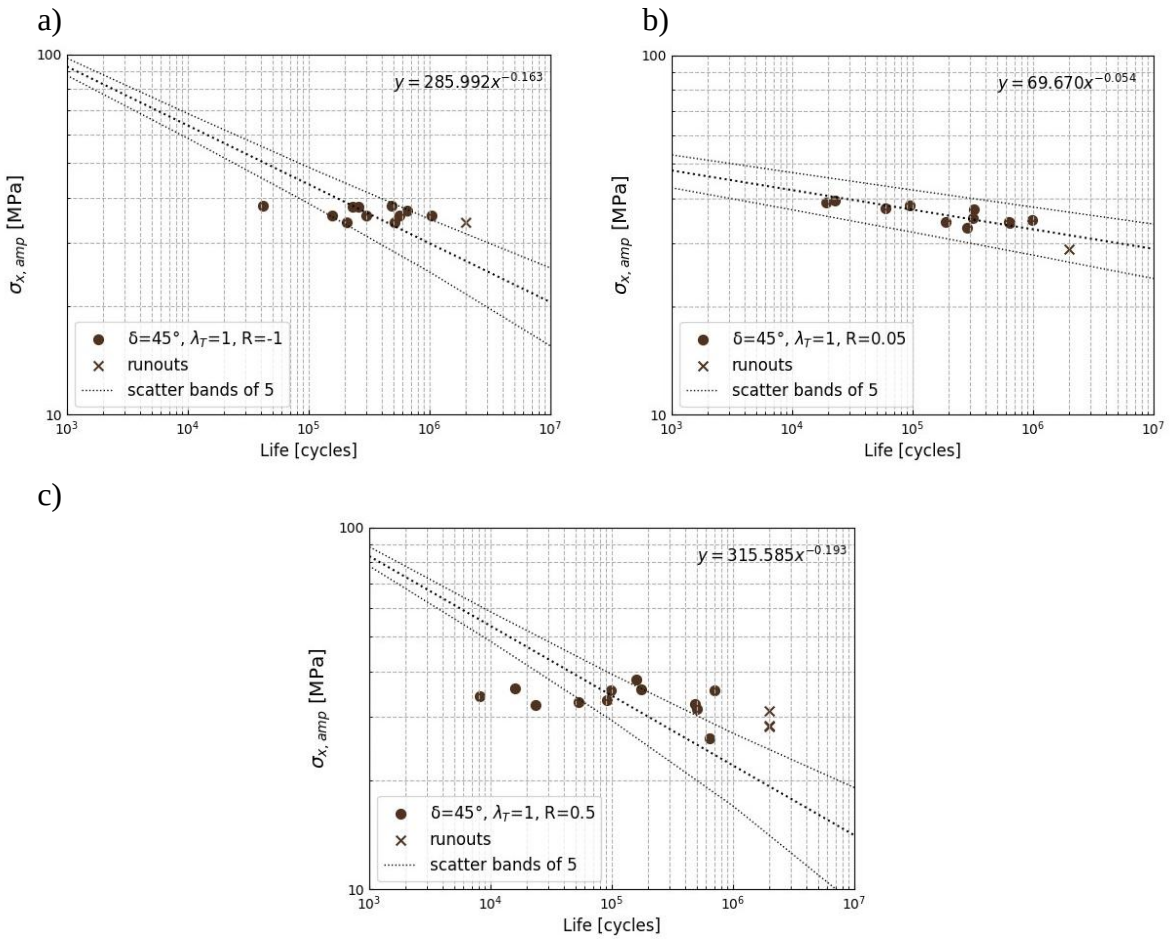

Fig. 39. Multiaxial fatigue S-N data for phase shifting 45° for a) R = -1, b) R = 0.05, and c) R = 0.5

90° out of phase load

The S-N data for the 90° out of phase multiaxial load are also plotted in the scatter band regime of 5. The reverse load ratio R = - 1 exhibits the largest discrepancy of the group, 6 points are out of the scatter band, remaining data for positive load ratios exhibit scatters within the bands of 5.

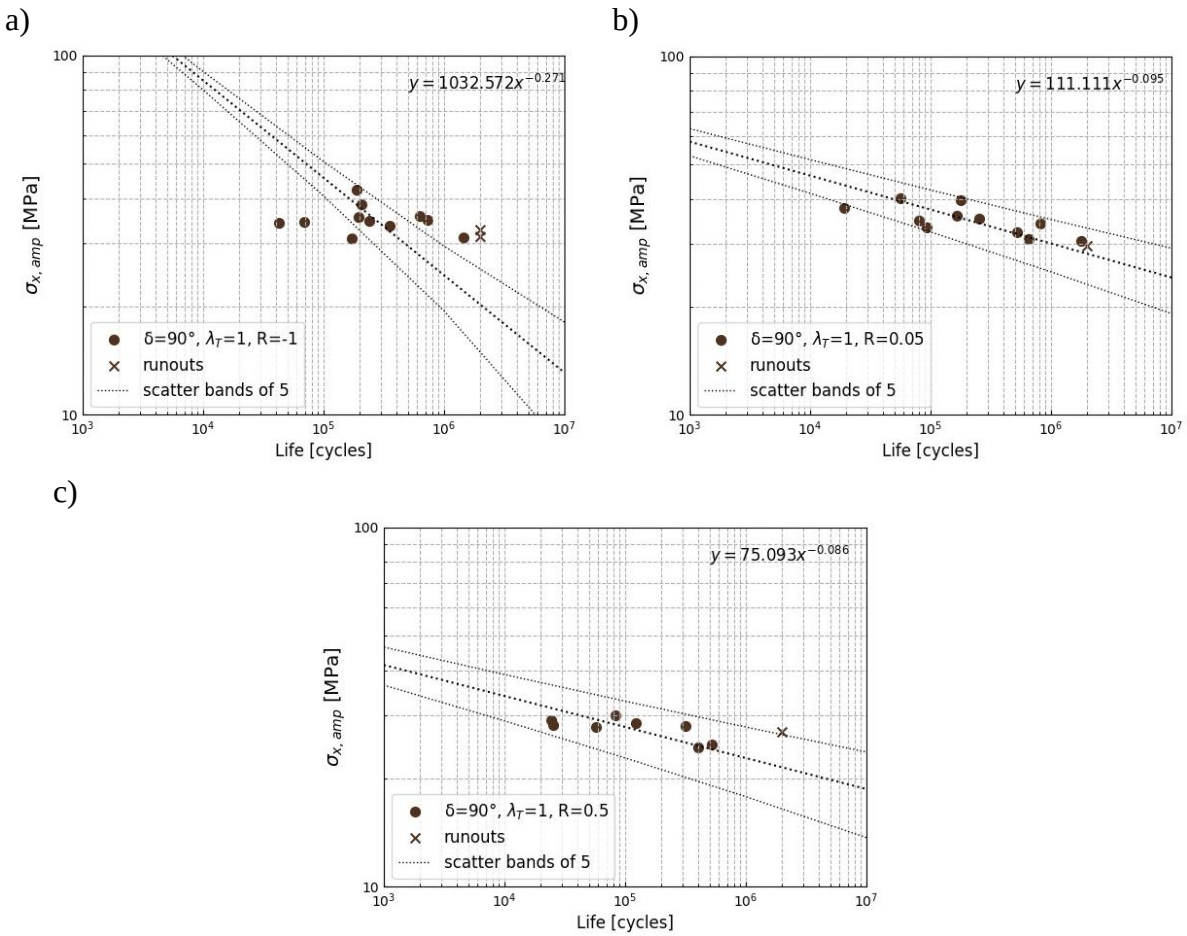

Fig. 40. Multiaxial fatigue S-N data for phase shift 90° for a) R = -1, b) R = 0.05, and c) R = 0.5

The results presented in the form of S – N curves approximated by regression show a scatter band of 5. The largest scatter is observed for 45° out of phase and the load ratio -1. The discrepancy observed for those cases may suggest that there is influence of other factors, e.g. a different failure mode such as local buckling. Therefore, those loading cases were excluded from the analysis. The regression equations with the coefficient of determination (R^2) are presented in Table 13. Taking into account the above statement, the R^2 coefficient also shows that the lowest prediction is observed for the results of the 45° out of phase and load ratio -1.

Table 13. Data from the regression analysis for the experimental results

Data set	Regression equation	R^2
$\delta = 0°; R = 0.05$	$y = 226.658x^{-0.140}$	0.8853
$\delta = 0°; R = 0.5$	$y = 83.041x^{-0.076}$	0.7011
$\delta = 0°; R = -1$	$y = 82.438x^{-0.065}$	0.5591
$\delta = 45°; R = 0.05$	$y = 69.670x^{-0.054}$	0.1960
$\delta = 45°; R = 0.5$	$y = 315.585x^{-0.193}$	0.2559
$\delta = 45°; R = -1$	$y = 285.992x^{-0.163}$	0.0323
$\delta = 90°; R = 0.05$	$y = 111.111x^{-0.095}$	0.6600
$\delta = 90°; R = 0.5$	$y = 75.093x^{-0.086}$	0.7000
$\delta = 90°; R = -1$	$y = 1032.572x^{-0.271}$	0.4000

Analysis of experimental results

To show the clear impact on mean stress and phase change, positive load ratio data was chosen for in-phase and 90-out-of-phase loading. Due to the large scatter, the data for 45° out of phase load and for load ratio -1 were excluded from the analysis. Furthermore, R = -1 was excluded due to the possibility of the influence of other failure mechanisms caused by compression.

To show the impact of out-of-phase loading, each load ratio was correlated and compared with the reference in-phase loading conditions. The results are plotted in Fig. 41, for load ratio 0.05 the phase shift of 90° decrease the life of the sample. The same situation appears for the load ratio R = 0.5.

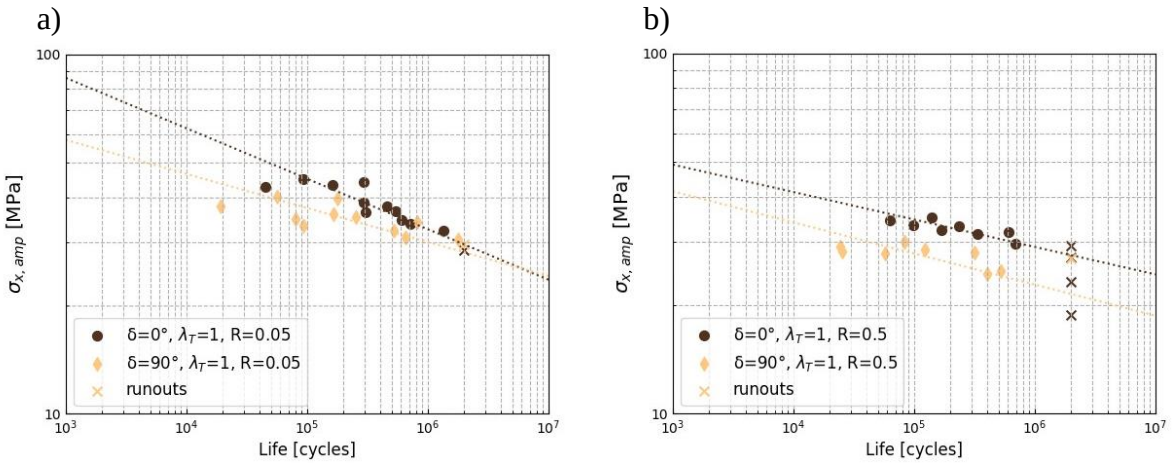

Fig. 41. Impact of phase shift on S-N data for a) R = 0.05 and b) R = 0.5

The slope of regressions for the load R = 0.05 load shows a slightly different gradient; the reference regression curve gives a higher slope compared to the out-of-phase load, suggesting a negative impact for this load ratio. The negative impact of the phase change is observed for a load ratio of 0.5 for 90° out of phase. The reference regression for in-phase loading exhibits a similar slope and with respect to 90° is shifted in the positive direction, giving greater fatigue strength. The S-N curves presented pointed out the negative effect of phase shift.

In addition to the impact of the phase load, the influence of the mean stress is considered. S-N data for two load ratios and in and out of phase load are presented in Fig. 42. For proportional load, the impact of mean stress is noticeable, and, as expected, a higher load ratio (R = 0.5) gives shorter fatigue life. It can be stated that the same effect is observed for phase shift of 90°. When loading in phase is considered, there is a discrepancy between the regression angles, but it does not affect the interpretation of the results. S-N data for 90° phase lag shows that the curves exhibit similar regression angles; however, they provide various life, where for higher load ratio, shorter life is observed. The impact of mean stress is recognized on the basis of the presented S-N data. As expected, a greater load ratio gives a shorter life.

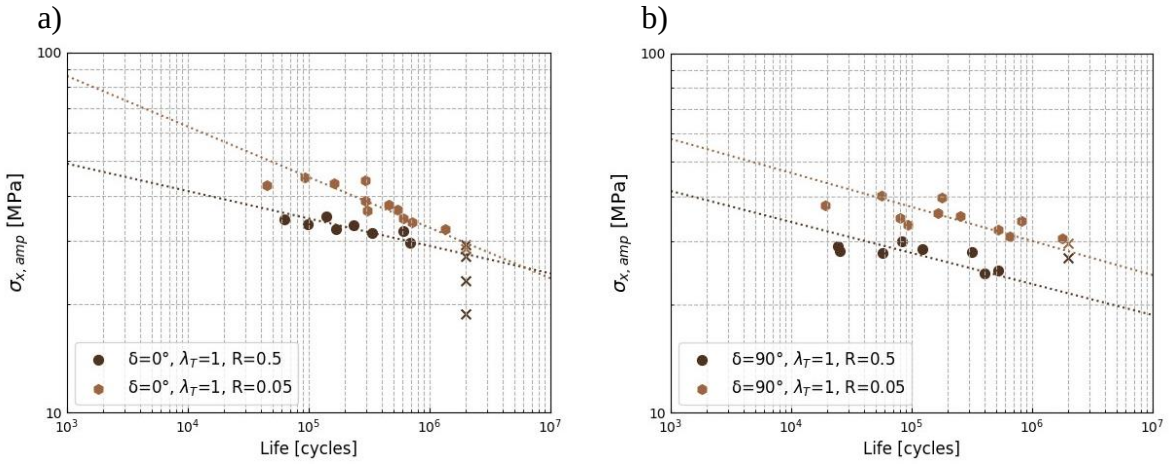

Fig. 42. Impact of mean stress on fatigue data; a) proportional load, b) out of phase load

Full data correlation

In addition to the analysis performed, the full data set of the results of the multiaxial fatigue test are presented in this subsection.

The phase shifting effect is presented in Fig. 43, due to the scatter bands and relatively small results variation, the effect is hided and cannot be determined explicitly.

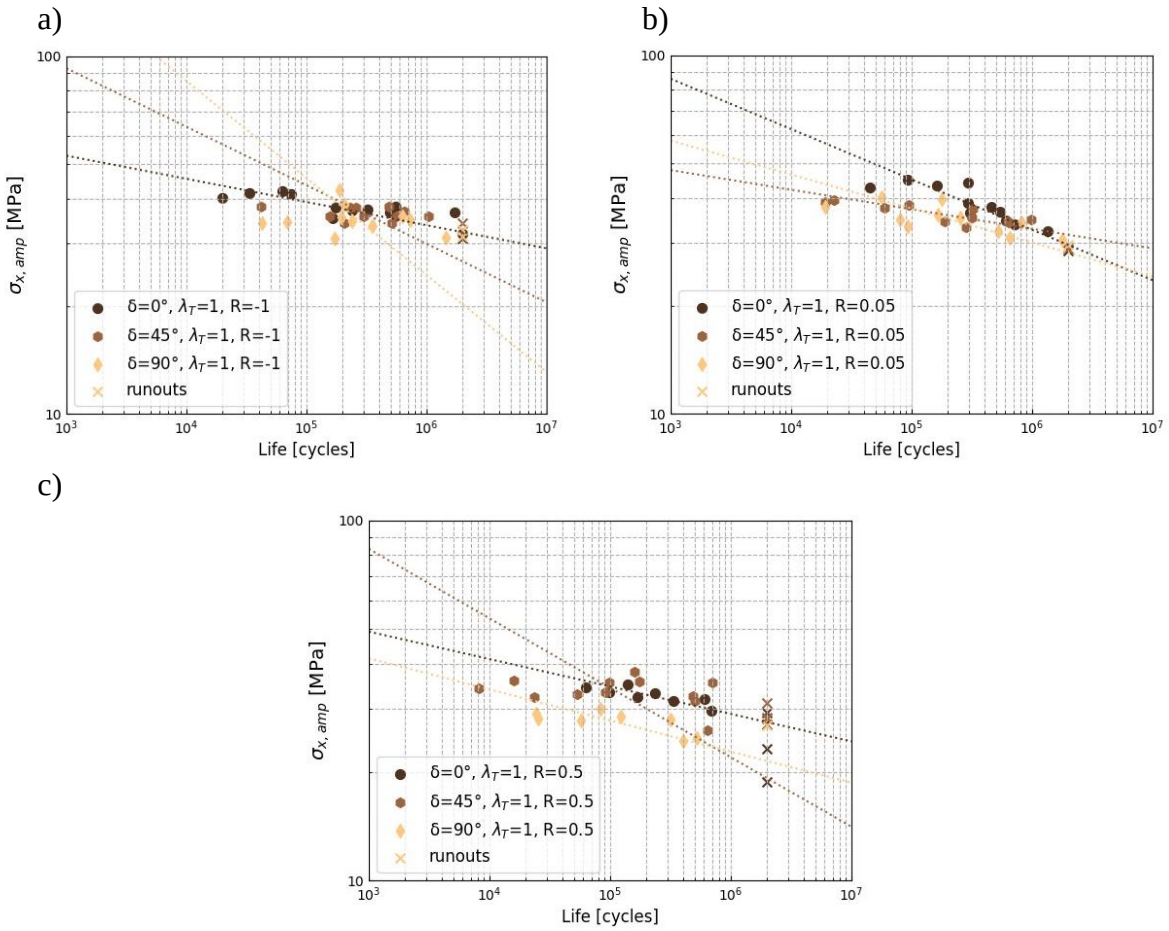

Fig. 43. Impact of phase shift on multiaxial fatigue data for a) R = -1, b) R = 0.05 and c) R = 0.5

For the mean impact of stress, presented in Fig. 44, there is a similar situation as highlighted before. The data for load ratio -1 exhibit a different nature, and may increase the level of interpretation of the results.

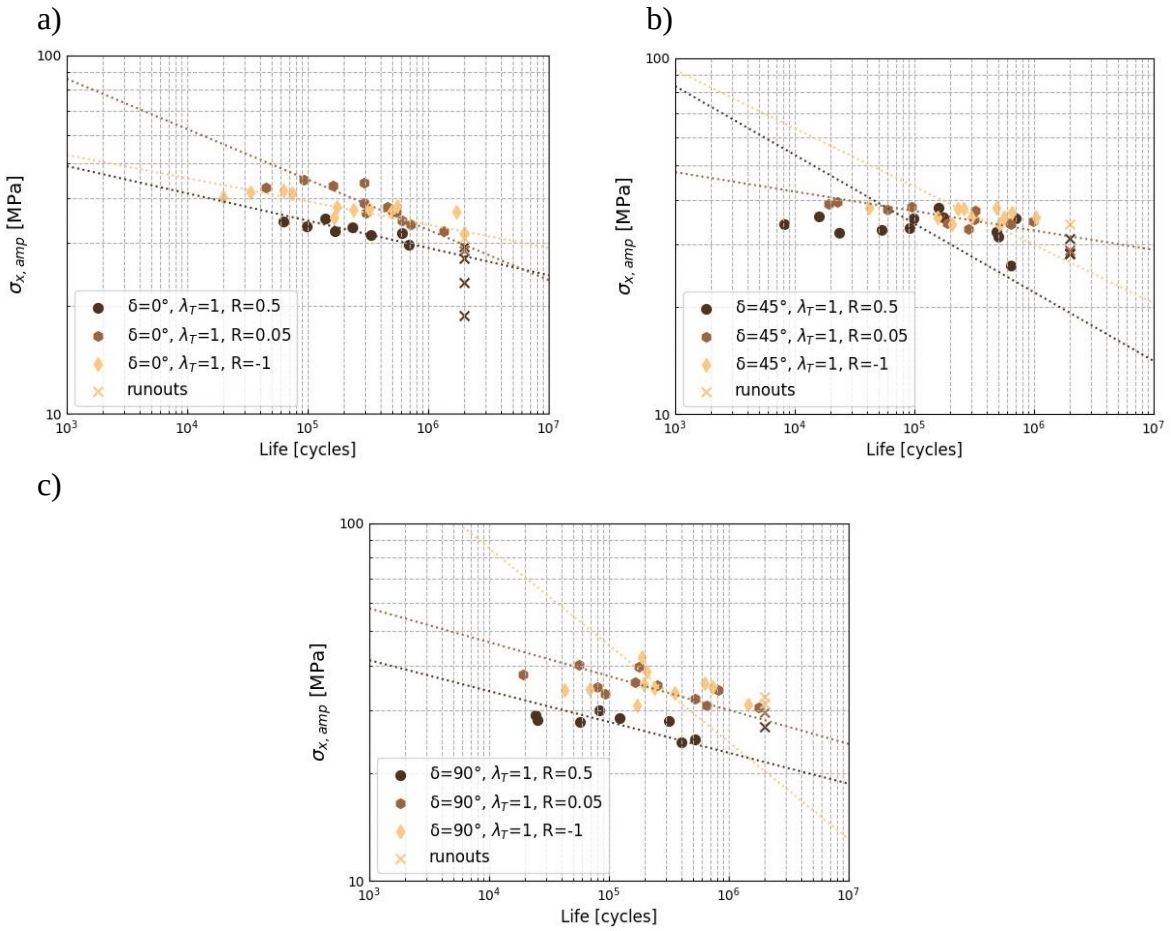

Fig. 44. Mean stress impact on multiaxial fatigue data for a) $\delta = 0°$, b) $\delta = 45°$, and c) $\delta = 90°$

As might be confirmed in Fig. 43 and Fig. 44, the impact of mean stress and phase shift cannot be recognized directly from plotted S-N curves.

5.3 Summary

On the basis of the experimental data and performed regression analysis, the following conclusions can be drawn:

- The negative impact of out-of-phase loading can be explicitly determined based on the data correlation for correlation of the data for 90° for R = 0.05 and 0.5 combined with the reference in-phase loading.
- The influence of mean stress on fatigue life was analyzed. It shows the negative impact of the mean stress. The higher mean stress, the shorter fatigue life, which was observed by correlating load ratio 0.05 and 0.5 for in-phase and out of phase loading.
- It was not possible to recognize the effect of 45° out of phase loading, due to large scatter band obtained from experiment. This data set was excluded from the analysis.
- The different nature of the results was also observed for R = -1, this load case provides, in addition to the tensile load, the compression load, which can develop additional or different failure mechanisms within the material.

6 Damage analysis

A comprehensive analysis of the fracture is required to understand the phenomena of fatigue. The following chapter is devoted to analyzing the failure that governs fatigue. The analysis is performed on the basis of collected acoustic signals and microcomputed tomography performed on the specimen after fatigue test. The main objective of the chapter is to define and understand the failure mechanisms that act during fatigue and their importance for fatigue life.

6.1 Quantitative analysis of acoustic signals

The acoustic signals acquired during the experiment under cycling load allowed the cumulative counts function to be delivered. It gives information on the acoustic events that appeared at a particular time and their compilation within the fatigue life of the specimen. This function was compared with the shape of the general damage accumulation function presented in Fig. 1. Due to the extremely large database, the results for three randomly chosen samples are analyzed and normalized to present the general fracture behavior of CFRP. The graphs presented in Fig. 45 – 47 combine 3 curves, that is, normalized displacement, rotation, and cycles, which represent their value divided by the maximum value. The displacement and rotation curves indirectly reflect the stiffness of the sample, the highest damage state in the sample, the smallest active cross-sectional area, and the decrease in the elastic properties, which directly influence the stiffness of the sample. The increase of the displacement and rotation indicates that a larger deformation is needed to keep the assumed load ratio.

Taking into account the general behavior of damage accumulation, the cumulative curves have been divided into 4 stages, which were defined according to the following assumptions.

- Region A starts from the beginning until CDS is defined after the first gradient of cumulative counts.
- Region B represents the gradual linear part of the cumulative curve until there is a significant deviation from linearity.
- Region C ends at a significant gradient of cumulative counts.
- Region D - the last stage, which covers rapid cumulation of events mainly due to fiber breakage.

The regions were estimated according to the highlighted assumptions and compared with the general accumulation of damage presented by the composite materials. Considering the sensitivity of acoustic piezoelectric sensors and very complex failure behavior of composite materials (failures occur simultaneously), the cumulative counts curve are analyzed without any additional analysis, which may exclude environmental noises and cluster the signal groups. Due to the complexity and additional data required, those methods were not considered within the investigation.

Each region is assumed to refer to the govern failure mechanism acting within these frames. The first region (A) covers matrix microcracking, mainly their initiation within the entire sample volume. As the crack saturation reaches a certain level, the cumulative curve progresses to the gradual linear part (region B). Within this region, interface failures appear, i.e. debonding. The next region (C) covers delamination, with a sudden increase in acoustic events being

observed because of the coalescence of cracks resulting in delamination. It significantly decreases stiffness and, in the end, leads to global decohesion. The last stage, in addition to delamination, covers fiber breakage. The analysis is devoted to showing the applicability and possibility of characterizing the damage accumulation of continuous fiber polymers on the basis of unfiltered AE data. In addition, the data were used to establish the S-N curves for the CDS point presented in Chapter 6.2.

Proportional loading

The proportional loading is investigated as a reference loading condition. Sample no. 0.5/1/0/15 was chosen as the representative for this loading case. It was subjected to a maximum geometric stress of 137.2 MPa and a load ratio of 0.5. The fatigue life totals 63 407 cycles.

Analyzing the graphs presented in Fig. 45, a similar curve nature between the displacement/ rotation curve might be highlighted. The gradual nature of the curves is observed after 15% of fatigue life, before after reaching the CDS the stiffness dropped rapidly. Region A is fulfilled where the significant counts gradient reaches a stable gradual phase; it perfectly correlates with the stabilization of normalized displacement and rotation. It can be assumed that the first part of the fatigue life is correlated with a significant loss of stiffness. In the next stages, the rotation and displacement curves are linear, gradually increasing the number of acoustic events in the material. Taking into account region C, there is a noticeable increase in acoustic events, suggesting that delamination failure initiates, however, there is no stiffness change. In the last region, these acoustic events are more intense, suggesting fiber breakage and growth delamination. The last approximately 10% of fatigue life is affected by very rapid damage growth, reflected in a high number of acoustic events, suggesting a very short propagation phase. The majority of the fatigue life of the specimen is governed by crack initation, their coupling, and small crack growth.

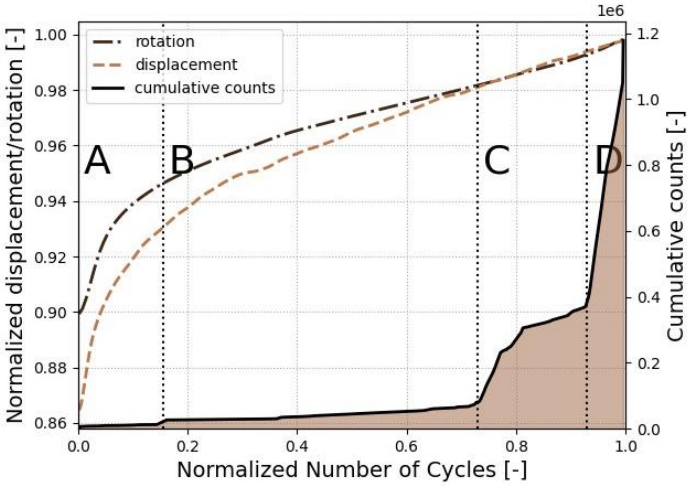

Fig. 45. Normalized displacement and rotation correlate with cumulative counts as a function of fatigue lifetime for sample 0.5/1/0/15 (lifetime 63 407 cycles)

Phase shifting (45°)

Sample no. 0.5/1/45/14 was chosen as representative of the 45° out of phase load. The sample was subjected to a maximum geometric stress of 114.9 MPa and a load ratio of 0.5. The failure appeared at 90 315 cycles. The initial behavior shows a high similarity to the proportional load

case; however, a significant difference appears at the final life stage. In this case, the CDS point was achieved earlier on the proportional loading. This might lead to the hypothesis that the sample's initiating state was different (more discontinuity in the microstructure) or that phase shifting affects the crack initation. On the basis of the available data in the analysis, it is not possible to directly answer which hypothesis has a higher impact on this matter. Additionally, an important aspect is the place in region D, where an increase in the displacement and rotation curve is noticeable, which indirectly refers to a significant stiffness drop at this lifetime (as the fatigue is force-controlled). Taking into account the decrese stiffness and the progressive nature of the curve of coumulative counts, the last stage of fatigue life is governed by the development of macrodamage.

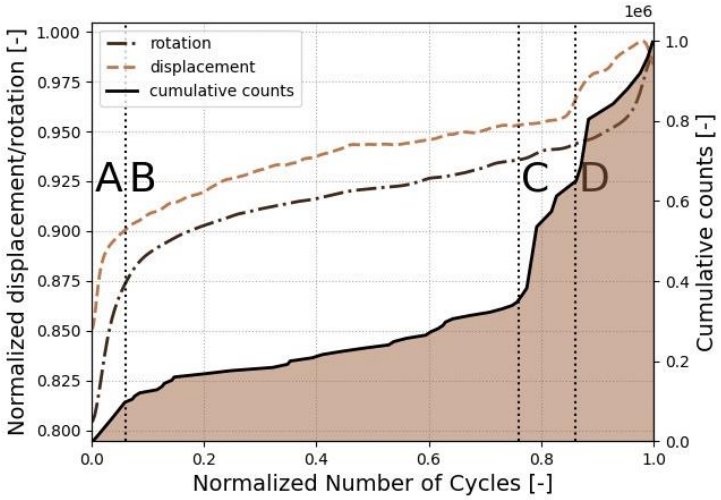

Fig. 46. Normalized displacement and rotation correlate with cumulative counts as a function of fatigue lifetime for sample 0.5/1/45/14 (lifetime 90 315 cycles)

Phase shift (90°)

Sample no 0.5/1/90/11 represents the 90° out of phase load case. It was subjected to a maximum geometric stress of 111.0 MPa, and a load ratio of 0.5. The failure occurred in 57 463 cycles. In terms of phase lag of 90°, a slightly different manner is observed in the duration of region D and the stabilization of the normalized displacement curve. The increase in the duration of part D suggests that the last fatigue life phase proceeds more stable and with a softness.

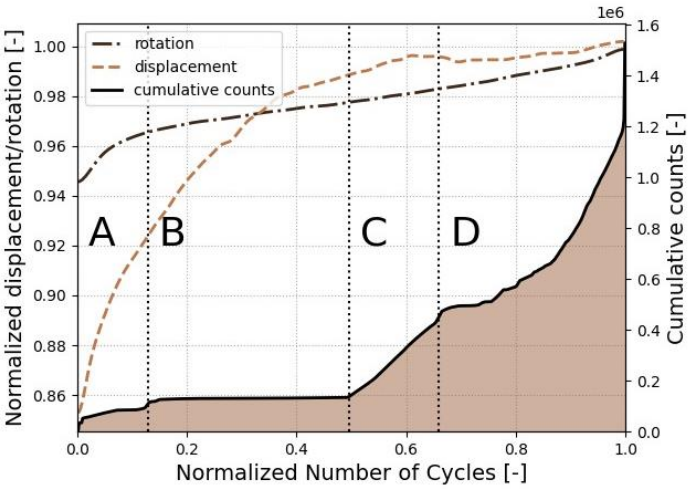

Fig. 47. Normalized displacement and rotation correlate with cumulative counts as a function of fatigue lifetime for sample 0.5/1/90/11 (lifetime 57 463 cycles)

The duration of the regions for each sample is presented in Table 14 in the form of fatigue lifetime indices for the end values, which close the region (where D ended at 1).

Table 14. Comparison of the index along samples under various phase-shifting loadings - each value stands for the end value of the index for a particular region.

	Fatigue lifetime index – end of the region		
Sample no	**A**	**B**	**C**
0.5/1/0/15	0.155	0.730	0.930
0.5/1/45/14	0.060	0.760	0.860
0.5/1/90/11	0.129	0.496	0.660

The conducted analysis shows the relatively high similarity of the damage accumulation obtained from AE data with the general function found in the scientific literature. It can be assumed that the first stage of the fatigue life (region A up to the CDS point) appears to be up to 15.5% of the fatigue life in terms of proportional, 6% for 45° out of phase and 12.9% for 90° out of phase. At the CDS point, the maximum density of crack saturation is assumed. A gradual accumulation of damage can be observed just after this region, lasting about 60% of the fatigue life. In the case of a 90° out of phase load, region B is significantly smaller. However, region D is larger than in other cases. In general, the curves show gradual stiffness change, which suggests that investigated CFRP specimens undergo majorly single fiber breakage, crack initation and their coupling (interfecial debonding) and small crack growth. Only for 45° out of phase load, the progressive stiffness change is observed at last life stage, suggesting development of macrodamage i.e. delamination and fiber breakage. In fact, each loading case covers the macrodamage failure; nevertheless, in case of investigated specimens this phase proceeds rapidly within several hundred cycles. This fact is a result of the lack of constrain layers (cross – ply layers), which could control the damage evolution as the primary cracks appear in the plies inclined to the principal tensile loading direction.

6.2 S-N curves for the first failure gradient

The acquired acoustic data were analyzed as presented in previous sections to provide the S - N curves for the first failure gradient recorded by AE. The first failure gradient is associated with the end value for region A (CDS) and is correlated with the amplitude of the geometric stress. The regression analysis was carried out to show the curves and is presented in Fig. 48 – 50. The data for proportional loading are covered by a scatter band of 5, where only two points of 9 are out of the bands for R = 0.05. The highest regression slope can be observed at R = 0.05. The best correlation and the smaller scatter exhibit R = 0.5.

Proportional loading

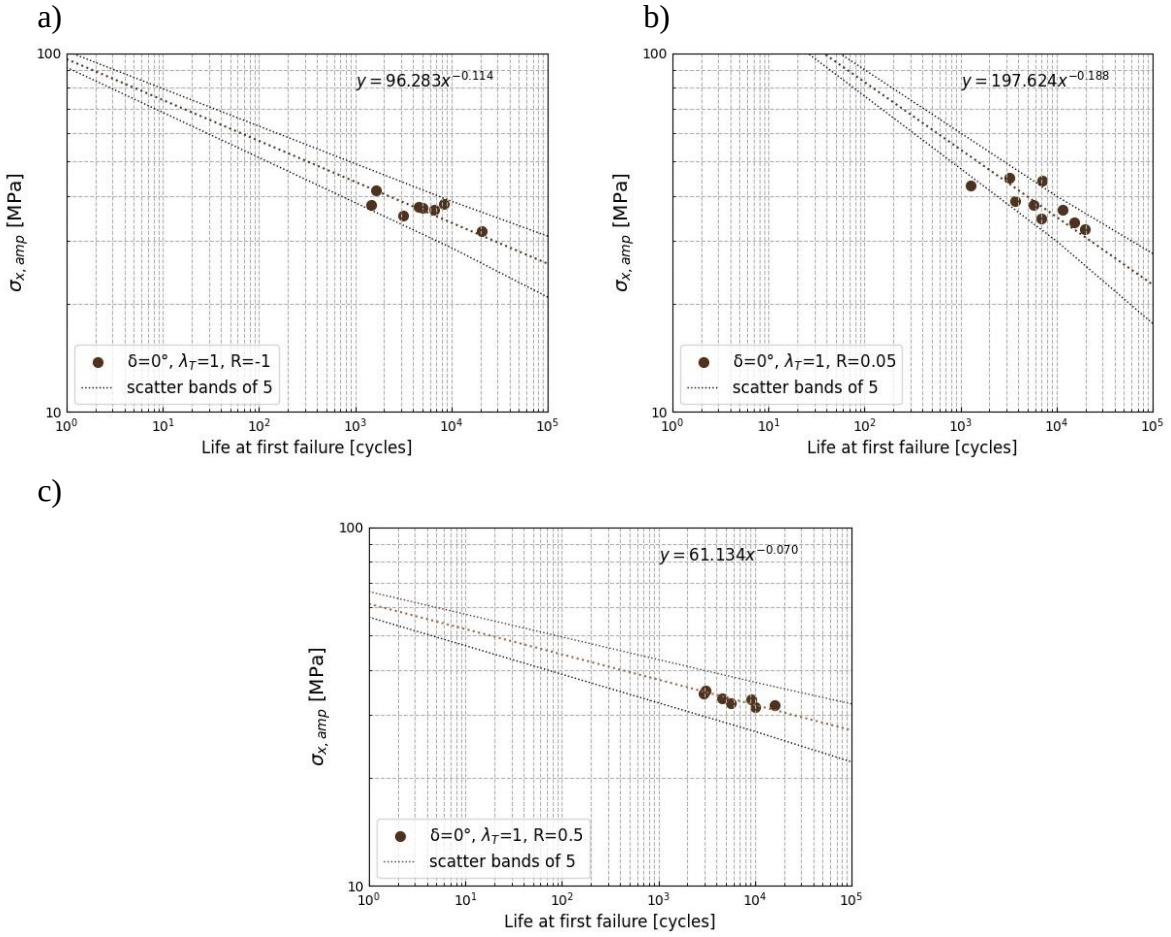

Fig. 48. Multiaxial fatigue S-N data at the first failure gradient for phase loading for a) R = -1, b) R = 0.05, and c) R = 0.5

45° out of phase loading

For 45° out of phase loading, a large scatter of data is observed. Only in the case of R = 0.05 all points are covered by scatter bands of 5. For R = -1, there are 3 points out of the scatter bands, and respectively 4 points out for R = 0.5.

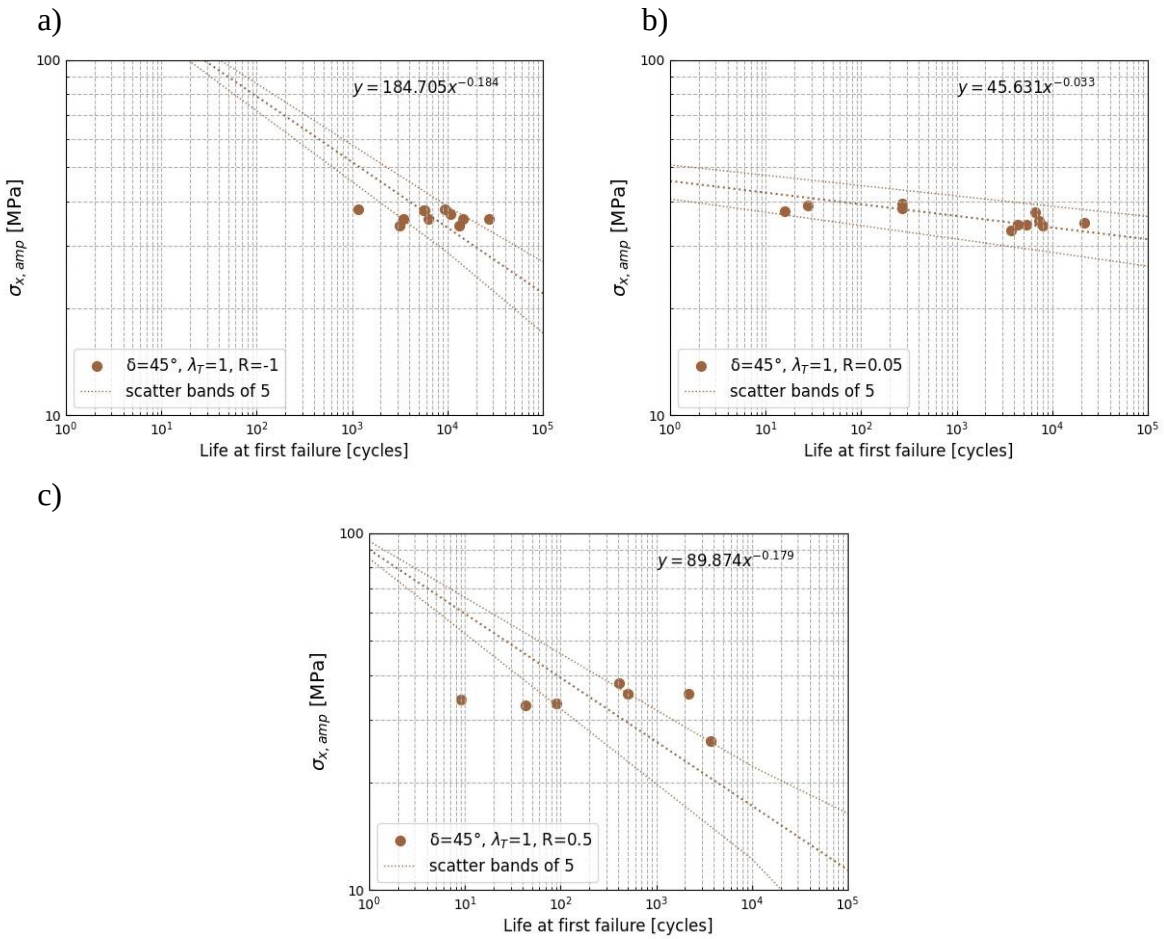

Fig. 49. Multiaxial fatigue S-N data at first failure gradient for phase shifting 45° for a) R = -1, b) R = 0.05, and c) R = 0.5

90° out of phase loading

For the remaining out of phase loading, all points are covered in terms of R = 0.5. For other cases, there are points out of the scatter bands of 5.

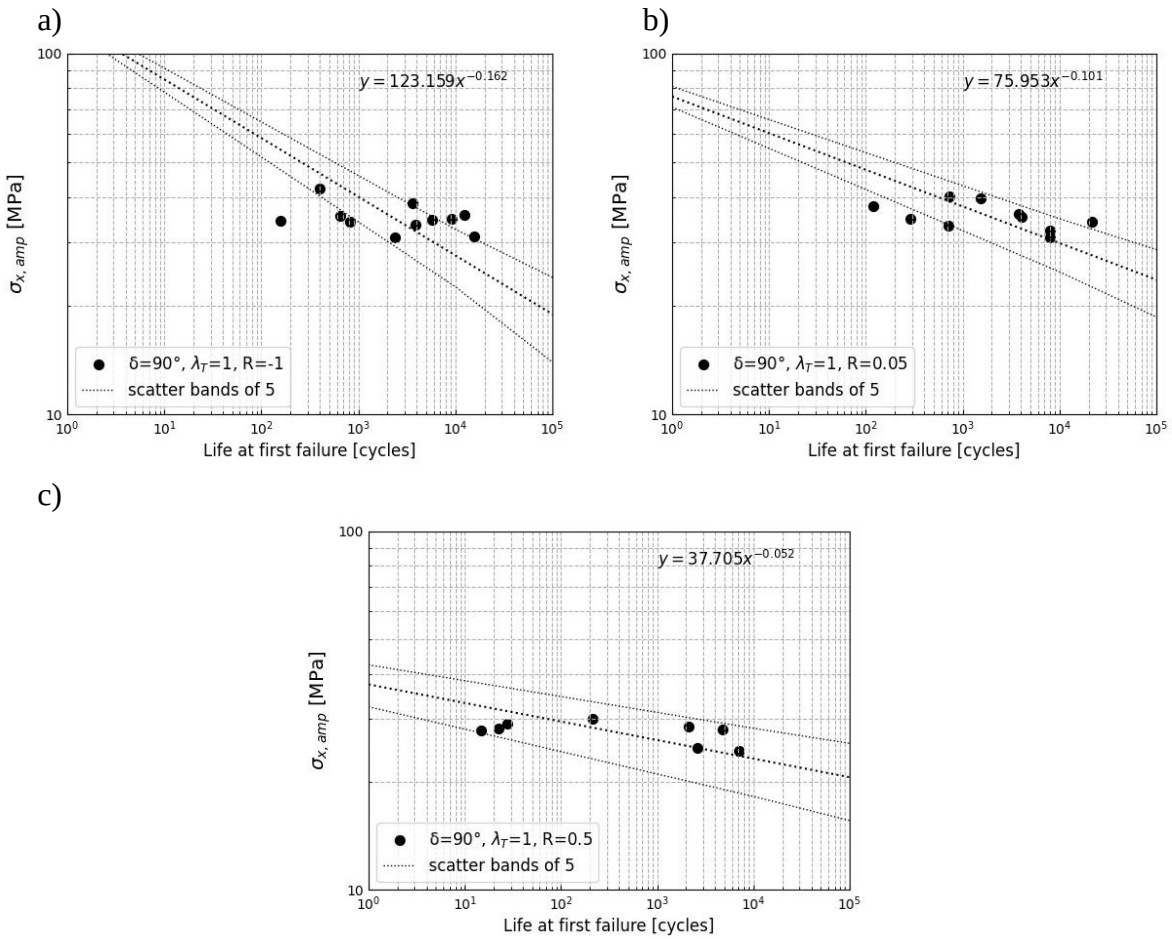

Fig. 50. Multiaxial fatigue S-N data at first failure gradient for phase shift 90° for a) R = -1, b) R = 0.05, and c) R = 0.5

The set of regression equations and R^2 is given in Table 15. The lowest value of R – sqaure is shown for the out-of-phase loading for the load ratios -1 and 0.05.

Table 15. Regression analysis data for S – N curves delivered from AE

Data set	Regression equation	R^2
$\delta = 0°; R = 0.05$	$y = 197.624x^{-0.188}$	0.7571
$\delta = 0°; R = 0.5$	$y = 61.134x^{-0.070}$	0.5858
$\delta = 0°; R = -1$	$y = 96.283x^{-0.114}$	0.8006
$\delta = 45°; R = 0.05$	$y = 89.874x^{-0.179}$	0.0233
$\delta = 45°; R = 0.5$	$y = 315.585x^{-0.193}$	0.6305
$\delta = 45°; R = -1$	$y = 184.705x^{-0.184}$	0.0529
$\delta = 90°; R = 0.05$	$y = 75.953x^{-0.101}$	0.1171
$\delta = 90°; R = 0.5$	$y = 37.705x^{-0.052}$	0.5371
$\delta = 90°; R = -1$	$y = 123.159x^{-0.162}$	0.1303

For further analysis of results, again the data for positive load ratios for in phase and 90° out phase were considered. At the beginning, the results for the proportional load are presented in Fig. 50a. The trend of the curves follows the behavior described in Section 5.2, showing earlier failure initiation for greater load ratio, which is correlated with shorter material fatigue load. In Fig. 51b, the out-of-phase loading case is shown, giving the same conclusion. The higher load ratio leads to earlier failure initiation and shorter life, respectively.

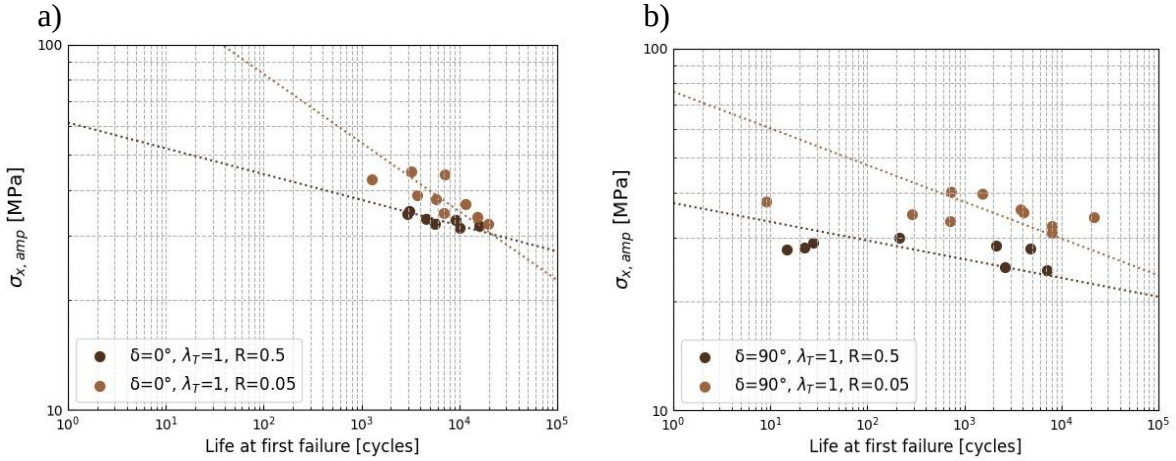

Fig. 51. S-N curves for first failure for the multiaxial fatigue testing of CFRP $[\pm 30]_{FW}$ on tubular specimens for a) in phase, b) 90° out of phase load

The impact of phase shifting for the following load ratios is presented in Fig. 52. There is a clear indication of negative influence of out of phase loading. When the S-N curves plotted are considered, damage begins earlier compared to phase loading, directly affecting fatigue lifetime.

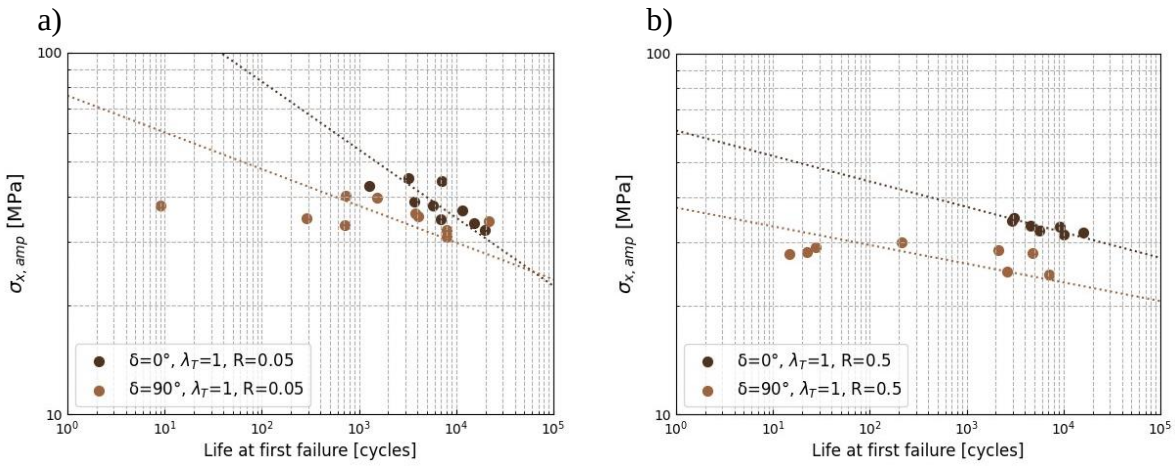

Fig. 52. S-N curves for crack saturation at CDS point for the multiaxial fatigue testing of CFRP $[\pm 30]_{FW}$ on tubular specimens for a) R = 0.05 and b) R = 0.5

6.3 Post failure analysis

The damage analysis supported by micro computed tomography (μCT) and visual observation gave an overview of the fracture behavior of the thin – walled specimen CFRP under cycling load. The results presented in this subsection aim to describe the material fracture in terms of the initation (microscale damage) and growth (mesoscale damage). Several specimens after multiaxial fatigue test were chosen for visual inspection, the pictures of the specimens are shown in Fig. 53.

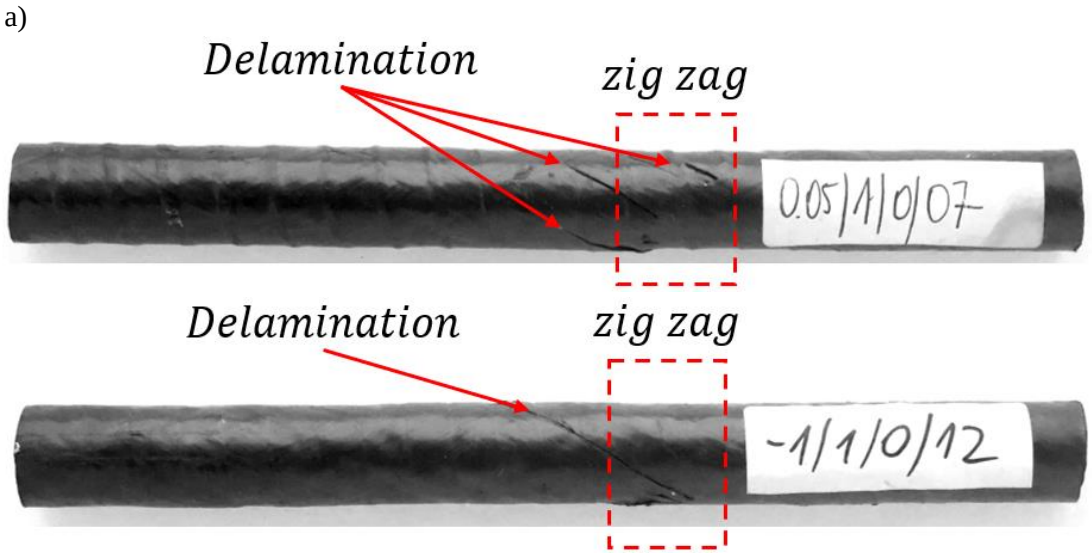

b)

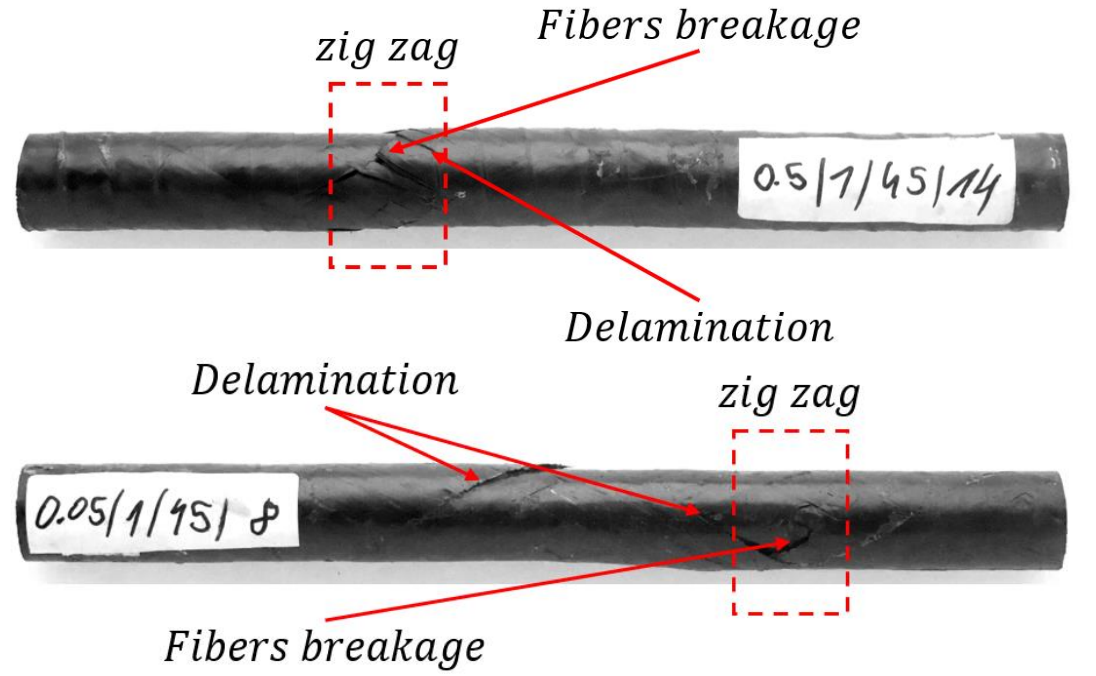

a)

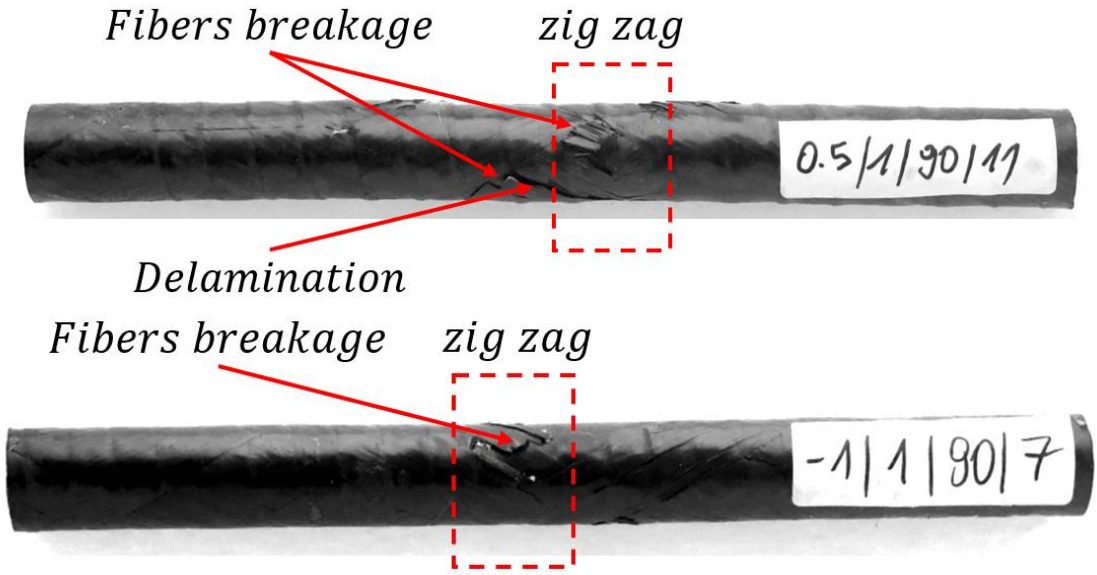

Fig. 53. Post-failure samples after a) in phase load, b) 45° out of phase, and c) 90° out of phase load case

The final failure can be reported on the basis of Fig. 53, the delamination and fibers breakage cause the loss of material integraity in the last several cycles. As soon as the cracks reach equilibrium or saturation spacing, interfacial debonding, and cracks coupling govern damage development. Delamination driven by strong interlaminar stresses along the alternating layers starts when the fracture area reaches a critical size due to crack growth and coupling. Due to the lack of a contrain layer (only two off-axis composite layer), the complete material decohesion due to delamination and fiber breakage occurs within several hounderd cycles.

Analysis of zig zag area

Having a closer look on the zig-zag area allowed showing the failures complexity. The failure area shown in Fig. 54 is a combination of two failure modes visible at first glance. It is fiber breakage through thickness and delamination. The final stage of fatigue life characterized by fiber breakage in zig – zag area occurs due to the large compression caused by the external layer on the internal layer at the place of layer undulation (zig – zag). The highlighted figure confirms the results from the numerical analysis as places of maximum stresses.

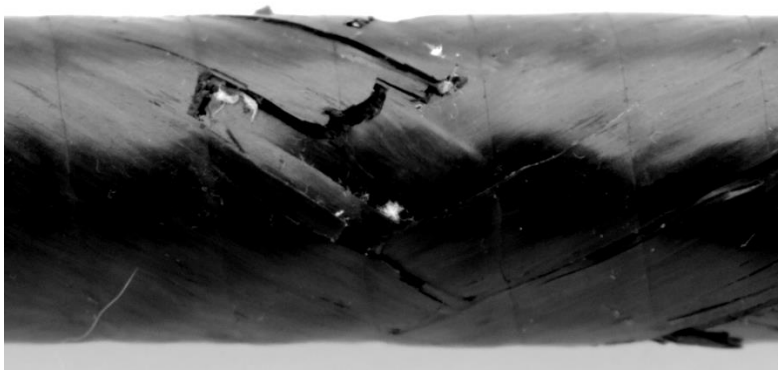

Fig. 54. Sample failure in the interweaving area

μCT analysis after multiaxial fatigue test

Microstructure analysis was possible by scanning the entire sample by microcomputed tomography. It is a nondestructive imaging technique to produce 3D images composed of 2D transaxial projections of a specimen. It allowed to obtain full 3D image of the microstructure with void volume content. The results are presented in Fig. 55 and Fig. 56 in the form of 3D geometry and transverse and longitudinal specimen cross sections. Considering the results in Fig. 55, the crack areas with various sizes are exhibited, as it was expected the fiber direction governs the direction of crack propagation. There are also white areas with irregular shapes, which indicate the delamination areas. The chosen sample exhibits a life of approximately 600 000 cycles. Excluding the gripping part of the sample (60 mm from both sides) the failure appears along the entire gauge length. The total length of the sample is 220 mm, and within this length, at least three zigzag areas are located. The damage observed after cycling load showed that there might be damage initiation at different zig-zag areas, and it coalesces by delamination, as is shown in Fig. 55b.

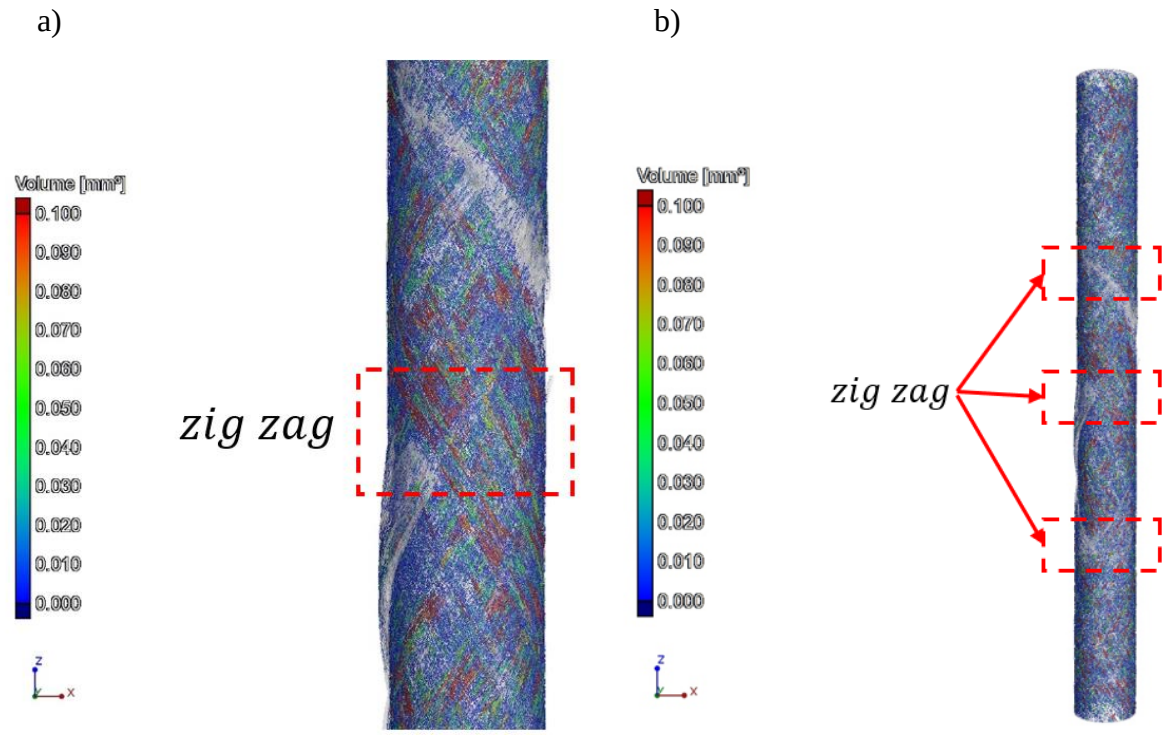

Fig. 55. Volume content of specimen after multiaxial fatigue test

The cross-sectional view of the specimen shows a clear indication of delamination as well as fiber breakage through specimen thickness. In Fig. 56, the transverse and longitudinal cross section in the zig-zag area in the middle length of the sample is presented.

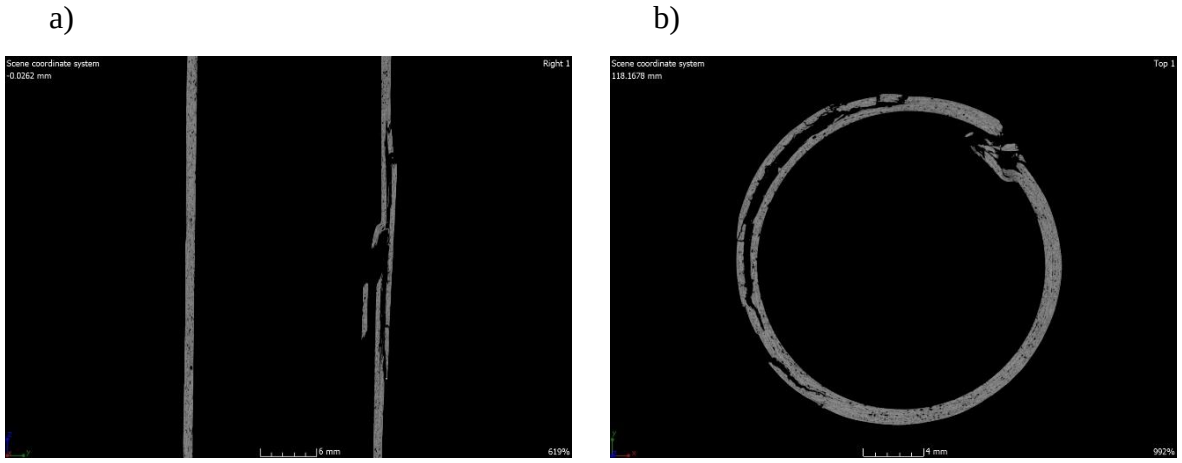

Fig. 56. Cross section of samples after fatigue test from µCT scan, a) longitudinal direction, b) transverse direction

The development of damage is shown in Fig. 57, based on the numerical analysis and optical observation, the failure initiates at the maximum damage value and is given at area no I (resin rich area). Plane A – A is a critical plane, which gives the direction of failure; however, the fracture plane is given by the red arrows, which refers to the growth direction of the delamination. Delamination initiates if the area between I and II reaches a critical fracture size. The delamination will grow along the final fracture plane, oriented 60° counterclockwise along the fibers (red arrows); this failure stage progresses rapidly. The failure area I – II is the object of interest from the use of damage parameter, it is a place of damage initiation (matrix cracking)

and small crack propagation (microcrack growth, coupling and debonding). As soon as the initiation phase reaches critical size, delamination and fiber breakage cause a decrease in axial and torsional stiffness, leading to the final fracture.

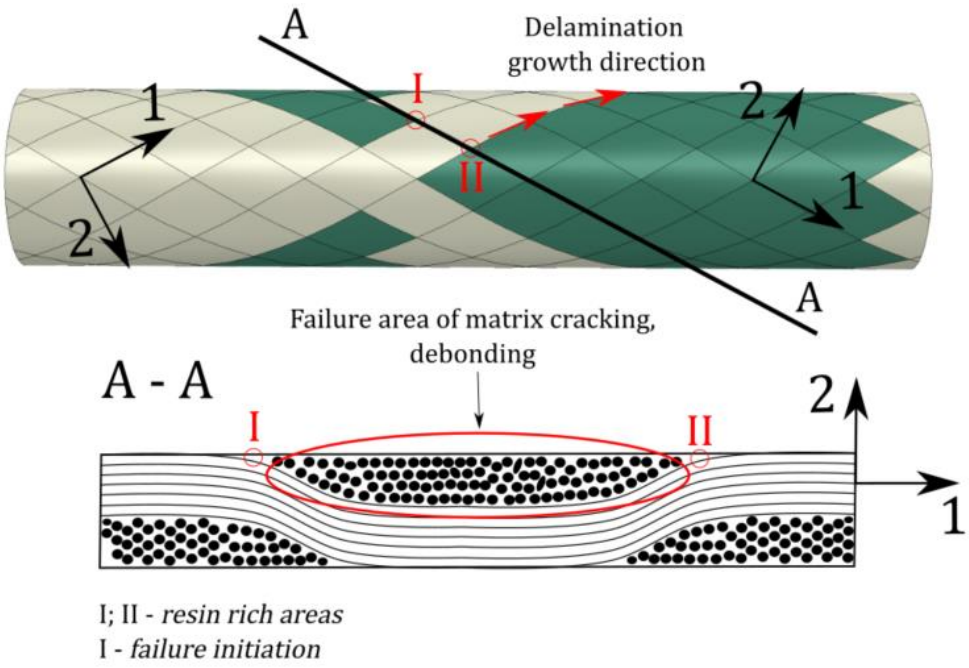

Fig. 57. Damage initiation and propagation observed in FW tubular with mosaic pattern 1/1

6.4 Summary

To summarize observations from Chapter 6, the following conclusions can be drawn:

- Analysis of damage evolution in the form of cumulative counts curve indicates the absence of a stable macrodamage growth in terms of 45° out-of-phase load. The results suggest that the initation phase and small crack growth cover most of the total fatigue life. On the other hand the propagation phase is relativly short, which might be expalined by sudden and unstable propagation of delamination. This fact is reported in [63] and expressed as a lack of additional layer, which should provide a constraint effect for stable growth of damage.
- The negative effect of mean stress is also confirmed by the data provided for the first failure gradient (based on AE), showing that the failure initiation occurred earlier for a greater load ratio. Also, the detrimental effect of the 90° out-of-phase load is recognized, which by the early initiation of failure decreases the fatigue life.
- The S – N curves delivered for the first failure gradient give the possibility of designing composite structures reinforced with continuous fibers for short and long service operations without the presence of damage. These data also confirm the applicability of acoustic emission in early damage detection for in-service parts, based on the S – N curves delivered for particular composite material, without applying any sophisticated analysis.

- The post failure visual observation of the specimens allowed to define two failure mechanisms i.e. fibers breakage and delamination. Those failure mechanisms were confirmed by conducted μCT analysis.
- In general, the results show that most life is governed by damage initation (crack nucleation and small crack growth at the microscale) occurring in the zig-zag area. The macrodamage growth is observed on the basis of the displacement and rotation curves within the last hundreds of cycles.

7 Modeling of multiaxial S-N behavior

This chapter presents the S-N results in the form of the material stress component based on the stress analysis performed and the modyfied damage parameter by Fatemi – Socie. At the beginning, stress analysis is introduced for the defined critical point, which gives the stresses. Consequently, the impact of the phase shift and mean stress on the results is plotted and discussed. The objective of this chapter covers the possibility of a new approach for analyzing fatigue data under multiaxial loading conditions, including the mean stress effect.

7.1 Stress analysis

The fatigue experimental campaign was carried out under constant biaxiality ratio (λ_T) determined by geometrical stresses; however, due to material complex nature (fiber orientation, interweaving areas, layup configuration) those stresses do not precisely define the material stress state. Mechanics of materials, in terms of composite materials, is based on the stresses according to the material coordinate system denoted 1 – fiber direction, 2 – direction perpendicular to fiber, and 3 – direction perpendicular to plane 12, which are the principal stresses of the lamina. To define those stress components, the analysis is performed using the finite element method at the mesoscale (homogenity of the lamina). As multiaxial loading conditions are investigated, another biaxiality ratio must be introduced according to Eq. (11). The biaxiality λ_{12} provides the ratio between τ_{12} and σ_2, and in high cycle fatigue regime those components play significant role as the fatigue material behavior is govern by matrix – dominant failures. Since the initation of damage is considered, two major failures should be taken into account, i.e. matrix cracking and crack coupling (debonding) as presented in Fig. 58. Both failures are covered as the mesoscale stresses are considered.

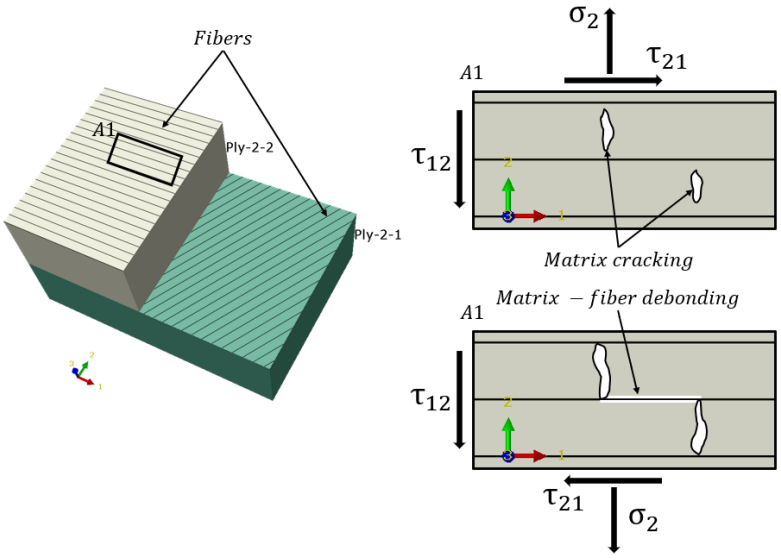

Fig. 58. Crack development and its coupling under τ_{12} and σ_2 stress components

The analysis began with the identification of the critical stress point based on the numerical analysis performed. The maximum stresses defined for the critical point are considered as the initiation place of failure and are used in the fatigue analysis provided in this chapter. The finite element analysis for the multiaxial loading conditions showed that the critical stress point is in

the area of interweaving, where the local stress concentration occurs due to fiber undulation. This point is shown in Fig. 59 and is represented by node no. 185. The stresses were calculated for the internal layer at the middle integration point of the composite layer. Numerical analysis was performed for the axial load range of -2800 N to 8300 N and the torque of -31 Nm to 87 Nm, which directly reflects the load range applied in the experimental fatigue campaign.

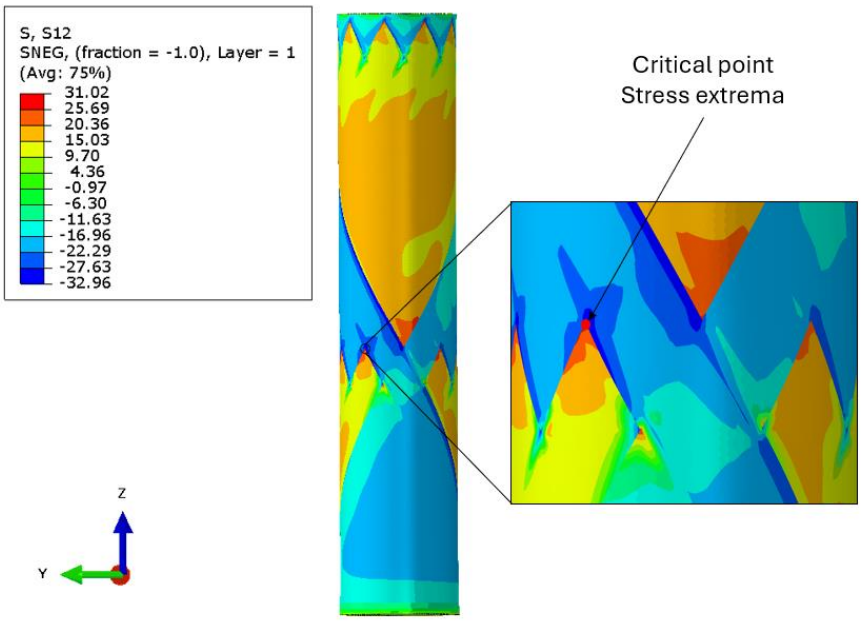

Fig. 59. Stress extremum point for S12 (τ_{12}) at the zigzag area taken from the external surface at the bottom integration point for the layer [MPa]

Considering the biaxiality (λ_{12}), the value of the ratio is not constant due to the shear stress nonlinearity presented in Fig. 60 especially in the range ±2 kN. Some nonlinearity is also observed for σ_1 component, which for tension load gives compression stress and reverses in opposite direction. On the other hand, remaining σ_2 The component exhibits linear behavior in tension and compression. The stress history versus the applied force presented in Fig. 60 gives the stress functions for the critical point at node 185 for the internal composite layer.

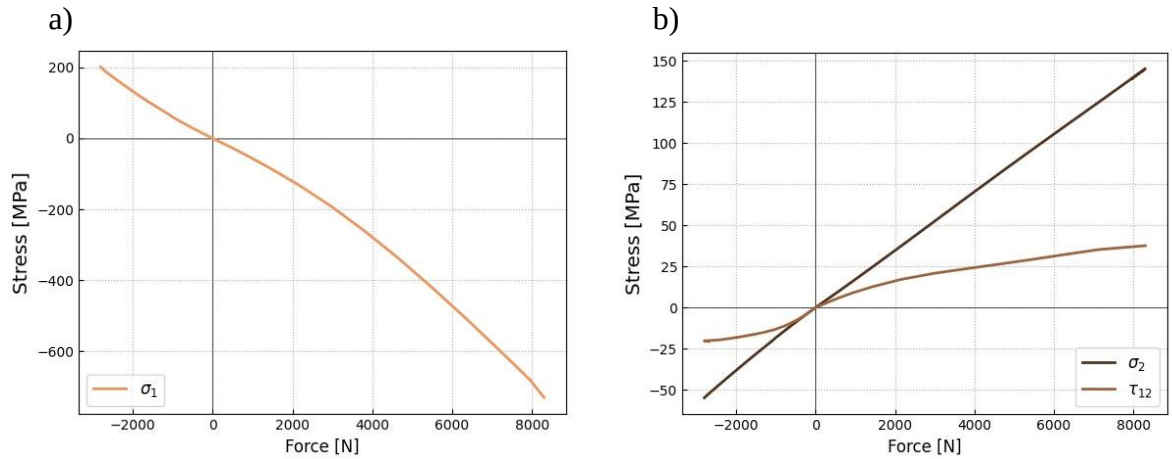

Fig. 60. Stress history for a) $\sigma_1$and b) σ_2, τ_{12} over the force range from -2.8 kN up to 8.3 kN for node 185

The biaxiality λ_{12} calculated based on the stress analysis performed for each load level is presented in Table 16.

Table 16. Biaxiality ratio calculated for investigated load ratios

	R = -1	R = 0.05	R = 0.5
λ_{12}	0.35	0.25	0.18

The stress distribution exhibits an inhomogeneous nature, which is presented in Fig. 61, and was confirmed by the DIC method. Additionally, the complex structure of composite materials gives various stress distributions on each composite layer, because the stresses need to be plotted for each layer separately. On the basis of the results, the samples can be divided into two regions between zigzag areas with approximately similar stress ranges. Those areas with an alternating fiber orientation $\pm 30°$ provide different stress levels. Except for that, the large stress gradient is observed in the zigzag area, which was discussed. These results confirm the need to model the FW geometry, including the zigzag areas. Based on the stress analysis, it can be concluded that the internal composite layer gives greater stress values.

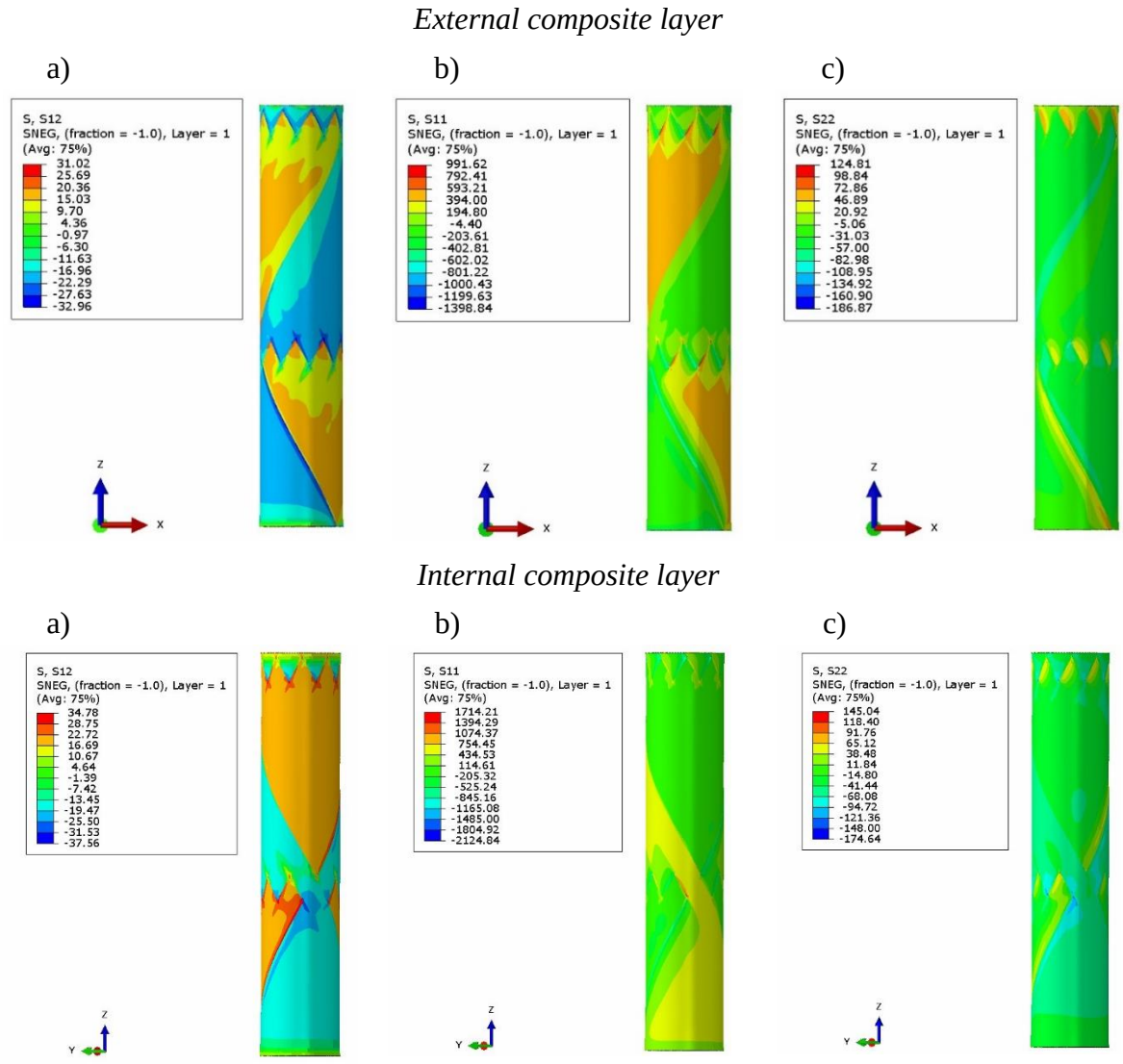

Fig. 61. General stress field for the internal and external composite shell for the following components a) shear stress (τ_{12}) b) normal stress (σ_1) and c) normal stress (σ_2) on the external surface [MPa]

The alternating stresses were analyzed for different phase shifting and stress ratios. The exemplary stress paths for R = 0.5 for each phase shifting are presented in Fig. 62 – 64. Based on those data, particular stress components were delivered for each load level and analyzed. As can be noticed, the shear stress nonlinearity causes the stress path deformation.

a)

b)

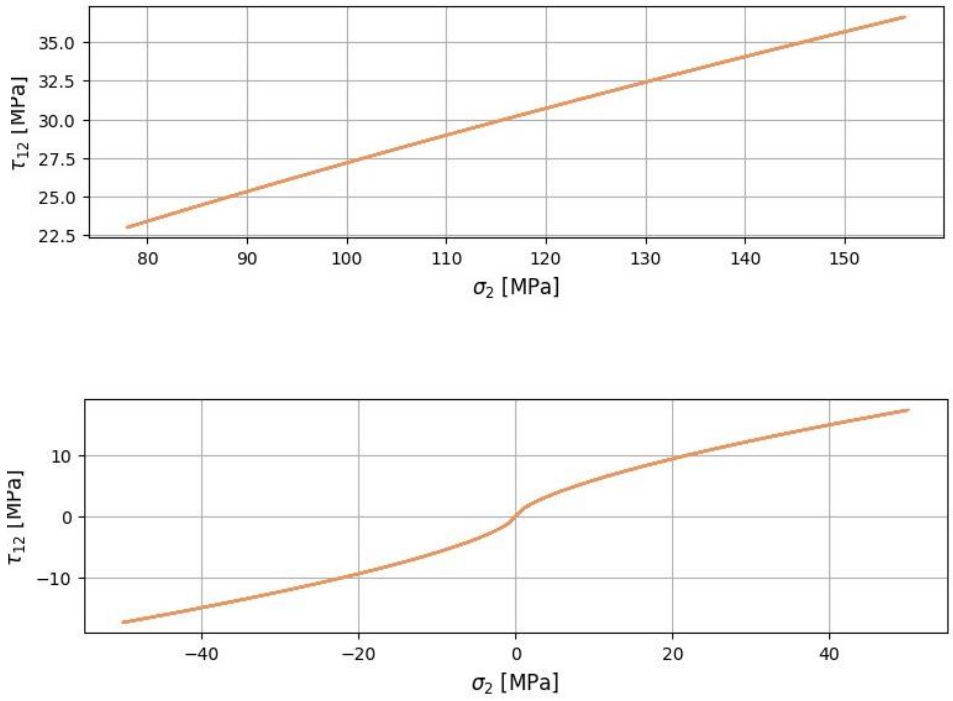

Fig. 62. Stress path (τ_{12} vs σ_2) for proportional loading for a) R = 0.5 and b) R = -1

a)

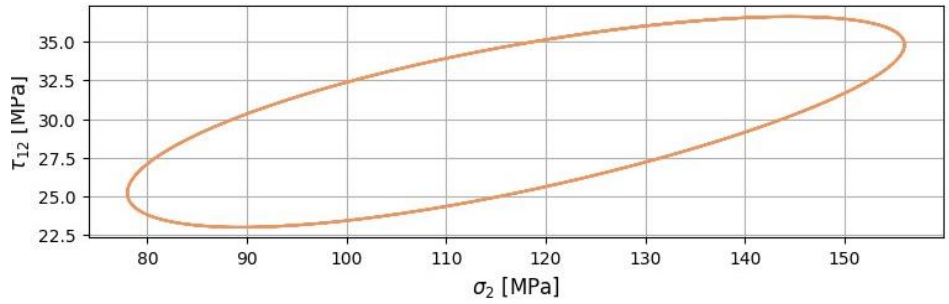

b)

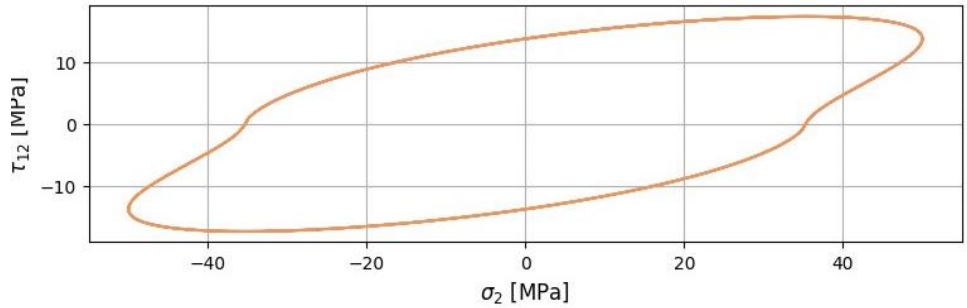

Fig. 63. Stress path (τ_{12} vs σ_2) for nonproportional loading (45°) for a) *R* = 0.5 and b) *R* = -1

a)

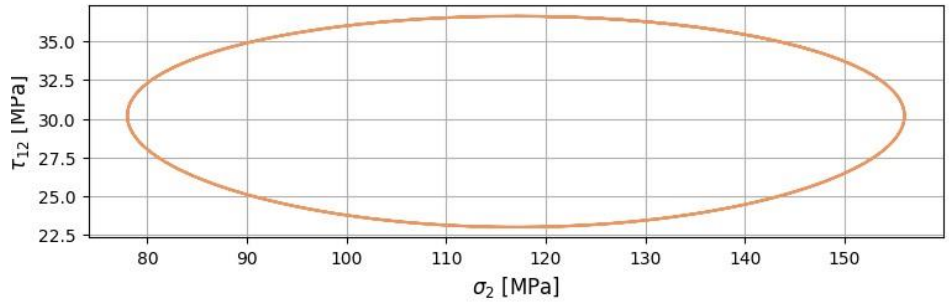

b)

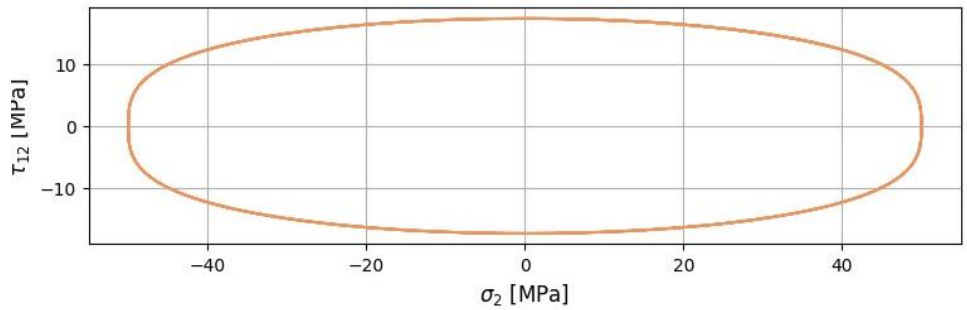

Fig. 64. Stress path (τ_{12} vs σ_2) for nonproportional loading (90°) for a) *R* =0.5 and b) *R* = -1

This sub-chapter provides the importance of the stress components chosen in the development of failure mechanisms and their importance in fatigue analysis. Moreover, numerical analysis shows the critical point for the stresses that need to be analyzed.

7.2 S-N multiaxial fatigue behavior

The stress analysis conducted allowed to define stress components for the entire FW structure. In the modeling process, the critical point described in the the previous subsection is considered. The presented S-N curves are plotted for amplitude of τ_{12}, the value of biaxiality ratio given for each load ratio allowed to calculate the corresponding amplitude of σ_2. At the beginning, the results are presented separately to show the scatter bands obtained. The data for in-phase load is presented in Fig. 65, the assumed scatter band of 2, fits well the results. On the other hand, the load ratio 0.5 provides an even lower scatter band.

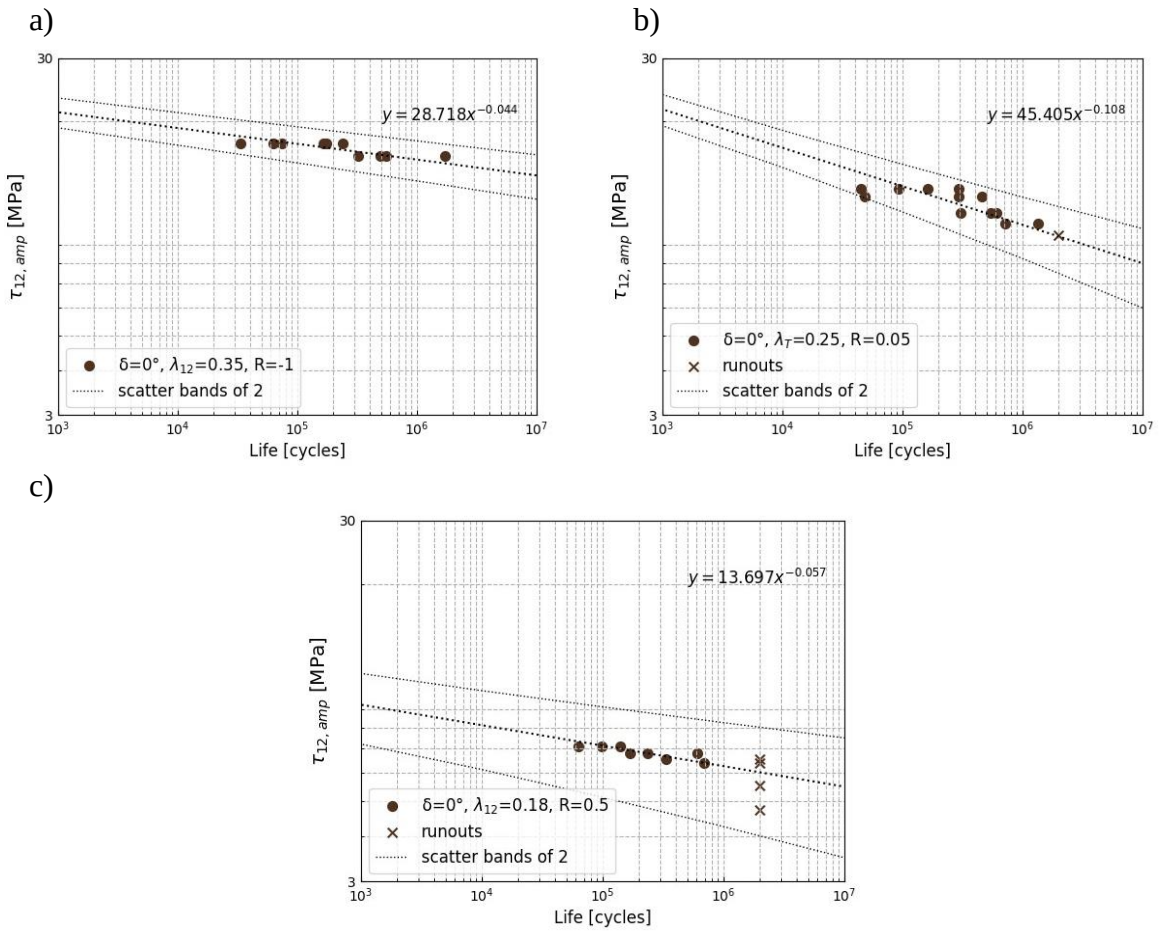

Fig. 65. S-N data for the material shear stress component for proportional loading for a) R = -1, b) R = 0.05, and c) R = 0.5

For the 45° out-of-phase results presented in Fig. 66, the largest scatter band can be observed for R = 0.5. In this case, two points are outside the scatter band of 2. For R = -1, the scatter does not cover 1 point. In case of a negative load ratio, an improper failure could have been reached, due to material sensitivity to microstructural discontinuity under compressive load.

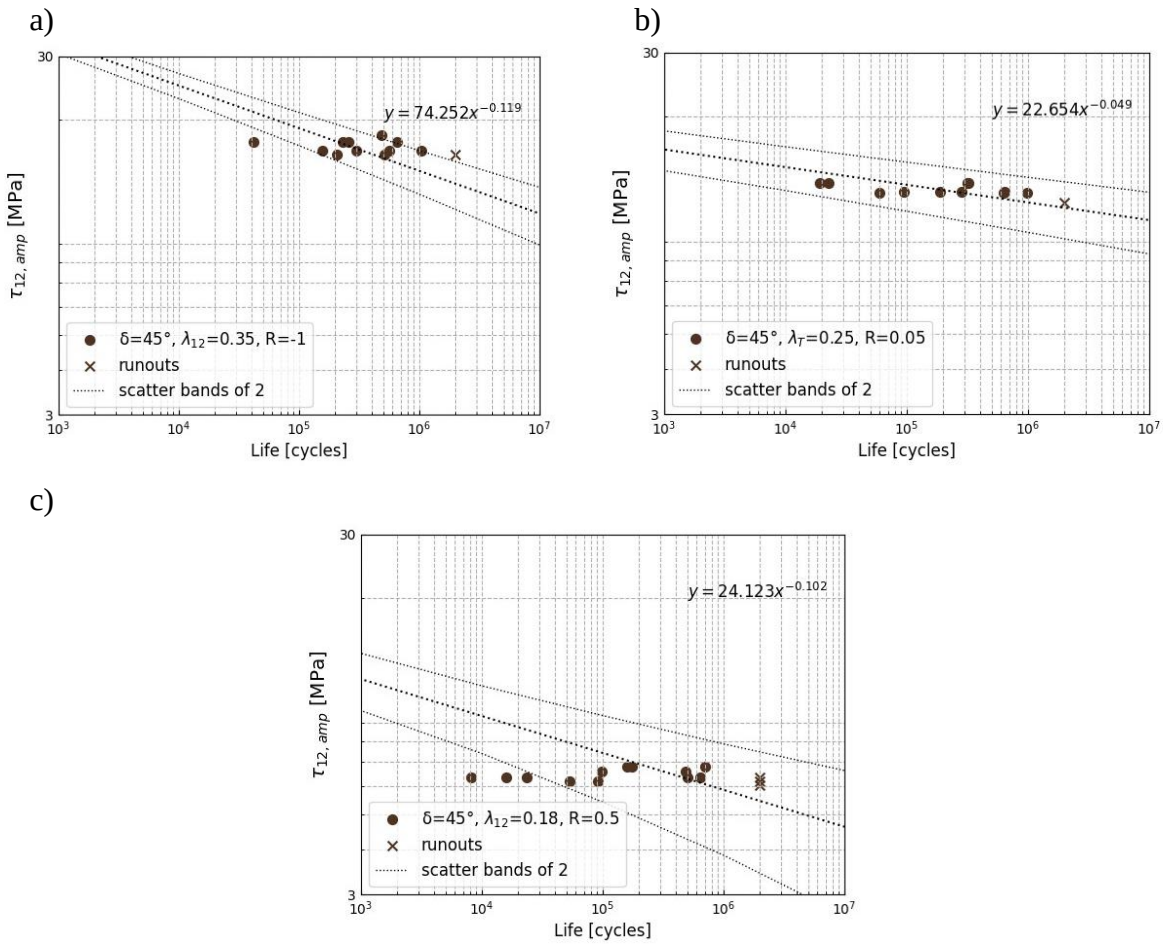

Fig. 66. S-N data for material shear stress component for 45° out of phase loading for a) R = -1, b) R = 0.05, and c) R = 0.5

The 90° phase lag provides well correlated results, all points are covered by scatter band of 2, and in case of R = 0.5 could be reduced.

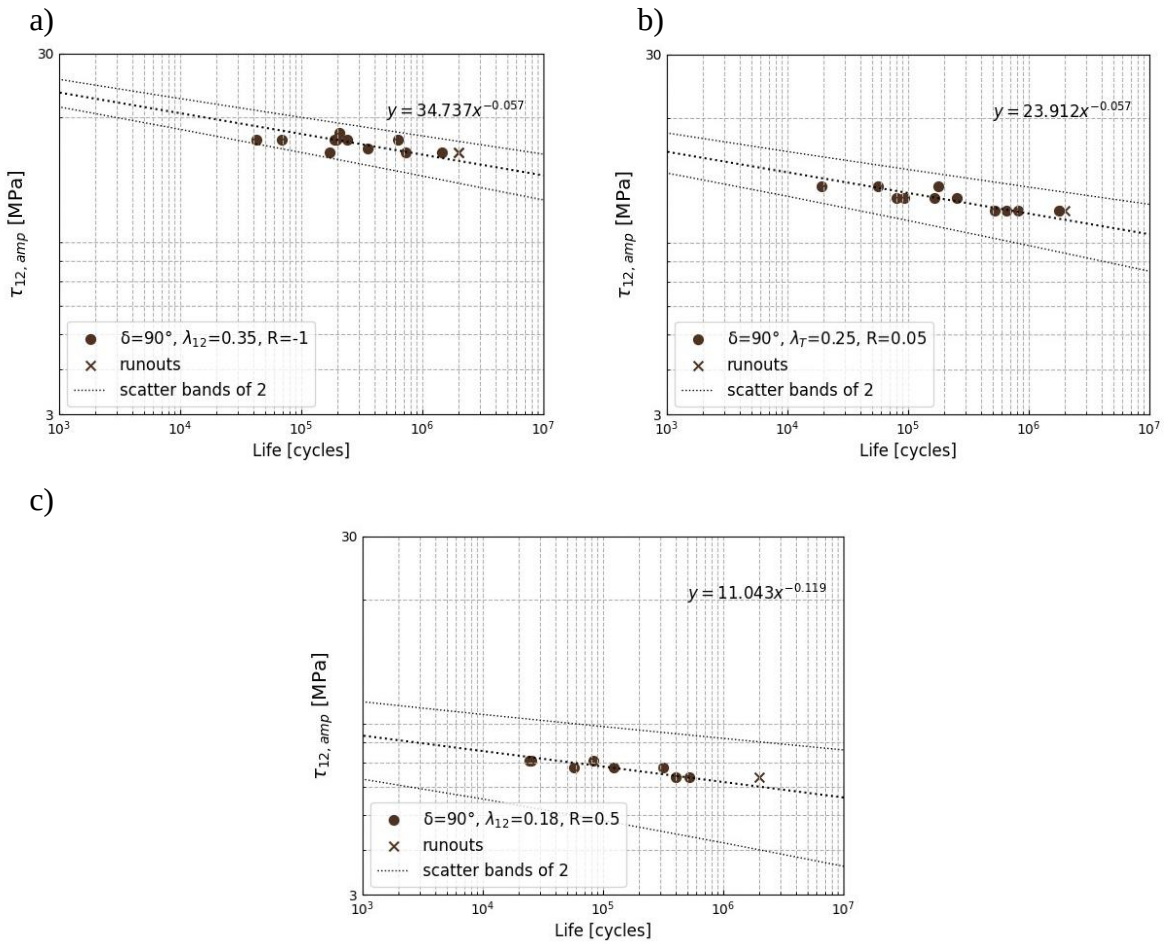

Fig. 67. S-N data for material shear stress component for 90° out of phase loading for a) R = -1, b) R = 0.05, and c) R = 0.5

The comparison of the regression data obtained is given in Table 17. The smallest R^2 is observed for phase shift 45°.

Table 17. Regression analysis data for mesoscale stresses calculated by FEA

Data set	Regression equation	R^2
$\delta = 0°; R = 0.05$	$y = 45.405x^{-0.108}$	0.7403
$\delta = 0°; R = 0.5$	$y = 13.697x^{-0.057}$	0.6100
$\delta = 0°; R = -1$	$y = 28.718x^{-0.044}$	0.4400
$\delta = 45°; R = 0.05$	$y = 22.654x^{-0.049}$	0.1906
$\delta = 45°; R = 0.5$	$y = 24.123x^{-0.102}$	0.0816
$\delta = 45°; R = -1$	$y = 74.252x^{-0.119}$	0.0107
$\delta = 90°; R = 0.05$	$y = 23.912x^{-0.057}$	0.6251
$\delta = 90°; R = 0.5$	$y = 11.043x^{-0.119}$	0.8020
$\delta = 90°; R = -1$	$y = 34.737x^{-0.057}$	0.5089

Phase-shifting effect

According to Fig. 68, the impact of load proportionality is shown for two different load ratios. The correlated regression curves exhibit a different nature; however, it cannot be explicitly determined.

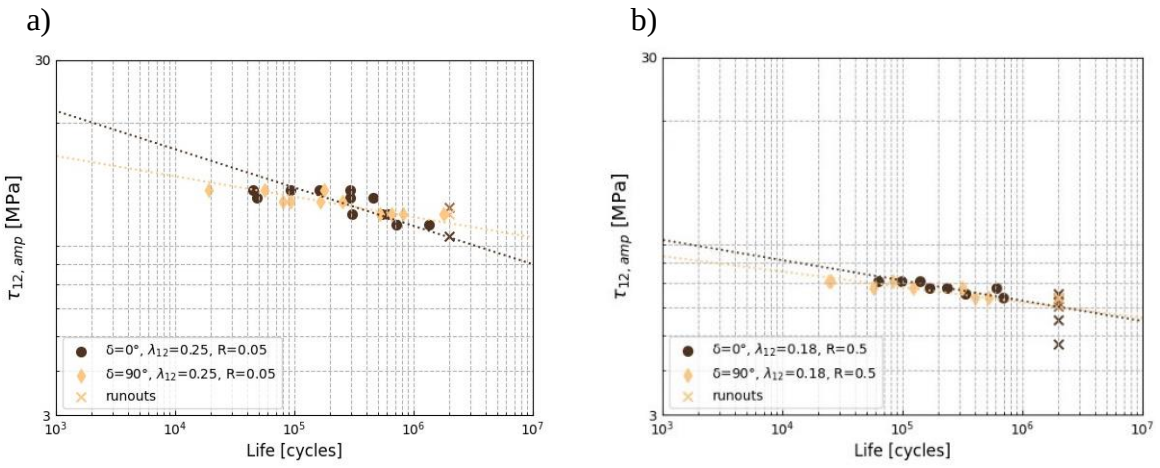

Fig. 68. Impact of phase shift on multiaxial fatigue data for a) R = 0.05 and b) R = 0.5

From the modelling point of view, there is no significant impact of phase shifting on the fatigue life. The comparison for remaining results for 45° and R = -1 is presented in Fig. 69.

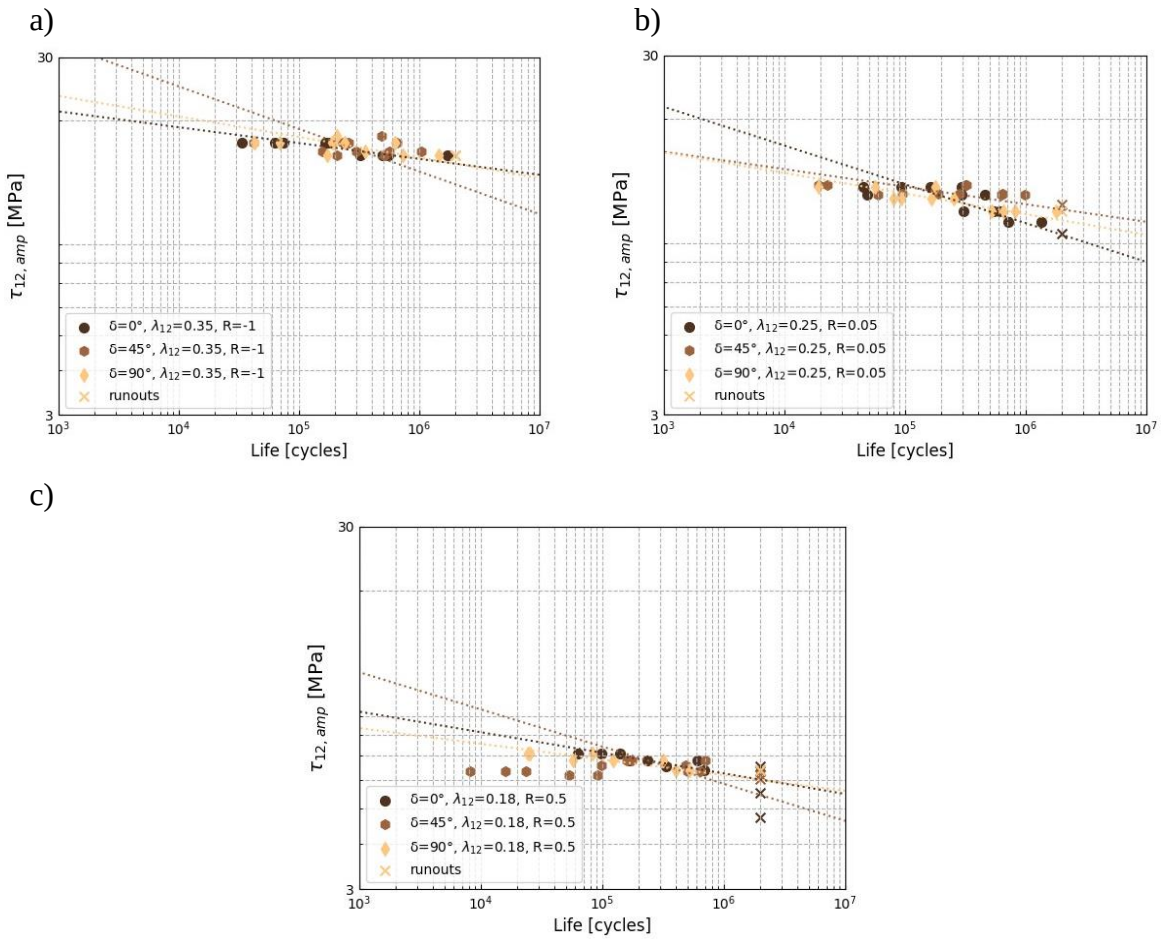

Fig. 69. Impact of phase shift on multiaxial fatigue data for a) R = -1, b) R = 0.05 and c) R = 0.5

Mean stress effect

The S-N curves highlight the mean impact of stress on fatigue lifetime in the CFRP specimen. In general, the mean stress effect is observed for each phase shift. However, it should be noted that there is another factor that could hide the full impact of the load ratio. The biaxiality ratio, which, due to nonlinearity of the stress, varies in the range of 0.18 to 0.35, gives a slightly different stress state in the material. The research on the biaxiality ratio in reference [63] confirms a clear and detrimental effect of the shear stress component on fatigue strength; Due to this, the results are plotted for the shear stress amplitude, which allowed comparison of the results. The differences for $\sigma_{2,amp}$ The stress component is relatively small and does not provide a significant impact on the scientific literature investigated.

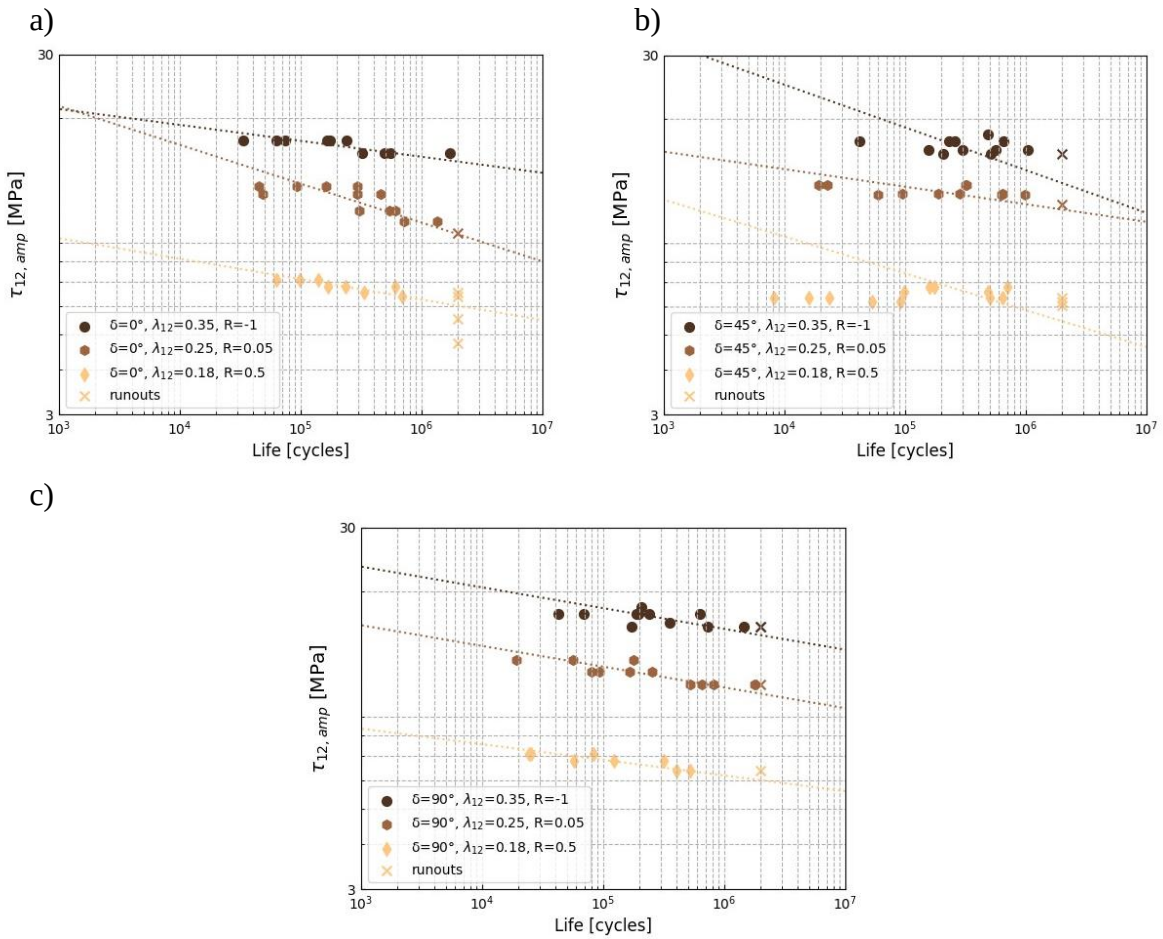

Fig. 70. Mean stress impact on multiaxial fatigue data for a) δ=0°, b) δ=45°, and c) δ=90°

The results provided in 48 show that for each load case, the load ratio R = -1 gives the highest fatigue strength due to the zero-mean value, and is the reference. When the load ratio is increased to R = 0.05, a noticeable reduction in fatigue strength can be observed. The lowest fatigue strength can be expected due to the highest mean value by the load ratio R = 0.5. The sensitivity of CFRP material to mean stress is significant and noticeable in terms of out-of-phase and in-phase loading conditions, reducing its life drastically.

7.3 Critical plane damage model

The critical plane approach was applied to this research to describe the damage state in the CFRP material, properly defined damage in the material allows to exclude the impact of parameters that influence fatigue life i.e. load non-proportionality and mean stress. For this purpose, the Fatemi – Socie damage parameter was redeveloped for the investigated composite material. The S-N data for proportional 90° out of phase for positive load ratios were considered since the unambiguous impact of out of phase and mean stress was defined in this case.

The Fatemi-Socie (FS) damage parameter [110] is a physics-based critical plane parameter used for the prediction of fatigue life of metallic materials under multiaxial loading conditions. The original form of the FS damage parameter is given by Eq. (20).

$$D = \frac{\Delta\gamma_{max}}{2}(1 + k\frac{\sigma_{n,max}}{S_y}) \tag{20}$$

where $\Delta\gamma_{max}$ is a maximum shear strain range, $\sigma_{n,max}$ is a maximum normal stress corresponding to the maximum shear strain plane over the cycle, k is a material constant calibrated by superimposing pure axial and pure torsion data together and S_y is the yield strength. Taking this parameter into account, shear strain plays a crucial role and is a driver of small crack growth; on the other hand, normal stress plays a secondary role. It has an impact on friction according to the applied load; in tension, the crack growth rate increases due to the reduction in friction between the crack faces and decreases the crack growth rate in compression due to friction between the crack faces. The presented model takes into account normal mean stress, which is covered by $\sigma_{n,max} = \sigma_{n,m} + \sigma_{n,a}$, where $\sigma_{n,m}$ is a normal mean stress, and $\sigma_{n,a}$ is a normal amplitude stress.

The theory of the critical plane postulates that the initiation and growth of cracks within material appear on certain planes and that particular stresses or strains to those planes govern the fatigue crack growth process. Taking into account the investigated continuous fiber composite materials, it was necessary to modify the original form of the damage parameter. To provide physical meaning, proper failure mechanisms must be incorporated. The HCF behavior for these materials is governed by matrix dominant failure mechanisms, which require considering debonding, matrix cracking, and fiber pull-outs. The importance of the stress components that govern these mechanisms is described in Chapter 7.1. Moreover, the brittle behavior of investigated material questions the relevance of shear stress, since plasticity is not a relevant aspect (used mainly for ductile materials). Proper stress components that correspond to the driving force of these failure mechanisms should be taken into account. In terms of composite materials, the most appropriate form is to use stresses with respect to the material coordinate system, which also refers to principal stresses of the lamina. The shear stress component plays an significant role in the development of damage in CFRP material thus its range is considered crucial. In terms of $\sigma_{2,max}$, it also important, it considers the effect of mean stress value as well as impact the damage state in material. The form of the redeveloped damage parameter applied in the analysis is presented in Eq. 21.

$$D = \Delta\tau_{12}(1 + k\frac{\sigma_{2,max}}{\Delta\tau_{12}}) \tag{21}$$

where $\Delta\tau_{12}$ is a maximum shear stress range, $\sigma_{2,max}$ is a maximum normal stress along 2 - direction, k is a material constant calibrated by superimposing the fatigue data for different load cases together. Due to the insufficient data in the literature for the CFRP tube, the value of the k parameter was chosen 0.2 as suggested in [42].

Calculating damage requires finding its maximum value for the plane, which is critical to crack initiation. In terms of composite material, the plane due to stress extrema is oriented along the

fibers; however, considering multilayer composite materials, it must be calculated for each layer. The maximum value gives the orientation of the critical plane. For the investigated thin-walled CFRP specimen, there are 2 possible orientations, either -30° or 30° with respect to the specimen symmetry axis. For both cases, the value was computed at the critical point for each layer. The highest value was obtained for the internal composite layer. The orientation of the layer is presented in Fig. 71a. Simultaneously, to confirm the validity of the orientation, the results of the void analysis from μCT scan are presented in Fig. 71b. Taking into account the fracture behavior of laminated composite materials, the crack begins between the fibers and then their coalescence cases of delamination and a significant drop in stiffness.

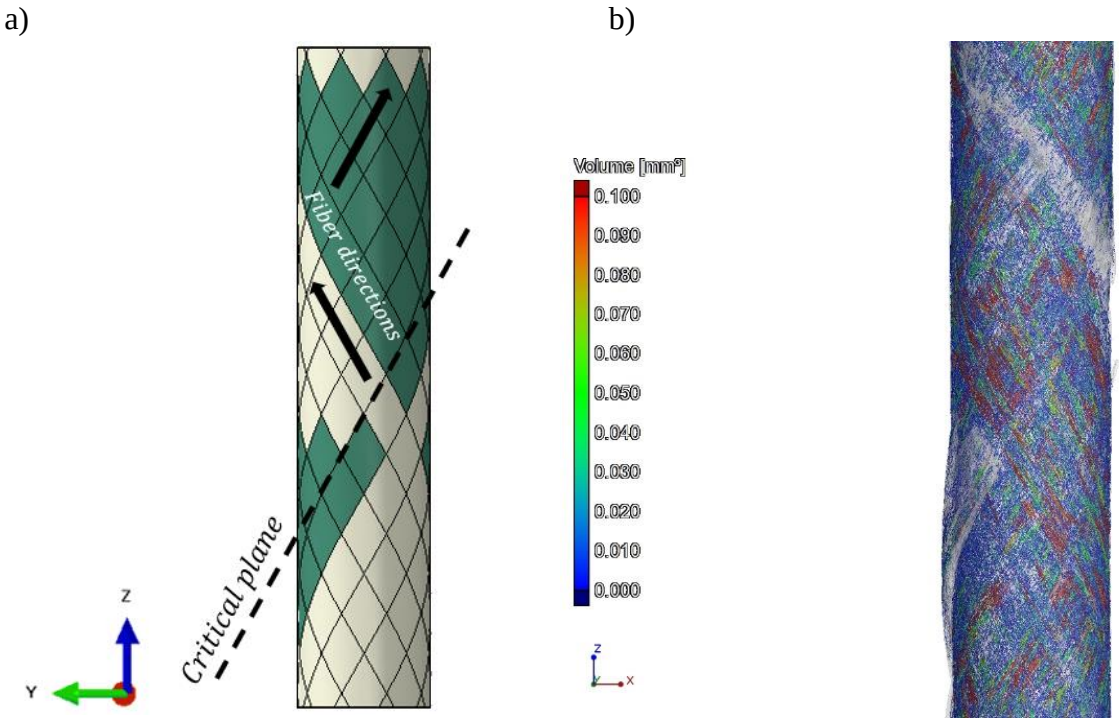

Fig. 71. a) The orientation of the critical plane with respect to the tube axis is equal to the fiber orientation 30°, b) void content in the CFRP material after multiaxial fatigue test

Results for multiaxial fatigue

As the clear impact of mean stress and phase shift was recognized for the particular data set, the same set was used for damage calculations. The correlation of the results for multiaxial data fits within the scatter band of 5. The mean stress effect is taken into account, and its accuracy can be observed in Fig. 72.

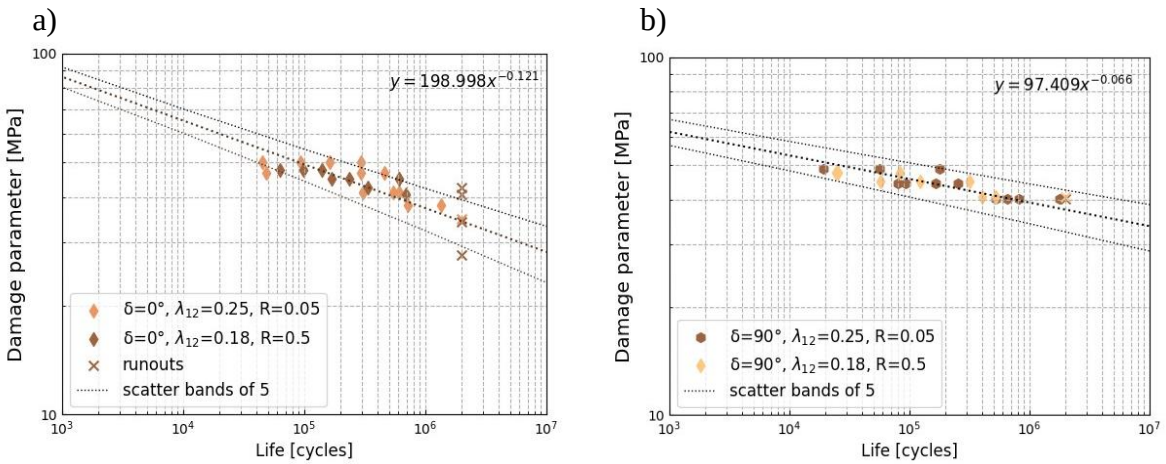

Fig. 72. Multiaxial fatigue data correlation of CFRP using the damage parameter *D* [MPa] in scatter bands of 5 for a) $\delta = 0°$; and b) $\delta = 90°$

The entire data set is plotted in Fig. 73. As can be seen, the data correlate well using the proposed damage parameter within the scatter band of 5. The reference line was approximated using regression analysis (described by the power law), with the following parameters: A = 135.826, B = -0.092. The presented S-N curve exhibits the effectiveness of the applied damage parameter based on stresses. It takes into account the mean stress and the phase-shifting effect.

a)

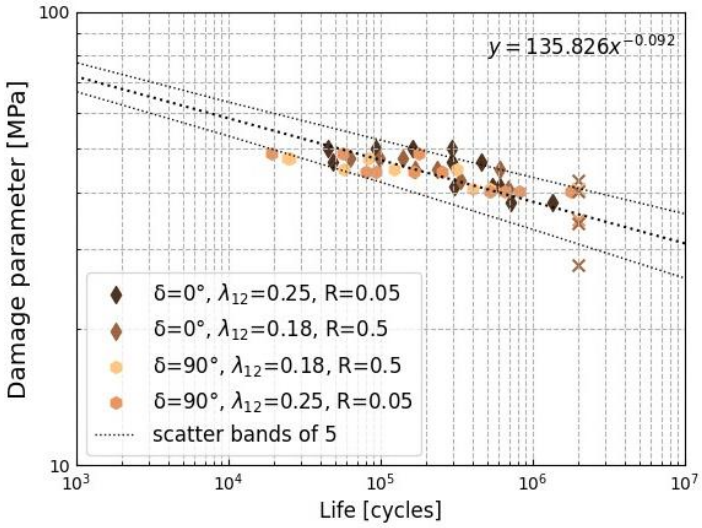

b)

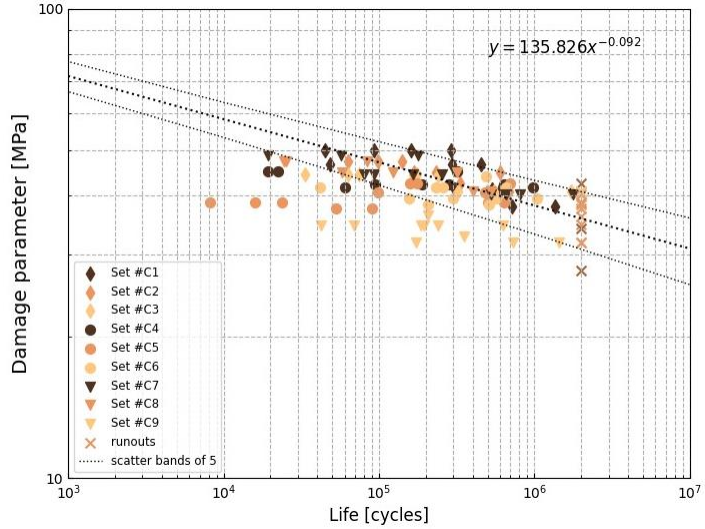

Fig. 73. Multiaxial fatigue data correlation of CFRP using damage parameter D [MPa] in scatter bands of 5, where C1 ($\delta = 0°, R = 0.05$), C2 ($\delta = 0°, R = 0.5$), C3 ($\delta = 0°, R = -1$), C4 ($\delta = 45°, R = 0.05$), C5 ($\delta = 45°, R = 0.5$), C6 ($\delta = 45°, R = -1$), C7 ($\delta = 90°, R = 0.05$), C8 ($\delta = 90°, R = 0.5$), C9 ($\delta = 90°, R = -1$)

Fig. 73 shows that sets C5 and C9 are almost completely outside the scatter band, showing a flat nature. It may result in instability on different length scales, especially under R = -1. Considering the buckling phenomenon controlled by the fibers, the failure is governed by normal stress along fibers (σ_1), which is not considered in the applied damage parameter. The numerical study on global buckling conducted in Chapter 4.3 gave a relatively large safety margin and suggests that instability can occur at the microscale rather than the macroscale. The source of large scatter and the flat nature of the data for 45° out of phase load was not recognized.

Regression analysis of the data sets

To show the difference in regression curves, the data were plotted separately in Fig. 74. As can be noticed, the regression for R = 0.05 in phase loading exhibits a larger slope compared to others that give approximately similar gradient.

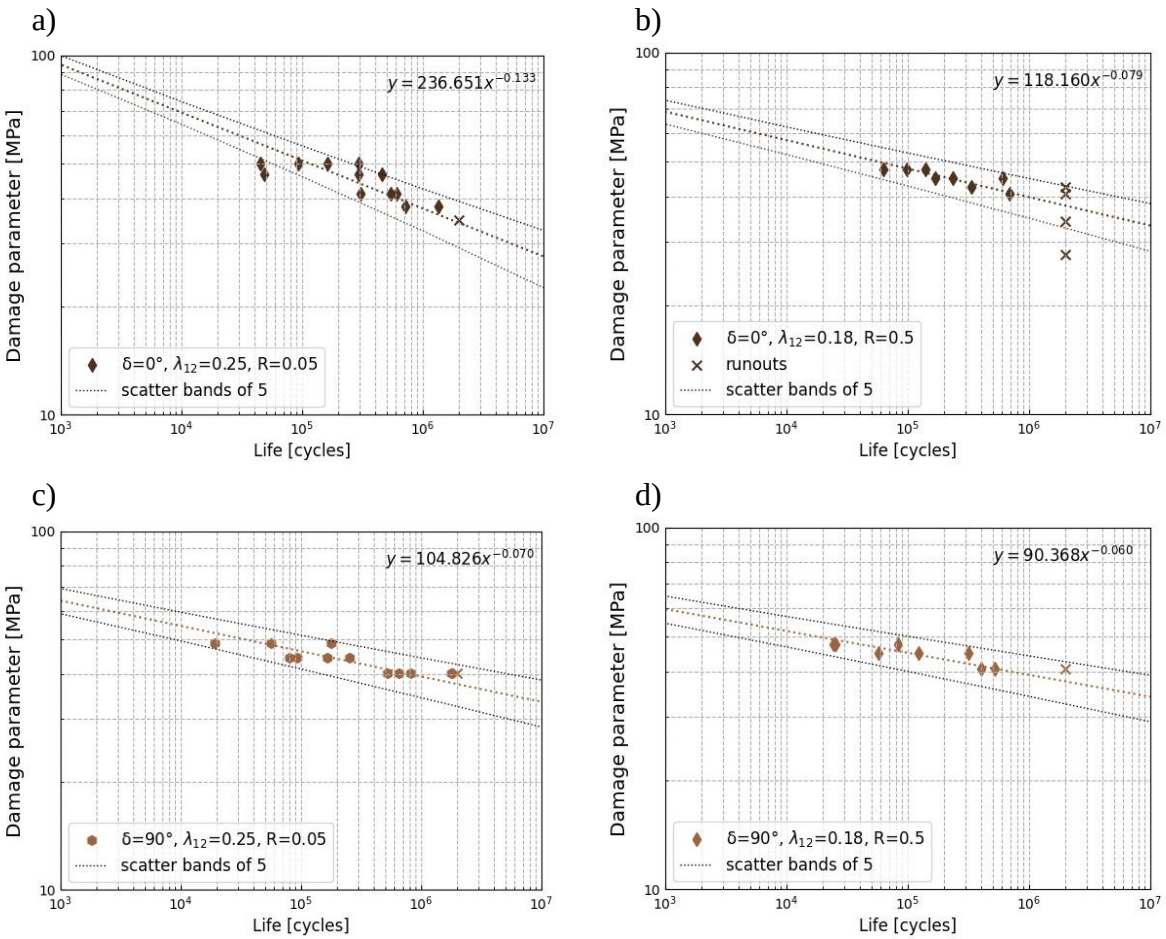

Fig. 74. Regression analysis of the multiaxial data set a) R = 0.05; in phase, b) R = 0.5; in phase, c) R = 0.05; 90° d) R = 0.5; 90° out of phase for damage parameter D [MPa]

The regression analysis performed gave the following parameters presented in Table 18.

Table 18. Regression analysis data for the damage parameter D (modyfied FS)

Data set	**Regression equation**	**R^2**
$\delta = 0°; R = 0.05$	$y = 236.651x^{-0.133}$	0.7416
$\delta = 0°; R = 0.5$	$y = 118.160x^{-0.079}$	0.6109
$\delta = 90°; R = 0.05$	$y = 104.826x^{-0.070}$	0.6235
$\delta = 90°; R = 0.5$	$y = 90.368x^{-0.060}$	0.7967

7.4 Summary

The following conclusions can be drawn based on the results presented in this chapter:

- The stress analysis performed provided the stress components of the material, which more precisely reflect the behavior of the CFRP material. It can be confirmed by the noticeable impact of mean stress on fatigue strength, which is expected in these materials. The mean impact of stress on the thin-walled CFRP tube is detrimental,

significantly reducing the life of the material. However, the impact of phase shifting is not recognized on the basis of the presented results.

- Considering the scatter band of 5 obtained for the experimental data, it can be assumed that the correlation of the damage parameter with respect to fatigue life for different load ratio and phase shift defines a reasonably actual damage state within the same scatter band.
- The assumed k-parameter based on the literature seems to fit the investigated data very well, providing a reasonable scatter band.
- Analysis of the particular terms of the damage parameter equations shows that, except for the importance of the shear stress range; the stress component σ_2 plays an important role, confirmed by the significant value variance of the second term in parentheses in Eq. 21. Normal stress (σ_2) becomes more important as long as small crack growth is considered.
- Since the damage parameter is in reasonably good correlation with the data for multiaxial loading conditions covering mean stress and phase shift, it is legitimate to use the formulae for the prediction of fatigue life.

8 Application of the critical plane damage approach

Fatigue life prediction is an important aspect of the design process, which significantly reduces experimental costs. Moreover, fatigue failure is one of the most important aspects to consider when designing. This phenomenon needs to be properly defined, and an experimental study is often required due to the lack of data, especially in the case of composite materials. Experimental investigation of the material under cycling loading is time consuming and cost consuming. It requires special testing systems operated by qualified engineers. These aspects require researchers to provide an approach to estimate the durability and fatigue lifetime of the the engineering material, which improves the effectiveness of the design process. In this chapter, the prediction method based on the proposed damage parameter is shown for the experimental data delivered and the fatigue data available in the literature. The objective of this chapter is to show the applicability of the delivery approach to life prediction of continuous fiber-reinforced polymers.

8.1 Fatigue life prediction based on uniaxial tension test

The idea of modeling based on the critical plane approach is to define and describe the damage state in the material by the parameter regardless of the loading conditions, the stress ratio, and other parameters that impact the fatigue life. In this work, the damage parameter (based on the FS parameter) was presented on the basis of the material stresses considering mean stress and phase lag. The properly determined parameter covers the damage state in the material for various experimental conditions and collect data at a certain scatter band. Because of this, the S-N curve can be delivered as a function of the damage parameter versus the fatigue life. This is finally compared to the uniaxial static tensile load to superimpose the predicted S – N. The flow chart of the approach is presented in Fig. 75. The first part of the approach concerns the modeling of fatigue experimental data. On the basis of those data, life prediction can be pursued. Moreover, the modeling part confirms the applicability of the redeveloped damage parameter and its effectiveness in describing the damage state.

The presented approach for life prediction is based on the delivery of the S-N curve constructed by incorporating the two values of the damage parameter at 1 and 1 million cycles. The damage state for 1 cycle reflects the ultimate static tensile strength (UTS); on the other hand, the parameter for 1 million cycles follows an adequate uniaxial tension load that gives the same damage value as in terms of multiaxial load. The relationship between UTS and stress at 1 million cycles caused by static tensile load gives a value for the second point to predict the S – N behavior.

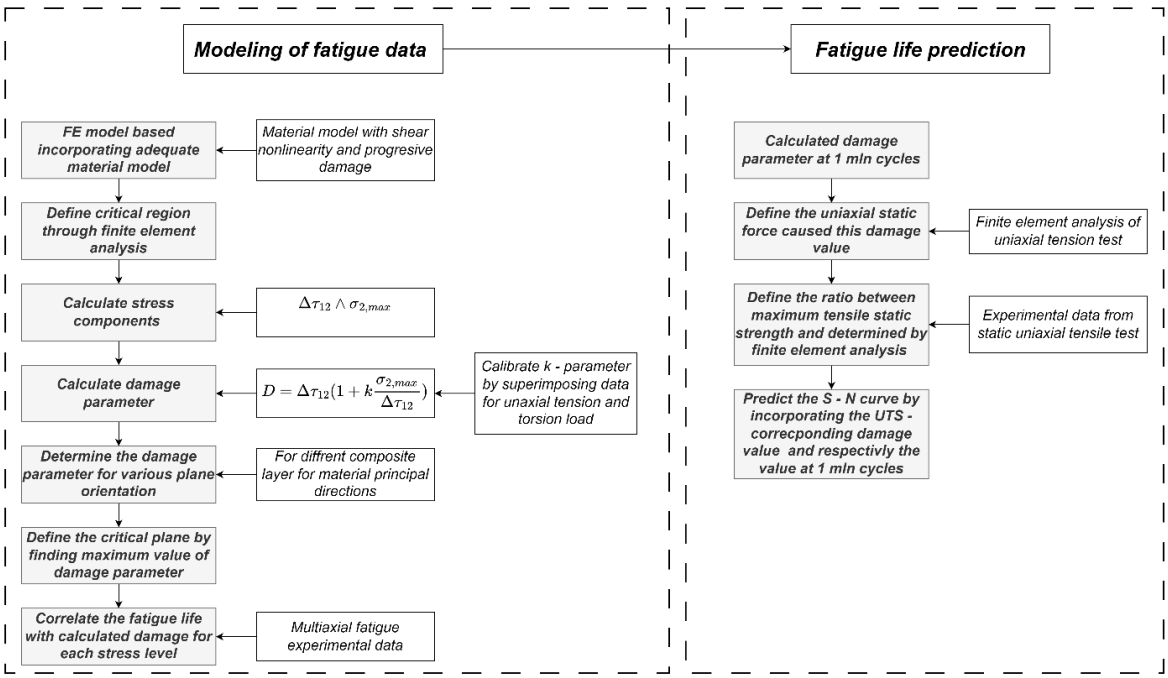

Fig. 75. The flow chart of the proposed fatigue life analysis based on the critical plane approach

The regression analysis of the data shown in Fig. 76 allowed to define the damage value for investigated data. It gives the damage parameter value of 135.8 MPa for 1 cycle, and the value of 38.1 MPa was defined for 1 million cycles.

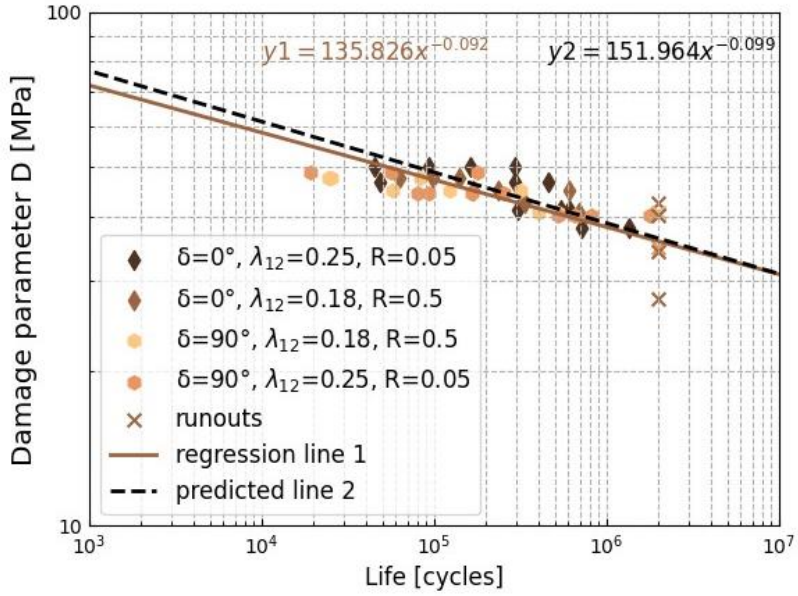

Fig. 76. Multiaxial fatigue data correlation of CFRP using damage parameter D [MPa]

To predict the S – N curve, the static uniaxial tension load was applied to the developed numerical model. The uniaxial tensile force of 6 kN gives the damage value of 38 MPa, considering the experimental maximum tensile force (23.5 kN), it is 25% of the maximum static tensile force that can be applied to predict the S – N curve. There is a small discrepancy between experimental and predicted curves, the predicted curve provides a value of 152 MPa at 1 cycle, where experimental 136 MPa. However, the HCF regime is considered and as it is shown, the

discrepancy in this life range is not significant. The delivered formulae for the prediction of fatigue for CFRP material are shown in Eq. (22).

$$\sigma_{amp} = \sigma_{UTS} N_f^{-0.10} \tag{22}$$

8.2 Applicability of damage parameter - literature data

To assess the applicability of the proposed fatigue life approach, the data for glass fiber reinforced polymer (GFRP) were collected from the literature. Damage calculation was performed for data sets presented in Table 19. The presented data cover various biaxiality and stress ratio and loading conditions i.e., apart from biaxiality equal 0, which gives uniaxial fatigue tension test, the remaining sets cover multiaxial load conditions.

Table 19. Fatigue datasets obtained from literature

Set	Reference	Layup	Biaxiality (λ_{12})	Load ratio (R)	$\sigma_{2,max}$ [MPa]	$\tau_{12,max}$ [MPa]	Fatigue life [cycles]
Set #G1	[31]	$[0_F/90_{U,3}/0_F]$	**0**	**0.05**	34.6	17.3	12 000
					34.2	17.1	6 500
					32.5	16.3	13 000
					29.5	14.8	99 000
					29.5	14.8	134 400
					27.6	13.8	215 300
					24.7	12.3	150 900
					23.7	11.8	942 300
					22.5	11.2	1 587 900
Set #G2	[31]	$[0_F/90_{U,3}/0_F]$	**0.5**	**0.05**	34.6	17.3	3 000
					32.9	16.4	9 100
					30.1	15.1	28 900
					28.1	14.0	33 200
					24.9	12.5	303 700
Set #G3	[31]	$[0_F/90_{U,3}/0_F]$	**1**	**0.05**	30.1	30.1	3 000
					30.0	30.0	4 700
					30.0	30.0	5 000
					24.9	24.9	18 000
					23.0	23.0	143 500
					20.1	20.1	809 600
Set #G4	[31]	$[0_F/90_{U,3}/0_F]$	**2**	**0.05**	18.0	35.9	2 800
					18.0	36.1	11 400
					13.8	27.6	29 900
					14.9	29.9	34 900
					14.9	29.9	45 200
					14.0	27.9	144 600
					12.9	25.8	816 000

Set #G5	[32]	$[0_F/90_{U,3}/0_F]$	**2**	**0.5**	21.5	43.1	4 800
					20.5	41.0	18 800
					18.7	37.3	254 700
					15.7	31.3	2 015 500
Set #G6	[32]	$[0_F/90_{U,3}/0_F]$	**2**	**-1**	12.0	24.0	2 500
					11.0	22.0	6 000
					9.0	18.0	58 500
					6.9	13.8	1 282 400
Set #G7	[33]	$[0/50_2/0/-50_2]$	**1**	**0.05**	30.1	30.1	3 000
					29.9	29.9	5 000
					24.9	24.9	18 100
					23.2	23.2	144 800
					19.9	19.9	790 300
Set #G8	[33]	$[0/60_2/0/-60_2]$	**0.5**	**0.05**	35.1	17.6	3 000
					33.3	16.7	8 400
					29.9	15.0	28 000
					28.0	14.0	33 500
					25.0	12.5	294 900

For the purpose of calibration of the *k* parameters, Set #G1, Set #G4 and set #G6 was chosen. Data for the uniaxial tension and torsional fatigue test should be superimposed to obtain the value of *k*. However, data on pure torsional fatigue are lacking in the literature, so sets were chosen for the same *R* ratio (to exclude the impact of mean stress). To determine the parameter *k*, sets G1 (pure axial) and G4 (multiaxial) were chosen, giving the *k*-value of 1. The *k* – parameter is not empirical; the determination shows a good correlation for the same load ratio. Furthermore, comparison with the set G6 for zero mean stress and the same stress state ($\lambda_{12} = 2$) also gave good agreement. There are no significant differences for $k = 1$ for the G1, G4, and G6 sets mentioned in terms of the regression lines obtained. It should be noted that the k-value is relatively high if the CFRP *k*-value ($k = 0.2$) is considered. However, the configuration of the sample based on 90° layers is highly sensitive to σ_2 Stress component (which is induced by the axial force applied to the samples)and, respectively, transverse cracking.

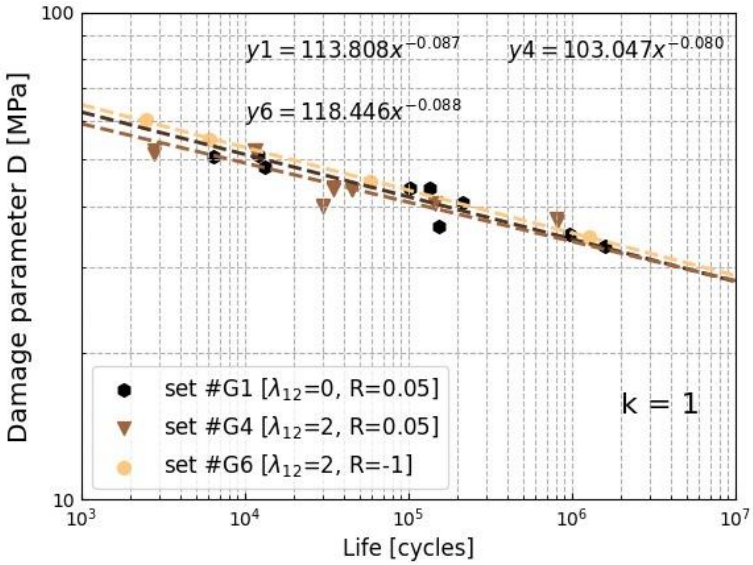

Fig. 77. Calibration of the *k* parameter based on Set #1 and Set #6

The calibration allowed to calculate the damage parameter for other multiaxial fatigue data sets and combined them. The results are given in Fig. 78, the regression analysis performed showed very similar function parameters as in terms of data chosen for calibration. It suggests the rationality of the *k*-value and the damage parameter itself. The full dataset is covered by a scatter band of 5 except for 2 points.

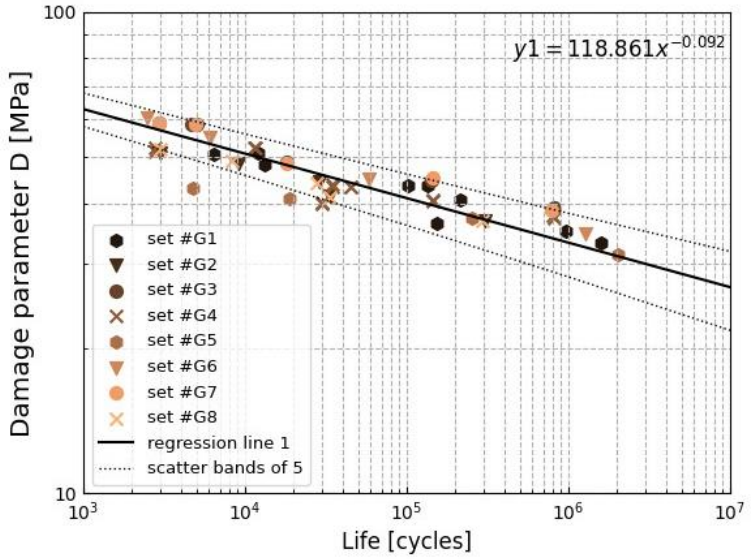

Fig. 78. Data correlation for GFRP material collected from literature

Comparison with different damage parameters

The damage patrameter *D* in a reasonable way correlates the literature data within the scatter band of 5. Comparison was carried out with other initiation parameters that evaluated their precision. Taking into account the damage-based approach proposed in [18], there are two initiation parameters based on microscale stresses used in the prediction of fatigue life.

- Local hydrostatic stress (*LHS*) – for the stress state without or limited presence of shear stress, Eq. (23).

$$LHS = \frac{\sigma_{rr} + \sigma_{\varphi\varphi} + \sigma_{zz}}{3} \tag{23}$$

- Local maximum principal stress (*LMPS*) – applied for multiaxial stress state with significant influence of the shear stress component, Eq. (24).

$$LMPS = \frac{1}{2}\left[\sigma_{rr} + \sigma_{zz} + \sqrt{\sigma_{rr}^2 + 4\sigma_{rz}^2 - 2\sigma_{rr}\sigma_{zz} + \sigma_{zz}^2}\right] \tag{24}$$

To define these parameters, local stresses in a polar coordinate (r, φ, z) need to be calculated. A unit cell of the fiber matrix is incorporated to define those local stress components, which was confirmed to provide reliable results regardless of many simplifications. The data correlation (sets #G1 – 4) for these two parameters was taken from [18], the results are presented in Fig. 79 with scatter bands of 5 and compared with the proposed damage parameter *D*.

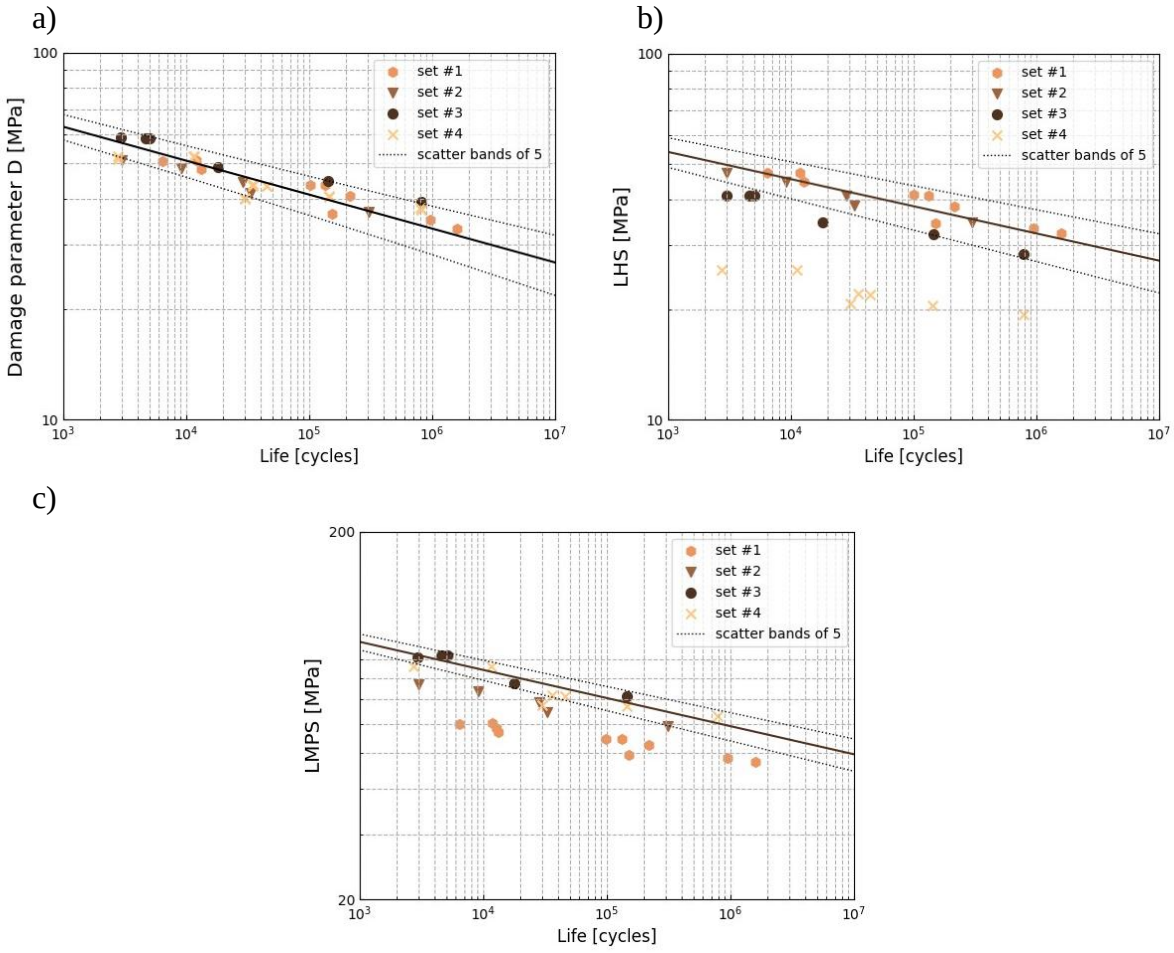

Fig. 79. Comparison of damage parameters for a) damage parameter D; b) LHS, and c) LMPS [MPa]

The damage parameters proposed as the driving force in [18] required a calculation of local stresses with the analysis of the parodic unit cell. However, there are certain conditions that define the use of damage parameter, i.e. fiber orientation and biaxiality ratio. For calibration of the modified FS parameter, the experimental data for uniaxial fatigue tension and torsion should be used to deliver the *k* – parameter. Taking into account the results, the damage parameter

proposed in this dissertation more precisely covers the experimental data within the scatter band of 5.

8.3 Summary

The application of the stress-based damage parameter for fatigue life prediction as well as its applicability for multiaxial data correlation is presented in the chapter and gives the following conclusions.

- The prediction of the fatigue life of multiaxial fatigue is based on uniaxial tensile testing. The numerical analysis was applied to determine stresses and correlate the uniaxial tensile force that reflects the reference multiaxial damage state at 1 million cycles. The results showed that 25% of the ultimate tensile strength can be applied to predict fatigue life for investigated thin – walled CFRP member.
- The delivered approach was applied to correlate the data found in the literature for the GFRP material. The correlation using the damage parameter *D* showed good agreement within the scatter bands of 5. A comparison made with the initiation parameters of the literature (*LHS, LMPS*) showed that the damage parameter *D* more effectively covers the results for multiaxial data. These parameters consider the initiation of damage at the microscale, i.e. only matrix cracking, whereby the applied damage parameter *D* is based on the mesoscale stresses covering matrix microcracking and debonding.

9 Conclusions

In this dissertation, comprehensive research on multiaxial phenomena is presented. CFRP thin wall with mosaic pattern 1/1 is considered, subjected to multiaxial global cycling loading conditions. The main objective of the dissertation is to develop an approach to estimating fatigue life; however, additional aspects are investigated within the presented research framework to provide fundamentals for modeling and assessing fatigue life. The research presented is focused on two parameters that influence fatigue life, that is, phase shift and the effect of mean stress on fatigue life. The schematic idea of the research conducted is presented in Fig. 80.

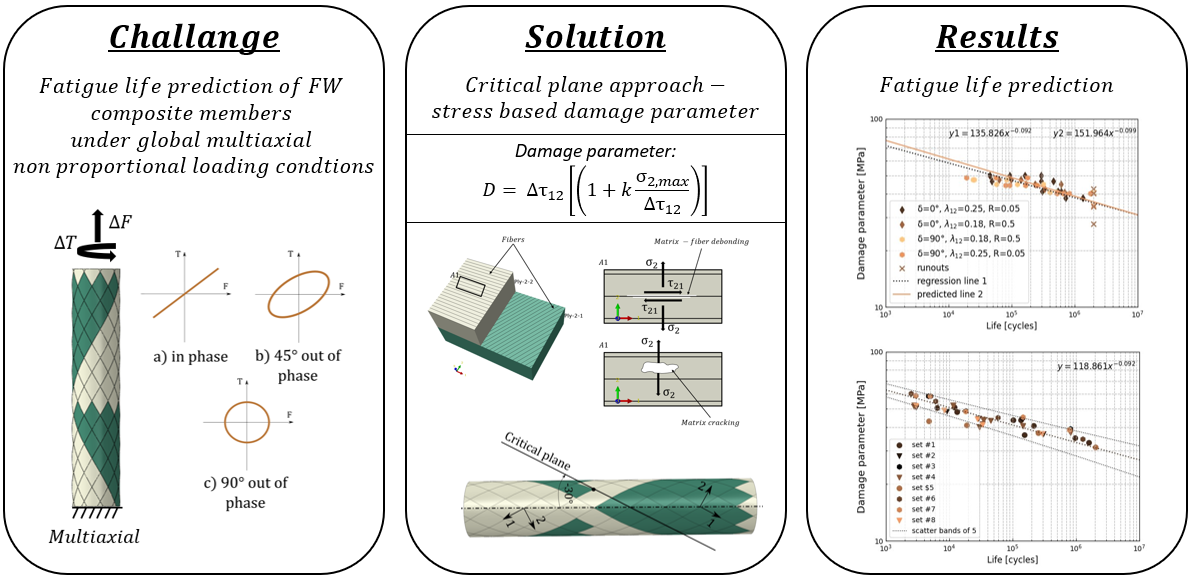

Fig. 80. Schematic summary of the conducted research

Conducted scientific research based on the comprehensive experimental and numerical part allowed to draw the following conclusions.

(1) The strain distribution on the external surface can be easily assessed by the DIC method. This method can be replaced or supported by external measurement, e.g. strain rosettes. However, there is some limitation, which excludes strain rosettes, in terms of maximum failure strain due to large deformation, the strain gauges deboned from the material surface at a certain load level. This aspect forces very precise surface preparation for strain gauges and requires the use of another method if maximum strain value is required, e.g. DIC.

(2) The inhomogeneous strain distribution in the FW tube caused by a complex material architecture requires a comprehensive experimental procedure supported by optical (DIC) and electrical methods (strain gauges). These data allowed to choose the proper material model and verify it in terms of the strain/stress distribution.

(3) From the point of view of stress analysis, a proper discrete model needs to be created that includes fiber orientation and interweaving areas caused by FW technology; otherwise, stresses are underestimated. The numerical model created from CFRP tube incorporated with a Python script allowed for providing precise geometry with zig-

zag areas. These areas are crucial from a stress-strain analysis perspective. The material model with shear nonlinearity and progressive damage was chosen based on the experimental static results obtained. The numerical results were compared with the experimental results. Good agreement can be confirmed between the experimental and numerical results. Furthermore, the strain fields of FEA and DIC exhibit a similar distribution. It confirms that the material model was chosen correctly and can reflect the mechanical performance of the CFRP tube under various loading conditions.

(4) The buckling phenomenon should be considered since the negative load ratio is investigated. The numerical analysis allowed to define the buckling safety margin for compression – torsional test. The analysis showed a higher compressive strength compared to the experiment, which can be explained by the fact that the FE model is a perfectly built discrete body, which does not include any imperfections, which very often appear in those materials. The experiment performed gives the actual value of the critical force and allows the establishment of a safety margin, which totals 2.6. Based on that, it can be assumed that there is no possibility of global buckling for multiaxial fatigue performed under R = -1. However, due to the possibility of structure discontinuity, local buckling might still affect the results.

(5) The effect of phase shift has been one of the main parameters investigated in the research. Regression analysis was performed to assess the influence on fatigue life in the HCF regime. For the impact analysis, the data of R = -1 for each phase were excluded, as well as the 45° out of phase load. This was important from the analysis point of view, due to the large scatter and the different nature of the data observed for those cases. It might be caused by the influence of additional unrecognized effects. The experimental results presented in the form of geometric stresses for in phase and 90° out of phase, and the positive load ratios show the negative influence of phase shifting.

(6) The mean stress effect is also analyzed for positive load ratios that exclude 45° out-of-phase loading. The effect is noticeable and, as expected, the higher the stress ratio, the shorter the fatigue life.

(7) The accumulation of damage was investigated by analyzing the acoustic data collected during multiaxial fatigue using a piezoelectric sensor. The analysis of cumulative counts curve allowed to divide the sample fatigue life into 4 regions with respect to major failure mechanisms acting within by comparison to the general accumulation curve reported in literature.

(8) Damage accumulation analysis suggests the unstable damage growth in terms of 45° out of phase loading conditions due to relatively short duration of the last two phases (i.e. C and D). The results suggest that the first initiation phase lasts even up to 70% of the total fatigue life. On the other hand, the propagation phase is relatively short, which might be explained by the sudden and unstable propagation of delamination. This fact is reported in [63], and is explained as a lack of an additional layer, which should provide a constraint effect for stable growth of damage. An approximately 20% increase in displacement/rotation value leads to decohesion of investigated thin-walled CFRP samples.

(9) By visual observation of the specimens, two failure mechanisms were recognized, i.e., fiber breakage and delamination, mainly observed in the zigzag area. The fiber failure observed in the fiber weaving borderline is caused by compression of the trough thickness caused by the top layer. These failure mechanisms were confirmed by conducted μCT analysis. It also showed the nature of the cracks and their directionality. The analysis confirmed the rationality of the numerical analysis performed, which also indicates the highest stress concentration and the initiation of failure in the zig-zag area.

(10) The in situ measurement of acoustic signals during the multiaxial fatigue experiment allowed a quantitative analysis of damage accumulation during the lifetime of fatigue. On the basis of the cumulative counts, the S-N curves were delivered. The negative effect of mean stress was also confirmed by the data provided, showing that failure initiation occurred earlier for a higher load ratio. The detrimental effect of the 90° out-of-phase load is recognized. The delivered S – N curves give the possibility of designing reinforced composite structures with continuous fibers for short and long-service operation without the presence of damage. These data also confirm the applicability of acoustic emission in early damage detection for in-service parts.

(11) A discrete model created with non-linear shear material behavior and progressive damage was applied to perform stress analysis to define the critical stress point, which gave the stress extrema. The defined critical point is located in the zig-zag area and is located in the internal composite layer. The analysis allowed to define the biaxiality ratio (λ_{12}) to be 0.35 for R = -1, 0.25 for R = 0.05 and 0.18 for R = 0.5.

(12) The damage analysis performed confirmed the rationality of this place as a damage initiation area. Additionally, material stress components were defined, which are more likely to reflect the behavior of CFRP materials. It can be confirmed by a noticeable impact of mean stress on fatigue strength, which is expected to be detrimental in these materials. However, the impact of phase shift is not recognized on the basis of the S – N curves delivered for material stresses.

(13) The Fatemi – Socie damage parameter was a base equation for proposed stress – based damage parameter. The damage parameter incorporates the shear stress range and $\sigma_{2,max}$ stress component as crucial stress that causes damage. Furthermore, the parameter includes k – material constat, which was defined as 0.2 as suggested in the literature. Considering the scatter band of 5 obtained for the experimental data, it can be assumed that the damage parameter with respect to fatigue life for different load ratio and phase shift correlate data are in good agreement within the same scatter band. Since the damage parameter is in reasonably good correlation with the data for multiaxial loading conditions covering mean stress and phase shift, it is legitimate to use the formulae for the prediction of fatigue life.

(14) To predict fatigue life in terms of the S – N curve, the numerical simulation for the uniaxial tension test was carried out. The S – N curve was interpolated using two points that refer to the damage parameter in 1 cycle that exhibits the ultimate tensile strength and point in 1 million cycles, which gives the same damage value for multiaxial experimental data and performed uniaxial analysis. Analysis showed that

25% of UTS should be used in 1 million cycles to predict the S – N curve for the multiaxial load case.

(15) The application of the developed approach was verified using multiaxial fatigue data from the literature. The glass fiber reinforced polymer was chosen to check the applicability of the damage parameter. It shows a good correlation with fatigue data for various R and λ_{12} ratios. Moreover, the proposed damage parameter appears to be a better alternative with comparison with those proposed in the literature based on local hydrostatic stress and local maximum principal stresses.

Outlook for further research

The dissertation is part of the scientific project entitled *Fatigue behavior and life assessment of CFRP members under global nonproportional multiaxial loading conditions.* Preliminary material characterization is presented in Ref. [11], and covers the quasi-static experimental and numerical investigation of the mechanical performance of thin-walled CFRP tubes.

Multiaxial fatigue experimental data analysis is currently under review in Composite Materials Part B: Engineering. The manuscript covers an evaluation that has been carried out based on the behavior of the S-N material, nondestructive damage analysis, and statistics.

Apart from that, the project covers additional aspects that will be covered after the graduation such as:

- Analysis of the influence of the biaxiality ratio on fatigue life. Currently, just biaxiality $(\lambda_T = 1)$ was investigated. The next stage covers the same experimental campaign for $(\lambda_T = 0.5)$, which allowed to analyze the influence of shear stress.

There are several ideas on how to continue this research; the following are highlighted:

- Acoustic signals analysis is based on advanced algorithms using machine learning. It will allow you to cluster the signals and define the failure mechanisms.
- Redesigning of the samples to obtain more stable propagation phase and investigation of its evolution by delivering Paris-like curves for propagation. This step would advance the prediction of fatigue life by implementing a fracture mechanics approach for the propagation of cracks.
- Optimization of a discrete model in terms of strength parameters to precisely reflect mechanical performance. Furthermore, the impact of material imperfections should be considered and included in the modeling.
- The analysis of phase impact by means of equivalent stress appropriate to use for composite materials.

Appendix 1

The filament winding process is an automated open molding process that uses a rotating mandrel as the mold to provide preimpregnated fibers on it. This process is used to produce tanks, pipes, pressure vessels, and other round-form products that require a high degree of structural integrity.

The mosaic pattern is characterized by the specific numeration presented in Eq. (1).

$$\pm X/Y \tag{1}$$

where
X – leading number
Y – lagging number

From a geometric point of view, the leading number (X) defines the number of diamonds in the circumference created during the filament winding process. The lagging number (Y), also called the skip index, determines whether there is a skip of the next positions (put the next band skip of the positions Y-1). The example of a diamond-shaped form for leading number 1 is presented in Fig. 81.

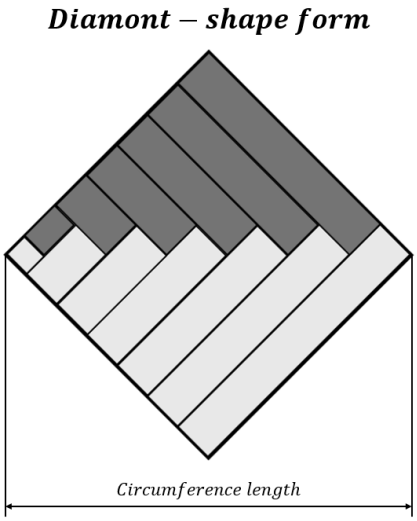

Fig. 81. Detail of the diamond-shape form for X = 1

The cylindrical specimen with 1/1 pattern investigated in dissertation is outlined in Fig. 82. The graphics were created using WindingExpert software.

Fig. 82. Winding path generation in WindingExpert software

Table list of figures

List of Tables

References

[1] T. Kizaki, J. Zhang, Q. Yao, and J. Yanagimoto, “Continuous manufacturing of CFRP sheets by rolling for rapid fabrication of long CFRP products” *Compos B Eng*, vol. 189, p. 107896, May 2020, doi: 10.1016/j.compositesb.2020.107896.

[2] “Composites Market Size to Worth Around USD 191.36 Bn By 2032.” Accessed: Mar. 05, 2024. [Online]. Available: https://www.precedenceresearch.com/composites-market

[3] A. Bona, “Theoretical and Experimental Review of Applied Mechanical Tests for Carbon Composites with Thermoplastic Polymer Matrix” *Transactions on Aerospace Research*, vol. 2019, no. 4, pp. 55–65, Dec. 2019, doi: 10.2478/tar-2019-0023.

[4] J. Weng, T. Meng, W. Wen, and S. Weng, “Multiaxial fatigue life prediction of composite laminates” *Chinese Journal of Aeronautics*, Jun. 2020, doi: 10.1016/j.cja.2020.06.016.

[5] P. Lucía Zumaquero, E. Correa, J. Justo, and F. París, “Transverse biaxial tests on long fibre reinforced composites” *Compos Struct*, vol. 297, p. 115868, Oct. 2022, doi: 10.1016/j.compstruct.2022.115868.

[6] N. Venkateshwaran, A. ElayaPerumal, A. Alavudeen, and M. Thiruchitrambalam, “Mechanical and water absorption behaviour of banana/sisal reinforced hybrid composites” *Mater Des*, vol. 32, no. 7, pp. 4017–4021, Aug. 2011, doi: 10.1016/j.matdes.2011.03.002.

[7] K. Jarukumjorn and N. Suppakarn, “Effect of glass fiber hybridization on properties of sisal fiber–polypropylene composites” *Compos B Eng*, vol. 40, no. 7, pp. 623–627, Oct. 2009, doi: 10.1016/j.compositesb.2009.04.007.

[8] Y. J. Liang, C. G. Dávila, and E. V. Iarve, “A reduced-input cohesive zone model with regularized extended finite element method for fatigue analysis of laminated composites in Abaqus” *Compos Struct*, vol. 275, p. 114494, Nov. 2021, doi: 10.1016/j.compstruct.2021.114494.

[9] S. Gholizadeh, “A review of non-destructive testing methods of composite materials” in *Procedia Structural Integrity*, 2016, pp. 50–57. doi: 10.1016/j.prostr.2016.02.008.

[10] M. Quaresimin, “50th anniversary article: Multiaxial fatigue testing of composites: From the pioneers to future directions” *Strain*, vol. 51, no. 1, pp. 16–29, Feb. 2015, doi: 10.1111/str.12124.

[11] S. Duda *et al.*, “Experimental characterization and modeling of cylindrical CFRP structures under quasi-static multiaxial loading conditions” *Thin-Walled Structures*, vol. 195, p. 111364, Feb. 2024, doi: 10.1016/j.tws.2023.111364.

[12] V. V. Vasiliev and E. V. Morozov, *Advanced Mechanics of Composite Materials, Second Edition*. Elsevier Science, 2007. doi: 10.1016/B978-0-08-045372-9.X5000-3.

[13] H. Fang, Y. Bai, W. Liu, Y. Qi, and J. Wang, “Connections and structural applications of fibre reinforced polymer composites for civil infrastructure in aggressive

environments" *Composites Part B: Engineering*, vol. 164. Elsevier Ltd, pp. 129–143, May 01, 2019. doi: 10.1016/j.compositesb.2018.11.047.

[14] M. Quaresimin and P. A. Carraro, "Damage initiation and evolution in glass/epoxy tubes subjected to combined tension-torsion fatigue loading" *Int J Fatigue*, vol. 63, pp. 25–35, Jun. 2014, doi: 10.1016/j.ijfatigue.2014.01.002.

[15] M. Quaresimin, "Multiaxial fatigue of composites: Experimental evidences and life prediction methodology" in *Comprehensive Composite Materials II*, Elsevier, 2017, pp. 249–274. doi: 10.1016/B978-0-12-803581-8.09915-X.

[16] M. Quaresimin, P. A. Carraro, and L. Maragoni, "Influence of load ratio on the biaxial fatigue behaviour and damage evolution in glass/epoxy tubes under tension-torsion loading" *Compos Part A Appl Sci Manuf*, vol. 78, pp. 294–302, Nov. 2015, doi: 10.1016/j.compositesa.2015.08.009.

[17] M. Quaresimin, L. Susmel, and R. Talreja, "Fatigue behaviour and life assessment of composite laminates under multiaxial loadings" *Int J Fatigue*, vol. 32, no. 1, pp. 2–16, Jan. 2010, doi: 10.1016/j.ijfatigue.2009.02.012.

[18] P. A. Carraro and M. Quaresimin, "A damage based model for crack initiation in unidirectional composites under multiaxial cyclic loading" *Compos Sci Technol*, vol. 99, pp. 154–163, Jul. 2014, doi: 10.1016/j.compscitech.2014.05.012.

[19] M. Quaresimin *et al.*, "Damage evolution under cyclic multiaxial stress state: A comparative analysis between glass/epoxy laminates and tubes" *Compos B Eng*, vol. 61, pp. 282–290, 2014, doi: 10.1016/j.compositesb.2014.01.056.

[20] P. A. Carraro, M. Simonetto, and M. Quaresimin, "Fatigue damage evolution in glass/epoxy cross-ply laminates under spectrum loadings" *Compos Part A Appl Sci Manuf*, vol. 173, pp. 1359–835, 2023, doi: 10.1016/j.compositesa.2023.107680.

[21] M. Quaresimin, "50th anniversary article: Multiaxial fatigue testing of composites: From the pioneers to future directions" *Strain*, vol. 51, no. 1, pp. 16–29, Feb. 2015, doi: 10.1111/STR.12124.

[22] J. Mei, "Modeling of Multi-Axial Fatigue Damage Under Non-Proportional Variable-Amplitude Loading Conditions," 2016.

[23] R. Olsson, "A survey of test methods for multiaxial and out-of-plane strength of composite laminates" *Composites Science and Technology*, vol. 71, no. 6. Elsevier, pp. 773–783, Apr. 12, 2011. doi: 10.1016/j.compscitech.2011.01.022.

[24] E. A. W. de Menezes, T. V. Lisbôa, J. H. S. Almeida, A. Spickenheuer, S. C. Amico, and R. J. Marczak, "On the winding pattern influence for filament wound cylinders under axial compression, torsion, and internal pressure loads" *Thin-Walled Structures*, vol. 191, p. 111041, Oct. 2023, doi: 10.1016/j.tws.2023.111041.

[25] T. V. Lisbôa, J. H. S. Almeida, I. H. Dalibor, A. Spickenheuer, R. J. Marczak, and S. C. Amico, "The role of winding pattern on filament wound composite cylinders under radial

compression" *Polym Compos*, vol. 41, no. 6, pp. 2446–2454, Jun. 2020, doi: 10.1002/pc.25548.

[26] C. B. Azevedo, J. H. S. Almeida, H. F. Flores, F. Eggers, and S. C. Amico, "Influence of mosaic pattern on hygrothermally-aged filament wound composite cylinders under axial compression" *J Compos Mater*, vol. 54, no. 19, pp. 2651–2659, Aug. 2020, doi: 10.1177/0021998319899144

[27] E. V. Morozov, "The effect of filament-winding mosaic patterns on the strength of thin-walled composite shells" *Compos Struct*, vol. 76, no. 1–2, pp. 123–129, Oct. 2006, doi: 10.1016/j.compstruct.2006.06.018.

[28] M. Sayem Uddin, E. V. Morozov, and K. Shankar, "The effect of filament winding mosaic pattern on the stress state of filament wound composite flywheel disk" *Compos Struct*, vol. 107, no. 1, pp. 260–275, Jan. 2014, doi: 10.1016/j.compstruct.2013.07.004.

[29] F. K. Chang and L. B. Lessard, "Damage Tolerance of Laminated Composites Containing an Open Hole and Subjected to Compressive Loadings: Part I—Analysis" vol. 25, no. 1, pp. 2–43, Jan. 1991, doi: 10.1177/002199839102500101.

[30] W. Van Paepegem, I. De Baere, and J. Degrieck, "Modelling the nonlinear shear stress–strain response of glass fibre-reinforced composites. Part II: Model development and finite element simulations" *Compos Sci Technol*, vol. 66, no. 10, pp. 1465–1478, Aug. 2006, doi: 10.1016/j.compscitech.2005.04.018.

[31] Y. He, A. Makeev, and B. Shonkwiler, "Characterization of nonlinear shear properties for composite materials using digital image correlation and finite element analysis" *Compos Sci Technol*, vol. 73, no. 1, pp. 64–71, Nov. 2012, doi: 10.1016/j.compscitech.2012.09.010.

[32] B. Fedulov, A. Fedorenko, A. Safonov, and E. Lomakin, "Nonlinear shear behavior and failure of composite materials under plane stress conditions" *Acta Mech*, vol. 228, no. 6, pp. 2033–2040, Jun. 2017, doi: 10.1007/s00707-017-1817-4/metrics.

[33] C. N. O'Brien and A. E. Zaghi, "Modelling the nonlinear shear stress-strain response of composites with metal and non-metal reinforcement" *Compos B Eng*, vol. 221, p. 109009, Sep. 2021, doi: 10.1016/j.compositesb.2021.109009.

[34] G. P. Sendeckyf, "Fitting Models to Composite Materials Fatigue Data" *ASTM International: West Conshohocken*, vol. ASTM STP 7, pp. 245–260, 1981.

[35] J. Kohout and S. Věchet, "New function for fatigue curves characterization and its multiple merits" *Int J Fatigue*, vol. 23, no. 2, pp. 175–183, Jan. 2001, doi: 10.1016/S0142-1123(00)00082-7.

[36] W. Weibull, "A Statistical Distribution Function of Wide Applicability" *J Appl Mech*, vol. 18, no. 3, pp. 293–297, 1951, doi: 10.1115/1.4010337.

[37] M. M. Shokrieh and F. Taheri-Behrooz, "A unified fatigue life model based on energy method" *Compos Struct*, vol. 1–4, no. 75, pp. 444–450, Sep. 2006, doi: 10.1016/j.compstruct.2006.04.041.

[38] A. P. Vassilopoulos and T. Keller, “Modeling of the fatigue life of adhesively-bonded {FRP} joints with genetic programming” *17th International Conference on Composite Materials, ICCM-17*, p. F13:13, 2009, Accessed: Mar. 21, 2022. [Online]. Available: http://www.iccmcentral.org/proceedings/iccm17proceedings/themes/behaviour/fatigue of composites/f13 13 vassilopoulos.pdf

[39] A. P. Vassilopoulos, E. F. Georgopoulos, and V. Dionysopoulos, “Modelling fatigue life of multidirectional GFRP laminates under constant amplitude loading with artificial neural networks” *Advanced Composites Letters*, vol. 15, no. 2, pp. 43–51, 2006, doi: 10.1177/096369350601500201.

[40] J. Petermann and A. Plumtree, “A unified fatigue failure criterion for unidirectional laminates” *Compos Part A Appl Sci Manuf*, vol. 32, no. 1, pp. 107–118, Jan. 2001, doi: 10.1016/S1359-835X(00)00099-3.

[41] M. Amjadi and A. Fatemi, “Multiaxial fatigue behavior of thermoplastics including mean stress and notch effects: Experiments and modeling” *Int J Fatigue*, vol. 136, p. 105571, Jul. 2020, doi: 10.1016/j.ijfatigue.2020.105571.

[42] M. Amjadi and A. Fatemi, “A critical plane approach for multiaxial fatigue life prediction of short fiber reinforced thermoplastic composites” *Compos Part A Appl Sci Manuf*, vol. 180, p. 108050, May 2024, doi: 10.1016/j.compositesa.2024.108050.

[43] P. Labossière and K. W. Neale, “A general strength theory for orthotropic fiber-reinforced composite laminae” *Polym Compos*, vol. 9, no. 5, pp. 306–317, Oct. 1988, doi: 10.1002/pc.750090503.

[44] P. KJ. Smith EW, “Biaxial fatigue of a glass-fibre reinforced composite. Part 2: failure criteria for fatigue and fracture” *In: Brown M, Miller KJ, editors. Biaxial and multiaxial fatigue. EGF 3. London: Mechanical Engineering Publications;*, pp. 397–421, 1989.

[45] F. Ellyin and H. El-Kadi, “A fatigue failure criterion for fiber reinforced composite laminae” *Compos Struct*, vol. 15, no. 1, pp. 61–74, Jan. 1990, doi: 10.1016/0263-8223(90)90081-O.

[46] Z. Fawaz and F. Ellyin, “Fatigue Failure Model for Fibre-Reinforced Materials under General Loading Conditions” *J Compos Mater*, vol. 28, no. 15, pp. 1432–1451, 1994, doi: 10.1177/002199839402801503.

[47] A. Plumtree and G. X. Cheng, “A fatigue damage parameter for off-axis unidirectional fibre-reinforced composites” *Int J Fatigue*, vol. 21, no. 8, pp. 849–856, Sep. 1999, doi: 10.1016/S0142-1123(99)00026-2.

[48] J. Petermann and A. Plumtree, “A unified fatigue failure criterion for unidirectional laminates” *Compos Part A Appl Sci Manuf*, vol. 32, no. 1, pp. 107–118, Jan. 2001, doi: 10.1016/S1359-835X(00)00099-3.

[49] M. M. Shokrieh and F. Taheri-Behrooz, “A unified fatigue life model based on energy method” *Compos Struct*, vol. 1–4, no. 75, pp. 444–450, Sep. 2006, doi: 10.1016/j.compstruct.2006.04.041.

[50] D. Qi and G. Cheng, “Failure analysis of fiber-reinforced composites under multiaxial cyclic stress” *Polym Compos*, vol. 29, no. 8, pp. 922–931, Aug. 2008, doi: 10.1002/pc.20419.

[51] T. F. Tan and C. K. H. Dharan, “Cyclic Hysteresis Evolution as a Damage Parameter for Notched Composite Laminates” *J Compos Mater*, vol. 44, no. 16, pp. 1977–1990, Aug. 2010, doi: 10.1177/0021998309360942.

[52] A. Movaghghar and G. I. Lvov, “An Energy Model for Fatigue Life Prediction of Composite Materials Using Continuum Damage Mechanics” *Applied Mechanics and Materials*, vol. 110–116, pp. 1353–1360, 2012, doi: 10.4028/www.scientific.net/amm.110-116.1353.

[53] M. Naderi and M. M. Khonsari, “On the role of damage energy in the fatigue degradation characterization of a composite laminate” *Compos B Eng*, vol. 45, no. 1, pp. 528–537, Feb. 2013, doi: 10.1016/j.compositesb.2012.07.028.

[54] A. Plumtree and G. Shen, “Prediction of Fatigue Damage Development in Undirectional Long fibre Composites” vol. 2, no. 2, pp. 83–90, Apr. 2023, doi: 10.1177/096739119400200202.

[55] M. Amjadi and A. Fatemi, “A fatigue damage model for life prediction of injection-molded short glass fiber-reinforced thermoplastic composites” *Polymers (Basel)*, vol. 13, no. 14, Jul. 2021, doi: 10.3390/polym13142250.

[56] M. W. Brown and K. J. Miller, “Biaxial and multiaxial fatigue.,” p. 686, 1989, Accessed: Oct. 09, 2023. [Online]. Available: https://www.wiley.com/en-be/Biaxial+and+Multiaxial+Fatigue+%28EGF+3%29-p-9780852986691

[57] S. Amijima, T. Fujii, and M. Hamaguchi, “Static and fatigue tests of a woven glass fabric composite under biaxial tension-torsion loading” *Composites*, vol. 22, no. 4, pp. 281–289, Jul. 1991, doi: 10.1016/0010-4361(91)90003-Y.

[58] K. E. Atcholi, C. Oytana, D. Varchon, and D. Perreux, “Superposed torsion-flexure of composite materials: Experimental method and example of application” *Composites*, vol. 23, no. 5, pp. 327–333, 1992, doi: 10.1016/0010-4361(92)90332-O.

[59] T. Fujii, T. Shiina, and K. Okubo, “Fatigue Notch Sensitivity of Glass Woven Fabric Composites Having a Circular Hole under Tension/Torsion Biaxial Loading” *J Compos Mater*, vol. 28, no. 3, pp. 234–251, Jul. 1994, doi: 10.1177/002199839402800303.

[60] H. Kawakami, T. J. Fujii, and Y. Morita, “Fatigue Degradation and Life Prediction of Glass Fabric Polymer Composite under Tension/Torsion Biaxial Loadings” *Journal of Reinforced Plastics and Composites*, vol. 15, no. 2, pp. 183–195, 1995, doi: 10.1177/073168449601500204.

[61] M. N. Aboul Wafa, A. H. Hamdy, and A. A. El-Midany, “Combined Bending and Torsional Fatigue of Woven Roving GRP” *J Eng Mater Technol*, vol. 119, no. 2, pp. 180–185, Apr. 1997, doi: 10.1115/1.2805991.

[62] D. Qi and G. Cheng, “Fatigue behavior of filament-wound glass fiber reinforced epoxy composite tubes under tension/torsion biaxial loading” *Polym Compos*, vol. 28, no. 1, pp. 116–123, Feb. 2007, doi: 10.1002/pc.20275.

[63] M. Quaresimin and P. A. Carraro, “On the investigation of the biaxial fatigue behaviour of unidirectional composites” *Compos B Eng*, vol. 54, no. 1, pp. 200–208, Nov. 2013, doi: 10.1016/j.compositesb.2013.05.014.

[64] Y. Qiao, A. A. Deleo, and M. Salviato, “A study on the multi-axial fatigue failure behavior of notched composite laminates” *Compos Part A Appl Sci Manuf*, vol. 127, 2019, doi: 10.1016/j.compositesa.2019.105640.

[65] T. Skinner, S. Datta, A. Chattopadhyay, and A. Hall, “Fatigue damage behavior in carbon fiber polymer composites under biaxial loading” *Compos B Eng*, vol. 174, 2019, doi: 10.1016/j.compositesb.2019.106942.

[66] Y. Wang and Z. M. Huang, “Analytical Micromechanics Models for Elastoplastic Behavior of Long Fibrous Composites: A Critical Review and Comparative Study” *Materials 2018, Vol. 11, Page 1919*, vol. 11, no. 10, p. 1919, Oct. 2018, doi: 10.3390/ma11101919.

[67] A. International and F. indexed by mero, “Designation: D 3039/D 3039M-00 e1 Standard Test Method for Tensile Properties of Polymer Matrix Composite Materials 1” *ASTM International*, vol. 95, no. D3039, pp. 1–2, 2002.

[68] ASTM, “D6641: Standard Test Method for Compressive Properties of Polymer Matrix Composite Materials Using a Combined Loading Compression (CLC) Test Fixture” pp. 1–13, 2014, doi: 10.1520/D6641.

[69] ASTM D7078/7078M-12, “Standard Test Method for Shear Properties of Composite Materials by V-Notched Rail, D30.04, Ed.” 2012, doi: 10.1520/D7078.

[70] M. Guadagnini, “Mechanics of Composite Materials: Preface,” *Mechanics of Composite Materials*, vol. 44, no. 3. Academic Press, pp. 197–198, 2008. doi: 10.1007/s11029-008-9011-3.

[71] C. T. Sun, B. J. Quinn, and J. Tao, “Comparative Evaluation of Failure Analysis Methods for Composite Laminates” *U.S. Department of Transportation*, no. May, p. 133, 1996, [Online]. Available: http://trid.trb.org/view.aspx?id=523207

[72] R. D. Adams, *Adhesive Bonding: Science, Technology and Applications*. 2021. doi: 10.1016/B978-0-12-819954-1.09990-1.

[73] N. E. Dowling, *Mechanical behavior of materials : engineering methods for deformation, fracture, and fatigue*. 1999. Accessed: Mar. 21, 2022. [Online]. Available: http://libnet.ac.il/~libnet/pqd/opac_tau.pl?000421915

[74] R. K. Goldberg, G. D. Roberts, and A. Gilat, “Incorporation of mean stress effects into the micromechanical analysis of the high strain rate response of polymer matrix composites” *Compos B Eng*, vol. 34, no. 2, pp. 151–165, Mar. 2003, doi: 10.1016/S1359-8368(02)00081-1.

[75] M. N. Rohman, M. I. P. Hidayat, A. Purniawan, M. N. Rohman, M. I. P. Hidayat, and A. Purniawan, "Prediction of composite fatigue life under variable amplitude loading using artificial neural network trained by genetic algorithm" *AIPC*, vol. 1945, no. 1, p. 020019, Apr. 2018, doi: 10.1063/1.5030241.

[76] N. L. Post, S. W. Case, and J. J. Lesko, "Modeling the variable amplitude fatigue of composite materials: A review and evaluation of the state of the art for spectrum loading," *Int J Fatigue*, vol. 12, no. 30, pp. 2064–2086, Dec. 2008, doi: 10.1016/j.ijfatigue.2008.07.002.

[77] W. p. Seneviratne and J. Tomblin, "Life of Composites under Variable Amplitude Fatigue" *AIAA Scitech 2021 Forum*, Jan. 2021, doi: 10.2514/6.2021-0923.

[78] R. M. Guedes, "Creep and fatigue in polymer matrix composites" *Creep and Fatigue in Polymer Matrix Composites*, pp. 1–586, Jan. 2019, doi: 10.1016/C2017-0-02292-9.

[79] A. V. Movahedi-Rad, T. Keller, and A. P. Vassilopoulos, "Creep effects on tension-tension fatigue behavior of angle-ply GFRP composite laminates" *Int J Fatigue*, vol. 123, pp. 144–156, Jun. 2019, doi: 10.1016/j.ijfatigue.2019.02.010.

[80] B. Vieille, W. Albouy, and L. Taleb, "About the creep-fatigue interaction on the fatigue behaviour of off-axis woven-ply thermoplastic laminates at temperatures higher than Tg" *Compos B Eng*, vol. 58, pp. 478–486, Mar. 2014, doi: 10.1016/j.compositesb.2013.11.005.

[81] T. P. Philippidis and A. P. Vassilopoulos, "Life prediction methodology for GFRP laminates under spectrum loading" *Compos Part A Appl Sci Manuf*, vol. 35, no. 6, pp. 657–666, Jun. 2004, doi: 10.1016/j.compositesa.2004.02.009.

[82] M. Quaresimin, L. Susmel, and R. Talreja, "Fatigue behaviour and life assessment of composite laminates under multiaxial loadings" *Int J Fatigue*, vol. 32, no. 1, pp. 2–16, Jan. 2010, doi: 10.1016/j.ijfatigue.2009.02.012.

[83] M. Quaresimin and P. A. Carraro, "Damage initiation and evolution in glass/epoxy tubes subjected to combined tension-torsion fatigue loading" *Int J Fatigue*, vol. 63, pp. 25–35, Jun. 2014, doi: 10.1016/j.ijfatigue.2014.01.002.

[84] M. Quaresimin, "2.13 Multiaxial Fatigue of Composites: Experimental Evidences and Life Prediction Methodology" in *Comprehensive Composite Materials II*, Elsevier, 2018, pp. 249–274. doi: 10.1016/B978-0-12-803581-8.09915-X.

[85] A. Rotem, "Load frequency effect on the fatigue strength of isotropic laminates" *Compos Sci Technol*, vol. 46, no. 2, pp. 129–138, Jan. 1993, doi: 10.1016/0266-3538(93)90168-G.

[86] C. R. Saff, "Effect of load frequency and lay-up on fatigue life of composites" *ASTM Special Technical Publication*, pp. 78–91, 1983, doi: 10.1520/stp31817s.

[87] "Standard Test Method for Tension-Tension Fatigue of Polymer Matrix Composite Materials" doi: 10.1520/d3479_d3479m-19r23.

[88] Y. Zhang, A. P. Vassilopoulos, and T. Keller, “Environmental effects on fatigue behavior of adhesively-bonded pultruded structural joints” *Compos Sci Technol*, vol. 69, no. 7–8, pp. 1022–1028, Jun. 2009, doi: 10.1016/j.compscitech.2009.01.024.

[89] M. Kawai and T. Teranuma, “A multiaxial fatigue failure criterion based on the principal constant life diagrams for unidirectional carbon/epoxy laminates” *Compos Part A Appl Sci Manuf*, vol. 43, no. 8, pp. 1252–1266, Aug. 2012, doi: 10.1016/j.compositesa.2012.03.003.

[90] M. Quaresimin, L. Susmel, and R. Talreja, “Fatigue behaviour and life assessment of composite laminates under multiaxial loadings” *Int J Fatigue*, vol. 32, no. 1, pp. 2–16, Jan. 2010, doi: 10.1016/j.ijfatigue.2009.02.012.

[91] R. Talreja, *Failure Analysis of Composite Materials with Manufacturing Defects*. Boca Raton: CRC Press, 2023. doi: 10.1201/9781003225737.

[92] R. Little and J. Ekvall, “Standard Practice for Statistical Analysis of Linear or Linearized Stress-Life (S-N) and Strain-Life (ϵ-N) Fatigue Data” in *Statistical Analysis of Fatigue Data*, vol. 10, no. Reapproved, ASTM International100 Barr Harbor Drive, PO Box C700, West Conshohocken, PA 19428-2959, 1981, pp. 129–137. doi: 10.1520/stp29332s.

[93] M. Smolnicki and P. Stabla, “Finite element method analysis of fibre-metal laminates considering different approaches to material model,” *SN Appl Sci*, vol. 1, no. 5, pp. 1–7, May 2019, doi: 10.1007/s42452-019-0496-2/figures/10.

[94] Paul. Robinson, E. S. Greenhalgh, and Silvestre. Pinho, “Failure mechanisms in polymer matrix composites : criteria, testing and industrial applications” p. 450, 2012.

[95] J. A. Nairn and S. Hu, “Matrix Microcracking,” in *Composite materials series*, 1994, p. 187.

[96] Paul. Robinson, E. S. Greenhalgh, and Silvestre. Pinho, “Failure mechanisms in polymer matrix composites : criteria, testing and industrial applications” p. 450, 2012.

[97] Sz. Duda, M. Smolnicki, T. Osiecki, and G. Lesiuk, “Determination of fracture energy (mode I) in the inverse fiber metal laminates using experimental–numerical approach” *Int J Fract*, pp. 1–10, Jul. 2021, doi: 10.1007/s10704-021-00566-3.

[98] “Development of a Composite Delamination Fatigue Life Prediction Methodology - NASA Technical Reports Server (NTRS)” Accessed: Mar. 22, 2022. [Online]. Available: https://ntrs.nasa.gov/citations/20090037430

[99] P. Liu, “Viscoelastic cohesive/friction coupled model and explicit finite element analysis for delamination analysis of composite laminates under dynamic three-point bending” *Damage Modeling of Composite Structures*, pp. 191–218, Jan. 2021, doi: 10.1016/B978-0-12-820963-9.00007-9.

[100] Y. Wang, L. P. Mikkelsen, G. Pyka, and P. J. Withers, “Time-lapse helical X-ray computed tomography (CT) study of tensile fatigue damage formation in composites for

wind turbine blades" *Materials*, vol. 11, no. 11, p. 2340, Nov. 2018, doi: 10.3390/ma11112340.

[101] P. Wagner, O. Schwarzhaupt, and M. May, "In-situ X-ray computed tomography of composites subjected to fatigue loading" *Mater Lett*, vol. 236, pp. 128–130, Feb. 2019, doi: 10.1016/j.matlet.2018.10.078.

[102] Y. Qiao and M. Salviato, "Micro-computed tomography analysis of damage in notched composite laminates under multi-axial fatigue" *Compos B Eng*, vol. 187, p. 107789, Apr. 2020, doi: 10.1016/j.compositesb.2020.107789.

[103] M. Smolnicki, S. Duda, P. Stabla, P. Zielonka, and G. Lesiuk, "Acoustic emission with machine learning in fracture of composites: preliminary study" *Archives of Civil and Mechanical Engineering*, vol. 23, no. 4, p. 3, 2023, doi: 10.1007/s43452-023-00795-4.

[104] M. Smolnicki, S. Duda, P. Zielonka, P. Stabla, G. Lesiuk, and C. C. C. Lopes, "Combined experimental–numerical mode I fracture characterization of the pultruded composite bars" *Archives of Civil and Mechanical Engineering*, vol. 23, no. 3, pp. 1–11, Aug. 2023, doi: 10.1007/s43452-023-00684-w.

[105] M. Saeedifar and D. Zarouchas, "Damage characterization of laminated composites using acoustic emission: A review" *Compos B Eng*, vol. 195, p. 108039, Aug. 2020, doi: 10.1016/j.compositesb.2020.108039.

[106] D. S. Abolin'sh, "Compliance tensor for an elastic material reinforced in one direction" *Polymer Mechanics*, vol. 1, no. 4, pp. 28–32, Jul. 1965, doi: 10.1007/bf00858888/metrics.

[107] H. Wang *et al.*, "Stress dependence of indentation modulus for carbon fiber in polymer composite" *Sci Technol Adv Mater*, vol. 20, no. 1, pp. 412–420, Dec. 2019, doi: 10.1080/14686996.2019.1600202.

[108] W. Van Paepegem, I. De Baere, and J. Degrieck, "Modelling the nonlinear shear stress–strain response of glass fibre-reinforced composites. Part I: Experimental results" *Compos Sci Technol*, vol. 66, no. 10, pp. 1455–1464, Aug. 2006, doi: 10.1016/j.compscitech.2005.04.014.

[109] P. Stabla, M. Smolnicki, and W. Błażejewski, "The Numerical Approach to Mosaic Patterns in Filament-Wound Composite Pipes," *Applied Composite Materials*, 123AD, doi: 10.1007/s10443-020-09861-z.

[110] A. Fatemi and D. F. Socie, "A critical plane approach to multiaxial fatigue damage including out-of-phase loading" *Fatigue Fract Eng Mater Struct*, vol. 11, no. 3, pp. 149–165, Mar. 1988, doi: 10.1111/j.1460-2695.1988.tb01169.x.

[111] S. Duda, M. Smolnicki, P. Zielonka, P. Stabla, and G. Lesiuk, "Comprehensive study on the multiaxial fatigue behavior of thin-walled CFRP tubes" *Composites Part B: Engineering - under review*.

[112] M. Quaresimin and P. A. Carraro, “Damage initiation and evolution in glass/epoxy tubes subjected to combined tension-torsion fatigue loading” *Int J Fatigue*, vol. 63, pp. 25–35, Jun. 2014, doi: 10.1016/j.ijfatigue.2014.01.002.